Università degli Studi di Palermo

AREA QUALITÀ, PROGRAMMAZIONE E SUPPORTO STRATEGICO
SETTORE STRATEGIA PER LA RICERCA
U. O. DOTTORATI

D057 - Information and Communication Technologies
Dipartimento di Ingegneria
Settore Scientifico Disciplinare ING-INF/07

DEVELOPMENT AND CHARACTERIZATION OF ADVANCED METERING AND ICT SOLUTIONS FOR SMART ENERGY DISTRICTS

IL DOTTORE
NICOLA PANZAVECCHIA

IL COORDINATORE
PROF. ILENIA TINNIRELLO

IL TUTOR
PROF. VALENTINA COSENTINO

CO TUTOR
ING. GIOVANNI TINÈ

CICLO XXXIV
ANNO CONSEGUIMENTO TITOLO 2022

SUMMARY

ABSTRACT

Climate change will have an influence on the world's 8 billion inhabitants, the majority of whom live in cities, which account for roughly two-thirds of the CO2 emissions that are at the root of the climate crisis. To attain a net-zero carbon future, a rapid transition across business models and policy is required. At the same time, policy and legislation are struggling to keep up with smart technology and the Internet of Things. The management of smart urban infrastructure is the key to successful decarbonisation and the achievement of sustainable cities. In this framework, the smart electricity infrastructure shall be equipped with integrated technologies, such solar panels, storage facilities, electric vehicle charging, intelligent public lighting system and sensor connected to a digital platform. This paradigm has changed the view of the power system itself, as decades ago the energy infrastructure was built for a centralised power system, not for a decentralised and digitalized system when energy flows in a bi-directional way within the grid. This increases the advanced metering and ICT solutions for a proper and safe management of the grid itself.

This Ph.D. thesis proposes a smart architecture, as well as smart equipment and solutions, to suit the needs of the new power grid that will support smart energy districts. The developed architecture provides a distributed measurement system to keep the distributor updated about the status of the grid. Power Line Communication (PLC) has been chosen as communication technology in order to allow the DSO to reduce the cost of the upgrade of the grid and keep the control over the communication medium. Within this architecture, several devices have been developed. In detail, a concentrator and a remote PLC bridge implementing the PLC-PRIME v1.4 protocol have been developed to fulfil the requirements of the architecture. An IEC-6100-4-3/4-7 Class S Power quality analyser has been implemented on a low cost STMicroelectronics platform already used for smart metering applications. Starting from field measurement data collection, a specific software has been developed as oracle for the SCADA system in order to provide Distribution System Operators (DSOs) with valuable information for a better management of the power grid.

1 INTRODUCTION

With the Winter Package, or Clean Energy Package, the European Union has outlined its energy and climate goals for the years 2021-2030. The package, which was passed between the end of 2018 and the beginning of 2019, builds on the Paris Agreement's pledges and comprises a number of legislative changes in the areas of energy efficiency, renewable energy, and the internal electricity market. The Agreement in question was adopted following the XXI Conference of the Parties (COP21) in Paris in December 2015, with decision 1/CP21. It defines the long-term objective of temperature increase well below 2°C and the pursuit of efforts to limit the increase to 1.5°C compared to pre-industrial levels. This is the first legally binding global agreement on climate change (190 parties). Each country communicates its own "contribution, decided at national level" (INDC - Intended Nationally Determined Contribution) upon admission, with the need to pursue domestic means for its execution. Each succeeding national contribution (to be announced every five years) must represent a step up from the initial contribution. The Paris Agreement went into effect on November 4, 2016 (30 days following the deposit of ratification documents by at least 55 Parties to the Convention representing at least 55% of global greenhouse gas emissions), and it will remain in effect until 2021. The EU and its Member States are among the 190 countries that have signed the Paris Agreement. On October 5, 2016, the EU formally accepted it, allowing it to enter into effect on November 4, 2016. The Paris Agreement fits into the 2030 Agenda for Sustainable Development's larger framework. Following these promises, the EU has outlined its own targets for the years 2021-2030, which are contained in the EU INDC, and to which all Member States are required to contribute. With the publication of the Commission communication on the European Green Deal, COM (2019) 640, at the end of 2019, the European Union reformulated on new foundations its commitment to address climate and environmental problems, and established an Action Plan aimed at transforming the EU into a competitive and resource-efficient economy by 2050, with no net greenhouse gas emissions, in line with the Paris Agreement. One of the Plan's main elements was the introduction of a European legislative proposal on climate change, which was recently finalised and became Regulation 2021/1119/EU. The Regulation legally establishes the aim of climate neutrality by 2050, as well as the binding Union climate target for 2030, which is a net internal reduction of greenhouse gas emissions (emissions net of removals) of at least 55% by 2030 compared to 1990 levels. This is a new and more ambitious objective, which goes beyond the one set for 2030 in Regulations 2018/1999/EU and 2018/842/EU (reduction of at least 40 percent of emissions at 2030 compared to 1990 values). Climate neutrality by 2050 and a 55% reduction in emissions by 2030 were also reference targets for the development of Green Transition investments and reforms in the National Recovery and Resilience Plans, and were among the basic fundamental principles set out by the EU Commission in the Annual Sustainable Growth Strategy - SNCS 2021 (COM (2020) 575 final). According to the rules of art. 18, par. 4, e), of Reg. n. 2021/241/EU, all National Recovery and Resilience Plans must firmly focus on both reforms and investments in support of the green transition, with at least 37% of spending for the climate. Europe wants to achieve climate neutrality by 2050 and, based on the Strategy's principles, will need to significantly boost its objective for reducing

greenhouse gas emissions by 2030. Member States will have to present reforms and investments to support the green transition in the sectors of energy, transportation, industrial decarbonisation, the circular economy, water resource management, and biodiversity, i.e. in sectors aligned with the main investment sectors identified in the context of the European semester, in order to meet the ambitious climate goal of reducing emissions by 55% in 2030 compared to 1990 levels. The 2030 objectives set by law in the Clean energy package are therefore currently in evolution, as an upward revision of the emission reduction targets is underway, renewable energy and energy efficiency originally planned. The EU is, in fact, working on the revision of these regulations in order to bring them into line with the new ambitions.

While cities only cover for 3% of the earth's geographic surface, they produce more than 70% of all carbon emissions, primarily from buildings, energy, and transportation, and consume 78% of the world's primary energy. Cities must attain net zero emissions by mid-century to satisfy the stated goals. As a solution to the current environmental, economic, health, and social challenges, an integrated energy approach, characterised as "systemic efficiency," is recommended. Clean electrification, smart digital technology, efficient buildings and infrastructure, as well as a circular economy approach to water, waste, and materials, are all examples of systemic efficiency. Cities may strengthen their resilience to endure a variety of future climate and health-related catastrophes by taking a holistic approach. Smart city infrastructure that tracks and communicates critical information in real time, such as electricity usage levels, is critical to reaching net zero carbon cities. This is a critical step toward making the large-scale transition from fossil fuels to renewables that is required to prevent climate change. Creating smart, green, functional and liveable cities will imply several intelligent approaches, involving complex solutions and multifaceted innovation actions [1].

The modernization of urban infrastructures relies on innovative technological and social solutions, including advanced sensors and meters and sophisticated dispatch and control tools to automate and optimize the entire process of energy generation, distribution, consumption, and storage. Homes and buildings, clustered as districts [2,3], will be connected and they will actively participate in the energy distribution and market, giving place to the so-called “Energy Internet” where all the energy players will exchange information. Each building, within its residential district, will send its demand of energy or gas or electricity, thanks to the more advanced ICT techniques, through innovative energy hubs and routers. Moreover, the widespread deployment of distributed energy resources (DERs) will lead to the implementation of self-controlled energy systems at home, building and district scales. The districts, that become “smart”, relies on three pillars: efficient use of energy through smart grids and district heating and cooling distribution systems, new mobility and the use of ICT. With the combination of the three pillars, energy loads can be reduced and shifted from peak to off-peak hours to maximize energy efficiency and integration renewable energies towards a net-zero energy balance. Energy management systems will cluster loads and DERs and promise to dramatically improve the survivability and efficiency of local energy service. Distributed energy systems can also be networked to further improve the economics, efficiency, security, sustainability, reliability and resilience of energy supplied to local citizens. In this regard, conventionally centralized energy infrastructure shall be replaced with a host of distributed, interoperable and intelligent systems at home, building and district scale, that are capable of

handling two-way energy and information flows. This kind of systems will generate data and they will be fed with data generated by other sub-modules and elaborated by themselves or by a central or a smart district control centres. These control centres need to exchange information with each other and they need to rely on solid, pervasive and light communication infrastructure. To handle heterogeneous devices deployed and the enormous data generated, a new paradigm of control need to be adopted, joining heavy and rigid centralized control with a more liquid, flexible, peripheral, autonomous and strong connected control node. In this scenario a solution for collecting, storing, process and distributing data need to be designed. New distributed and resilient systems for data acquisition and processing along with new algorithms for data analysis need to be adopted. Old and robust technologies, like SCADA systems, will be placed, side by side, to new paradigms like the "Internet of Things" (IoT), creating a mixed control system called SCADA-IoT. Along with this, cloud and big data technologies can be used to ingest and process the real-time, multidimensional and heterogeneous data flow generated by all the smart devices deployed.

Safe and cheap energy is one of more valuable aspects of liveable along with sustainable production of the energy that can bring to a strong reduction of city carbon footprint and an increment of decentralized and distributed renewable energy sources. Handling that kind of sources brings new challenges to the utility distributor (DSO) and forces to re-think to the whole electricity network. New distributed generation profiles (DG), along with new load profiles and the increment of the presence of distributed storage systems (DSS), like electric vehicles, need to be addressed. Moreover the modular approach to this kind of problems can bring to a new equilibrium of the electric network where the DSO is not the only actor. The increasing number of services, that a "digital" electrical network allows to implement, creates more room for new actors. Even the traditional consumer (user) can produce energy (producer) and can take role to the market as "prosumer" and can take advantage of personalized and custom services.

In this Ph.D. thesis a smart architecture is developed, together with some smart equipment and solutions, to meet the requirements of the future power grid that would enable smart districts and smart cities. In more detail, in order to enable the operation of the new smart energy district, the proposed architecture and related devices have been developed, contributing to the following goals:

- To meet the demand to monitor the network and remotely manage dispersed energy sources through an innovative interface device.
- To enable a better management of the interface devices connected to the same substation, thanks to a new intelligent device conceived to be installed in the secondary substations.
- To enable DSO with new features for the power grid management, by making use of power meters installed on the low voltage side of each secondary substation, which may be accessed remotely by the SCADA for the measurement of power flows and whose information can be further exploited by a new software acting as an oracle.
- To gain more information on the power system state, thanks to cutting-edge Smart Meters that can perform new measurements in addition to the classical energy metering.

This architecture includes a distributed measurement system that keeps the distributor up to date on the current status of the distribution grid. Power Line Communication has been selected as the communication technology because it will allow the distribution system operator (DSO) to reduce the cost of grid modernization, while maintaining control over the communication medium. In order to meet the needs of the architecture, a concentrator and a remote PLC bridge, both implementing the PLC-PRIME, have been developed. As regards additional metering functions, the attention has been focused on power quality analysis, according to IEC-6100-4-30/4-7 Standards; according to this, a power quality analyser has been developed on a low-cost STMicroelectronics platform that is already in use for smart metering applications, created. Moreover, starting from collected measurement data, an enhanced software application has been built to act as an oracle for the SCADA system currently in use at the DSO, so to provide meaningful information and analysis tools for key applications, as decision-making and forecasting.

The Ph.D. research work was carried out in collaboration with the National Research Council's Institute of Marine Engineering (INM-CNR); collaborations with industries, particularly STMicroelectronics, must also be mentioned, as their perspective allowed the research work to gain an industrial interest.

The thesis is structured as follows. In Chapter 2, the transition between the Automatic Meter Readings towards the Advanced Metering Infrastructure is analysed and the proposed architecture is presented and described. In Chapter 3 an overview on measurements for smart grid along with the relevant types of devices used is presented; a detailed description of the work done on the ST-Comet is presented along with some results of the IEC 6100-4-3/4-7 metric implementation. The physical implementation as well as experimental testing of the Power Flow Monitoring and Control system at the Ustica Island DSO are described, as well as the integration of measurements at the control centre level via SCADA system. The shift from a typical SCADA system to Hyperion, a Software as a Service (SaaS) decoupled software, is described. The network modelling and software modules are described in order to better understand how a digital twin can work in tandem with the DSO's SCADA system to assist in network control and monitoring. In Chapter 4 the PLC technology is introduced and its use is discussed; the PRIME protocol is presented and the developed devices for both low voltage and medium voltage network are shown, along with their implementation; a solution for time dissemination over medium voltage network is proposed. Chapter 5 contains the conclusion and future developments of the thesis work.

2 SMART GRID CONTEXT AND PROPOSED ARCHITECTURE

2.1 FROM TRADITIONAL POWER SYSTEMS TO SMART ENERGY GRIDS

In the traditional electric transmission/distribution grid as we know it, the power plants, exploiting different technologies, produce energy and transmit it via a network of High Voltage (HV) lines. The HV transmission grid ends at Medium Voltage (MV) and, downstream, Low Voltage (LV) substations where the distribution grids begins. From these substations the distribution grids reach the individual customers/end users. In this architecture, the energy basically flow in one direction, from the main producer to the end user Fig. 1

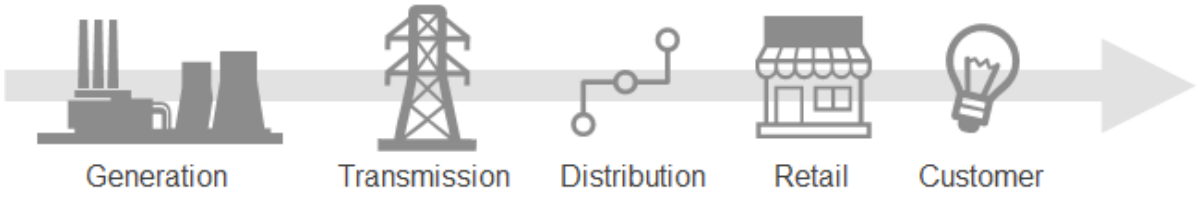

Fig. 1. Classical electricity network power flow

The electrical grid is a complex, interconnected system. Because of the greater reliability and cost savings, the grid has evolved in this fashion. In the event of a failure, different components of the system have multiple generation and transmission options as a backup. However, the grid's meshed network layout makes it vulnerable to cascading failure—known as blackout—caused by a slight fault in a tiny portion of the grid. The loading limit of the lines is the primary cause of a blackout in a heavily meshed network like the electrical grid. If a network line becomes overloaded and more power is forced through, the line may trip. This can sometimes cause a chain of low-probability events to cascade, resulting in a blackout. A direct relationship exists between number of blackouts in the power grid and increase in interconnectedness of its components [4]. The probability of cascading failures in the grid has increased significantly as a result of deregulation of the power sector. The 2003 Italian blackout, for example, was caused by an apparently innocuous event: a tree falling on a line somewhere in the network. One of the key reasons for the disastrous blackout was that the system was importing 6000 MW of low-cost power from neighbours at the time of the breakdown. This blackout is thought to be one of the worst in Europe's history, affecting 57 million people [5]. Although blackouts were caused by low-probability occurrences, the majority of them had a common thread, indicating that such failures may have been avoided or at least mitigated by improved sensing and control procedures. Many instances, the blackout was caused by the operator's or the equipment's failure to identify an otherwise manageable occurrence. Another crucial factor that utilities have overlooked is ensuring the appropriate quality of power for the newly established digital society. Variations in voltage and frequency can be as damaging to

digital equipment as a total blackout [6]. The electrical grid's core interconnected nature, which provides various benefits, is unlikely to change. Better monitoring and control techniques are required to offset the potential negative effects of the grid's meshed nature. The goal is to contain any potential flaws in a small area rather than completely eliminate the risk of blackout. Furthermore, even if a big problem or blackout happens, the system should be able to quickly recover. As a result, the power system must be updated to prevent the negative effects of large-scale blackouts and meet power quality requirements for the digital economy.

A "smart grid" [7] is an updated version of the electricity grid. A smart grid has three main characteristics: improved monitoring and control, increased knowledge of possible problems, and intentional islanding in the event of a grid disruption. Apart from blackouts, there are a slew of other reasons for the creation of a smart grid with improved monitoring, computing, and control employing cutting-edge technology. The following are some of the most essential drivers:

- Electricity market deregulation has led to unprecedented energy trading across many regional power grids. This arrangement has altered the fundamental character of the power network, introducing power flow situations and uncertainties that the traditional grid cannot handle.
- As renewable energy becomes more prevalent, bi-directional power flows are expected and distribution system will shift from a radial to a meshed network, necessitating enhanced and smarter monitoring and control functionalities. Because of the changing dynamics of the power system, the intermittent nature of these renewable energy sources also poses a hurdle.
- The new digital economy necessitates a high-quality and reliable power source.
- As the power grid becomes more networked as a result of increased use of wide-area communications, the threat of physical and cyber-attacks on the grid becomes more complex.
- One of the most pressing issues of our time is environmental preservation and the promotion of long-term growth. It include making the power grid more energy efficient, lowering peak demand, and enhancing the grid's integration of renewable energy sources.

Although there is no a unique and formal definition of the smart grid, various features have been presented in the literature. The smart grid is a power grid that employs enhanced sensing, control, and communication mechanisms based on these characteristics. In comparison to the traditional electricity grid, the smart grid is projected to be more efficient, stable, and versatile [8,9]. The smart grid is envisioned as a more dependable, versatile, secure, accommodating, resilient, and helpful version of the electric power grid for users.

Generally speaking, the smart grid vision includes [10]:

1. Optimal electricity delivery operations in the power grid.
2. At all levels of the grid, there is an integrated use of information technology, including two-way communications. In a paper from the US Department of Energy, the statement "using megabytes of data to transport megawatts of energy" captures the heart of this need.
3. Facilitating large-scale integration of renewable energy sources.

The Electric Power Research Institute (EPRI) in the United States has identified seven key features of a smart grid [11] :

1. Self-Healing in Nature

   Because of widespread real-time monitoring, the smart grid's self-healing capabilities means that the grid is more aware of its functioning state. In addition, the self-healing grid can isolate faulty portions from the rest of the system, allowing it to island. The smart grid's self-healing function will improve consumer service dependability while also assisting utility administrators in better managing the power infrastructure.
2. Resilient to Threats

   Disturbances, attacks, both physical and cyber threats, and natural calamities will not disrupt the smart grid.
3. Involve Active Consumer Participation

   In contrast to the traditional grid, the smart grid will involve customers in the decision-making process. By changing the way electricity is purchased and consumed, this active engagement will help balance supply and demand and assure reliability. These changes will occur as a result of consumer incentives that encourage a shift in usage patterns.
4. Provides High-Quality Power for the Digital Era

   The smart grid will deliver a very high-quality power supply that is fit for today's digital civilization. This will entail the employment of real-time sensing and control techniques, which will allow for quick diagnosis and resolution of power quality-related events such as switching surges, line faults, and harmonic sources.
5. Embraces and encourages the use of renewable energy sources

   The smart grid will have a high penetration of a big number of environmentally beneficial renewable energy sources on the distribution side. The smart grid will not only accommodate these sources, but it will also encourage their incorporation into the system.
6. Interactive with Market

   The smart grid will improve the climate in which the electricity trading industry may flourish. Consumers will be able to pick between competing services under such a system. The smart grid is designed to give utilities, regulatory authorities, and customers the ability to create appropriate operating regulations based on the needs of a specific location.
7. Optimize the Assets

   The use of current monitoring and communication technology to optimise the usage of the grid's assets is an important aspect of the smart grid goal. The smart grid will place a greater emphasis on asset condition-based maintenance rather than time-based maintenance.

In Europe, the smart grid is described by the European Commission report as [12]:

1. It's adaptable because it meets customers' expectations despite a variety of changes and problems.

2. Accessible in terms of integrating various distributed energy sources, particularly renewables, into the grid.
3. In the presence of disruptions and uncertainties, reliable in terms of security and power quality demands of the digital economy.
4. It is cost-effective because it maximises value through innovation, energy-saving techniques, and government regulation.

As previously indicated, the smart grid will emerge from the conventional grid if several key elements are included in the grid. Implementing these characteristics necessitates the usage of several technologies. The National Energy Technology Laboratory (NETL) has categorised the technology needs for a smart grid into five categories. The groups that have been identified are: integrated communications, sensing and measurement, advanced components and control techniques, improved interfaces and decision support. Integrated communications are required for the execution of functions such as advanced meter reading. A basic prerequisite for making the grid more aware of its operational conditions is advanced and pervasive sensing and monitoring. Sensing and measuring equipment should provide information such as power factor, power quality, phasor relationships, temperature, outages, power consumption patterns, and so on. Given the expansion of the electrical grid, these sensors must be low-cost and modest in size, with simple maintenance and security guaranteed. Power electronics such as inverters for solar PV, superconducting cables, and electric cars are examples of advanced components. Real-time measurements sent across a dedicated and secure medium are required for advanced control approaches. The control centre will evaluate data, identify problems, and take autonomous action based on the information gathered.

The following is a quick explanation of major technologies that are predicted to play a vital role in the creation of a smart grid.

2.1.1 Distributed Generation and Storage

One of the most significant technologies for the implementation of a smart grid is distributed generation. It is based on the extensive use of distributed energy resources, particularly environment-friendly renewables, to enhance electricity quality and reliability. Distributed generation is mostly utilised as backup power in traditional grids and is not incorporated into the grid. However, with a smart grid, these renewable and green energy sources would be smoothly incorporated into the system. This arrangement will eliminate the need for costly peaking infrastructure and can considerably lower the likelihood of blackouts, in addition to lessening the environmental effect of traditional sources. The primary idea behind distributed generation is that energy is created and delivered through smaller producing systems that are closer to the end users. The introduction of environment-friendly renewable energy sources such as wind turbines, solar photovoltaic cells, geothermal energy, and micro-hydropower plants has speed up the adoption of these technologies. The smart grid concept emphasises the integration of this kind of distributed energy sources. Distributed generation has

a number of advantages over traditional power systems, including lower costs for electricity transmission and distribution across long distances. Technology has progressed to the point that distributed generating units ranging in size from a few kW to hundreds of MW may now be incorporated into the power grid. Integration of dispersed power not only lowers operating costs, but it also has certain advantages for grid designers. Widely integrated DGs can help to minimise peak demand, making them a viable solution to the problem of high peak load shortages. It can also help to increase grid reliability. Furthermore, distributed generation, particularly in developing nations, provides an efficient means of supplying power to remote and inaccessible places. Because the generating systems employed are typically small capacity, they need shorter gestation periods, allowing for faster and easier capacity expansion as needed. Power electronics advancements have assured that these sources can be easily connected into the grid without causing serious concerns with power, voltage, or frequency maintenance. Distributed energy resources, particularly renewable energy sources, are critical to attaining the smart grid's intended qualities. Their capacity to generate electricity at the consumer site aids in the reduction of peak loads and, as a result, better grid system management, not only in terms of operation and control, but also in terms of better and more cost-effective planning. Consumers may now export excess power back to the grid thanks to the implementation of net metering for grid-connected generating sources. As a result, system planners are often exempt from having to invest in new high-voltage transmission lines to transport renewable energy from conventional facilities to distant towns and cities. Reduced power loss in long-distance transmission and improved voltage profile of customers at the tail end of the distribution system are additional advantages of locally based solar, wind, biomass generators, fuel cells, and other distributed generating systems. The islanding function of a smart grid can also be done via a network of distributed energy sources integrated with the grid. It will be possible to isolate a specific location from the grid during a disruption in island mode. This capability is intended to play a key part in the grid's self-healing capabilities. When the islanded area has restored to normal operation, it can automatically synchronise with the grid in a smooth manner. There are currently a few barriers to large-scale grid integration of renewable energy sources. The fundamental reason for these worries is that these energy sources are intermittent in nature, posing a threat to grid dynamics. What are the implications of distributed renewable energy sources on power quality issues such as harmonics, frequency, and voltage fluctuation, power fluctuation owing to a sudden change in weather or seasonal variations in weather, and so on [13].

Distributed storage systems (DSS) are utilised to ensure the optimal interaction between the grid and distributed generators at both the MV/LV levels. Indeed, they can reduce the variable effect of renewable energy sources, allowing DGs to avoid common issues such power flow inversions and undesirable variation of electrical power quantities due to load and generation mismatch [14]. DSS also encourages prosumers to share energy at various scales (households, virtual power plants, microgrids, and so on), allowing these smart users to better control energy and save costs [15,16]. A dependable measurement and communication infrastructure is required to support these solutions, which allows for grid monitoring and management while assuring its safe operation [17,18]. The usage of DSSs prevents DG systems from being disconnected during emergencies, allowing them to participate in frequency and voltage regulation. Only a constant contact

between DSO and prosumer, as proposed by recent standards such as the Italian CEI 0-21 [19], can achieve this. A critical part of this paradigm is the policies of DSOs and prosumers, with the goal of maximising economic gains while protecting grid safety. From the perspective of the prosumer, the goal is to maximise the amount of energy available based on their load profile and sell it when the price is high. DSOs, on the other hand, want to be able to control the charging and discharging times of DSSs in order to maintain system stability and network performance. To support these goals, the authors suggested in [20] an optimization algorithm for DSS management, in which the DSO interacted with a smart prosumer's energy management system (EMS) by adjusting energy selling and purchasing prices. Based on this, the EMS uses an optimization algorithm to schedule the daily power exchange in order to discover the most cost-effective solution for the prosumer. In addition to the energy costs, the algorithm takes into account daily energy output from distributed generators, load energy consumption, and data from a battery numerical model.

2.1.2 Real-time Monitoring and Control

The traditional power grid features centralised generating and radial one-way electricity and information distribution. Due to a lack of real-time monitoring, the power network is underutilised in order to avoid overloading. The ability to monitor the smart grid in real time is a critical requirement. The existing power network can be better utilised, resulting in higher efficiency, if a significant number of real-time monitoring sensors are deployed in the power grid. Consumer participation in traditional grid operations is modest, however with smart grid, the consumer is expected to be an active participant in grid operations. It will necessitate the establishment of a secure two-way exchange of data obtained from real-time sensors located in both the distribution system and the consumer's home. By better collecting meaningful information about a failure, the grid's performance can be improved by deploying a large number of sensors throughout it. It will also be useful in post-mortem analysis for generating a timeline of events and identifying remedial measures to avoid the failure from happening again. A greater penetration of sensors in the grid will also allow for more effective early detection of faults. These sensors are also required for new grid functions such as demand-side management to be implemented. Sensor application areas in the smart grid at all three levels: end-user, distribution, and transmission. The fast sampling data provided from these sensors will allow for quick diagnosis and correction of grid faults. The setup will also allow for a real-time display of component status and system performance over a large region. It will assist system operators in taking action well before a bigger area is affected. The data collected by these sensors will also aid in the smooth integration of intermittent nature of renewable energy sources.

2.1.3 Distributed Intelligence

Unlike traditional grids, which have a radial nature, the smart grid will have a two-way, networked flow of electricity and information. The implementation of such a structure, as well as its efficient management, necessitates a great deal of decentralisation and intelligence and control penetration on all sides of the grid. This configuration will aid in the real-time monitoring of grid component operational conditions, as well as dynamically balancing loads and resources to maximise energy efficiency and security. Appliances such as smart meters, as well as technologies such as the global positioning system and mobile computing devices, will be used to develop distributed intelligence.

2.1.4 Demand-Side Management

Demand-side management (DSM) entails the utility conceiving and conducting a variety of actions that result in a desired change in the load curve shape. The DSM activities mostly influence customer behaviour in terms of electricity usage in the consumer's home. DSM actions are expected to be cost-efficient and effective on the client side. The DSM activities include both planning and operational level strategies. DSM encompasses anything from replacing old incandescent light bulbs with energy-efficient LED lighting to adding complex metering infrastructure with load balancing capabilities. The growing consumption of power supplied mostly from fossil fuels has been a primary motivation for the notion of DSM. Energy efficiency techniques must be promoted in order to secure long-term growth. DSM approaches can be classified into the following categories based on the sphere of influence of the initiative on the consumer side:

- Energy conservation.
- The duration of use.
- Reaction to a demand.

Peak clipping is an example of DSM technology in action. It aims to lower peak load so that the requirement for expensive infrastructure for peak load can be reduced. Distributed generation and user participation can help reduce peak load and duration by providing appropriate incentives.

2.1.5 Demand Response

Demand response (DR) is another crucial technology for achieving the smart grid. The traditional method of running the electrical system has been to constantly balance supply and demand. The problems connected with large-scale electricity storage are a major issue in grid operation. The demand on the electricity network varies throughout the day, with a brief peak phase lasting a few hours. Reduce the gap between peak and base load to make the most of the electricity network is a major concern for grid operators and planners.

In other words, flattening the load curve is a crucial goal for smart grid adoption. The DR programmes are focused at lowering the load curve's peak and deferring the construction of new power plants to meet peak loads that last only a few hours. The value of DR is seen in the flexibility it provides at a minimal cost.

2.2 ACTUAL MID-TRANSITION PHASE

The transition towards smarter cities and communities requires a deep transformation of distribution electricity networks, at both LV and MV level, where a large quantity of energy users, producers and prosumers are connected. In the smart cities framework, modern distribution grids must be able to cope with new paradigms for energy production, distribution and use, providing the technical back-bone for smart energy applications[21,22]. In fact, the widespread diffusion of DG from renewable energy sources, lead power grids facing new bidirectional energy flows and random variations in the electrical quantities, due the intrinsically intermittent and unpredictable production profiles [23]. For real-time balancing energy supply and demand, a fundamental role can be played by distributed storage systems (DSS), by a proper control of charging and discharging periods and power exchange with the grid [21]. Also electrical vehicles (EV) can act as support for electricity storage and load shaping, by means of their optimal management in grid-to-vehicle (G2V) and vehicle-to-grid (V2G) paradigm[24,25]. In this framework, smart electricity users and prosumers are involved in new scenarios for energy metering and management. Energy demand is expected to become extremely flexible, under demand side management, demand response and dynamic energy price programs[16,26,27]. New smart strategies are expected to be implemented for aggregations of flexible energy resources and load demands, at different levels (homes, buildings, virtual power plants, micro-grids) [15,28,29]. In order to effectively enable the aforementioned scenarios, an increasing amount of measurement data and information must be acquired, transferred, processed, managed and stored. Thus, advanced information and communication technologies capabilities must be implemented to allow proper monitoring, management, automation and control features, ensuring safe and effective grid operation [30–33]. In this framework, advanced smart metering and distributed measurement infrastructures are key elements for a smarter power grid management, allowing new modalities of interaction among loads, DG and DSS (including those of EV) and the implementation of automatic meter reading (AMR), demand side management and other smart grid functionalities (real time power flows analysis, islanding detection, fault detection, power quality assessment and so on) [34,35]. A widespread diffusion of smart metering technologies is needed to acquire information on both electrical and non-electrical quantities (powers, voltages, currents, switches status, distributed generators power production, remote commands, security or safety warning signals, and so on). All these data must be exchanged among all different smart grid players: distribution system operators (DSOs), users, prosumers, etc.; thus a pervasive communication network is needed, which must be reliable, cost-effective and easy to install, in both MV and LV distribution networks [36,37]. In the aforesaid scenario, AMR systems play a fundamental role for grids management and the implementation of new interaction strategies between DSOs

and users/prosumers. Currently, in many countries (such as in Italy), AMR systems are already implemented. For each LV user or prosumer, a smart meter provide the information on the energy exchanges. In each secondary substation, an AMR concentrator collects and stores measured data coming from the LV smart meters installed downstream the substation itself. The AMR server is installed in DSO control centre and it queries the AMR concentrators periodically (usually once a day), to process and store the collected data (mainly for billing purposes). Usually, the data connection at LV level, between AMR concentrators and smart meters, is obtained via power line communications (PLC), while AMR server and concentrators communicate by means of a wireless modem (typically GPRS) which are widespread available in urban contexts. Thus DSO copes with economical and infrastructural dependence from a wireless communication provider. Furthermore, such systems can have weak reliability (particularly in bad weather conditions) and they can also be exposed to cyber-attacks. To overcome the aforesaid problems, a possible alternative for AMR communication can be represented by the use of PLC at both MV and LV level. This solution has several advantages: it has low installation cost, as power lines are already present; the PLC channel is totally under DSO control, thus commercial and technical dependence from communication providers can be avoided; PLC is also more secure from cyber-attacks, as the communication system is not easily accessible from an intruder. Moreover, PLC can be a suitable solution for last-mile applications or for reaching smart meters in peripheral urban or rural contexts, where other communication links can be not available [38,39]. As mentioned before, PLC is already used in distribution networks at LV level for AMR and it has been also proposed for DG applications [30,40]. On the other hand, PLC use at MV level has been investigated in the last years [41,42]. Some authors have verified that PLC signals cross power transformer, even if attenuation are expected in dependence of the selected frequency and modulation technique [43,44], especially in the CENELEC band. Further attenuations due to line length and derivations can reduce the signal amplitude below noise level, thus preventing its correct reception. Thus commercial couplers are usually suggested in substitution or in combination with PLC signal crossing techniques, to increase signal level in points of MV network where higher attenuations are expected. On the other hand, the use of MV commercial couplers generally entails high costs for both equipment and installation, including those of service interruption.

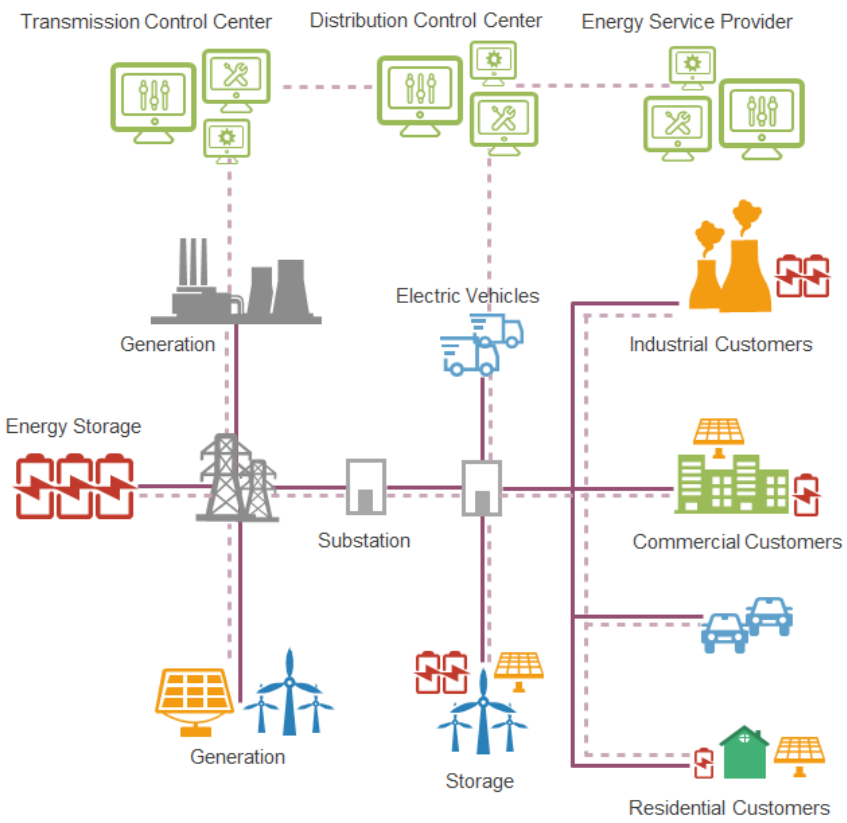

Fig. 2. New Distribution Network topology for Smart Grids

The measurement about energy, power quality and efficiency plays a fundamental role in the implementation of a smart grid [45,46]. In fact, a part of the smart grid vision entails enabling informed participation by customers, making them an integral part of the electric power system. With bi-directional flows of energy and coordination through communication, a smart grid should help balance supply and demand and enhance reliability by modifying the manner in which customers purchase and use electricity. These modifications can be the result of consumer choices that motivate shifting patterns of behaviour and consumption (Demand-Side Integration, DSI). These choices involve new technologies, new information regarding electricity use, and new pricing and incentive programs. From Distribution System Operator (DSO) viewpoint, the smart grid adds consumer demand as another manageable resource, joining to power generation, grid capacity, and energy storage. From consumers viewpoint, energy management in a smart grid environment involves making economic choices based on the variable cost of electricity, the ability to shift load, and the ability to store or sell energy. The new distribution network topology is depicted in Fig. 2, with dashed line representing data links and full lines representing power lines.

As the grid becomes more intelligent, it will be able to automatically self-monitor and assess its reliability and adapt to changing conditions. In such a grid, transmission/distribution networks and users loads can deteriorate the power quality or they can be affected by power quality disturbances. To deal with such issues, the smart grid shall adopt technologies such as advanced power quality meters, wide-area power quality

measurements, power quality enhancement devices for system components and sensitive loads, mechanisms that can provide fast diagnosis and correction of power quality disturbances in the grid, in accordance with the relevant standards in the field. Thus, to really enable the smart grid paradigm, an increasing amount of measurement data and information must be acquired, transferred, processed, managed and stored.

Advanced ICT capabilities must be implemented to allow proper monitoring, management, automation and control features, ensuring safe and effective grid operation. In this framework, advanced smart metering and distributed measurement infrastructures are key elements for smart grid management, allowing new modalities of interaction among loads, distributed generation and storage, as well as other smart grid functionalities (real time power flows analysis, islanding detection, fault detection, power quality assessment and so on). A widespread diffusion of smart metering technologies is needed to acquire information on both electrical and non-electrical quantities (powers, voltages, currents, switches status, distributed generators power production, remote commands, security or safety warning signals, and so on). All these data must be exchanged among all different smart grid players: distribution system operators (DSOs), users, prosumers, etc.

The key to allow the aforesaid capabilities is the Advanced Metering Infrastructure (AMI), which include smart meters and associated communication network. The AMI technology can enable the communication of real-time pricing data, grid conditions, and consumption information. When smart meters are coupled with other enabling technologies, such data management systems, information can be gathered and monitored by both the service provider and consumer. Such data can enable demand response, dynamic pricing and load management programs. In a more general framework, advanced Smart Metering (SM) capabilities can allow to measure, collect, analyse, and manage energy use (from generation to consumption), by using advanced ICT. The concept includes two-way communication networks between smart meters and various actors in the energy supply system, providing real-time or near-real-time information exchange and advanced control capabilities.

Automatic Meter Reading (AMR) programs were firstly developed, to transmit data on energy consumption from meters to DSO, using low-speed one-way communications networks. Since 2000, AMR, has given way to more advanced two-way communications supporting applications such as varying tariffs, demand-side bidding and remote connect/disconnect. The Smart Grid vision represents a logical extension of these capabilities to encompass two-way broadband communications supporting a wide range of Smart Grid applications including distribution automation and control as well as power quality monitoring.

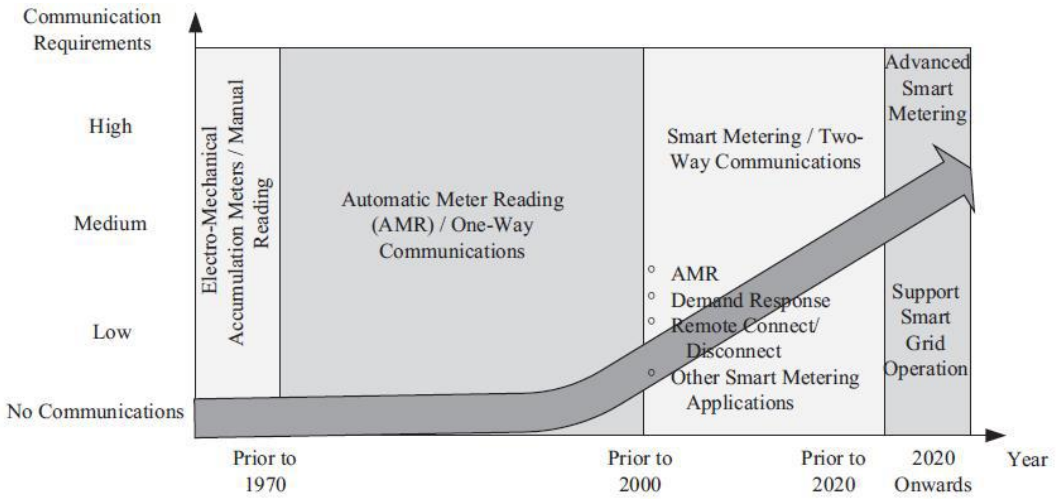

Fig. 3. Evolution of electrical metering, from simple electro-mechanical metering to advanced smart metering [46].

Modern smart meters have two-way communications to a Gateway and/or a Home Area Network (HAN) controller. The Gateway provides the bridge between the Smart Meters, the Meter Data Management system and other network actors, allowing the transfer of smart meter data to energy suppliers, Distribution Network Operators (DNOs) and other energy service companies (Fig. 4).

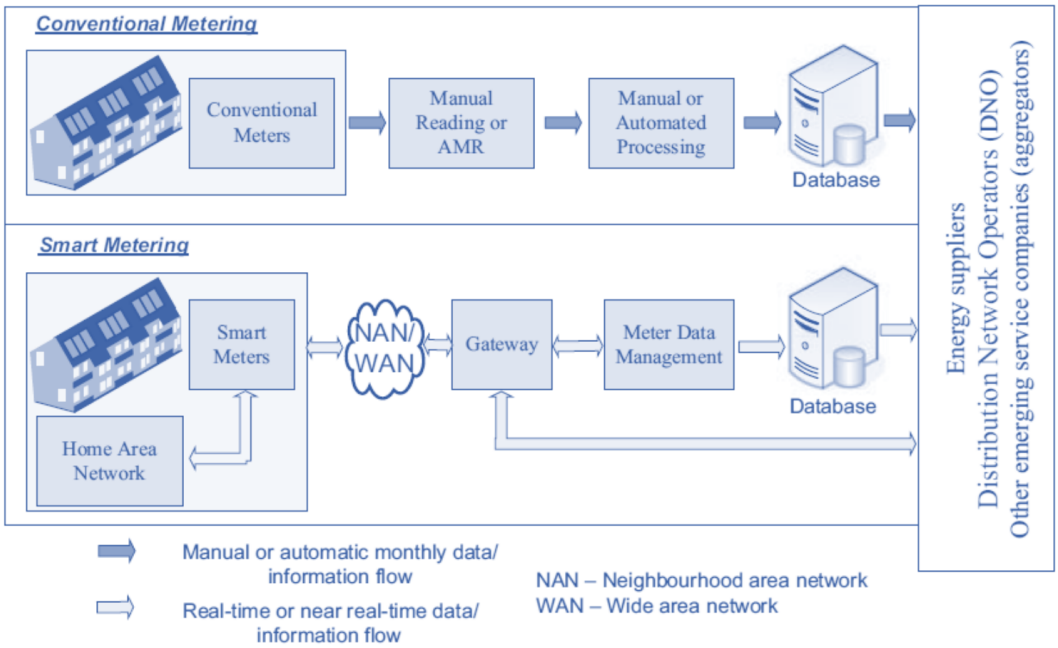

Fig. 4. Comparison between conventional and smart metering [46].

The evolution of electric metering generates transversal advantages both in short and long term horizon. In short-term, energy suppliers and DSOs can lowering metering costs and obtain more frequent and accurate reading from the controlled network. They can limit commercial losses due to easier detection of fraud and theft as well. From the customers' point of view, an increasing reading accuracy and frequency brings to a

more frequent and accurate billing, and to energy savings as a result of improved information and data correlation. Long term horizon, the DSO can reduce peak demand via DSI programs and so reducing cost of purchasing wholesale electricity at peak time. It can better planning generation and storage integration and network maintenance (Fig. 5).

	Energy suppliers and network operator benefits	All benefit	Customer benefits
Short-term	Lower metering costs and more frequent and accurate readings	Better customer service Variable pricing schemes	Energy savings as a result of improved information
	Limiting commercial losses due to easier detection of fraud and theft	Facilitating integration of DG and flexible loads	More frequent and accurate billing
Longer-term	Reducing peak demand via DSI programs and so reducing cost of purchasing wholesale electricity at peak time	More reliable energy supply and reduced customer complaints	Simplification of payments for DG output
	Better planning of generation, network and maintenance	Using ICT infrastructure to remotely control DG, reward consumers and lower costs for utility	Additional payments for wider system benefits
	Supporting real-time system operation down to distribution levels	Facilitating adoption of electric vehicles and heat pumps, while minimising increase in peak demand	Facilitating adoption of home area automation for more comfortable life while minimising energy cost
	Capability to sell other services (e.g. broadband and video communications)		

Fig. 5. Advanced metering benefits [46]

In fact a solid measurement infrastructure is the key for the implementation of a "digital twin" of the whole electricity network that need to be feed with precise and accurate measurements of electrical and non-electrical quantities. Such a digital twin can be used by the DSO for simulation purpose, for real time control and prediction or for predictive maintenance purposes.

2.3 From Automatic Meter Reading to Advanced Metering Infrastructure

The AMR system is used for remote reading and management of utility meters. AMR allows automatically collecting consumption, diagnostic, and status data from metering devices and transferring that data to a central database for billing, troubleshooting, and analysing.

This technology allowed DSOs to save expenses for manual meters reading and to obtain more information and field data. Thanks to daily, hourly or even shorter time meters readings availability, billing can be based on near real-time consumption rather than on estimates based on past or predicted consumption. This timely information coupled with analysis can help both utility and customers better control the use and production of energy. A typical AMR system has a structure as shown in the Fig. 6. Almost any AMR system consists of four primary components: Reading units, Communication system, Data receiving and processing unit and Billing system.

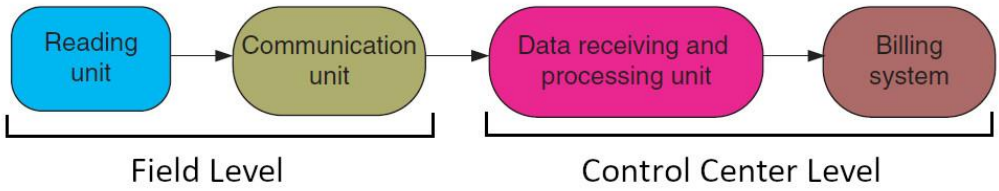

Fig. 6. Typical AMR system structure [45]

The reading units provide measurement data, in digital format (based on A/D conversion). Measurement data are available in the micro-controller for transmission. Metrological issues related to reading units concern measurement transducers and hardware devices technical features and implemented metrics.

The communication system must provide for efficient and successful data transmission, without any information loss. Many communication architectures and network structures can be used:

1. Cable ad-hoc network, in which the utilities set up their own cable network (for example optic-fiber);
2. Cable indirect network, which uses the power line or other communication network (for example telephone) to transfer the data they need. The solution using PLC (power line communication) has a wide range of applications and it is very common within the AMR network and it is more economic as DSO already owns the lines.
3. Wireless ad hoc network (for ex. RF, radio frequency), which, like the cable fixed ad-hoc network, requires the utilities to construct a new AMR communication network using wireless communication technologies and devices.
4. Wireless indirect network (for example GPRS, Wi-Fi), in which the utilities can use existing wireless communication networks to implement larger and wider AMR system. This approach needs to pay data communication fee to the wireless service providers.

Originally AMR devices just collected meter readings for billing purposes (one-way communication, occasional transmission of recorded energy, for example once a month). With the introduction of smart meters and two-ways communication network, metering devices can be controlled remotely and more data (i.e. events

alarms, tamper, reverse flow, interval data etc.) can be available to collect or control time-of-use or rate-of-use data for energy usage profiling, time-of-use billing, demand forecasting, demand response, remote shutoff, etc. Advanced metering infrastructure (AMI) represents the networking technology of smart metering, that goes beyond AMR into remote utility, distributed generation and storage management. AMI extends AMR technology by providing two way meter communications, allowing commands to be sent toward end users, producers and prosumers, for multiple purposes, including time-of-use pricing information, demand-response actions, or remote service disconnects. AMIs are systems that measure, collect, and analyse energy usage, and communicate with metering devices, either on request or on a schedule. These systems include hardware, software, communications, consumer energy displays and controllers, customer associated systems, meter data management (MDM) software, and supplier business systems. In Fig. 7 difference between AMR and AMI are showed.

Index to compare	AMR	AMI
Functionalities	Aggregated kWh usage reading by drive-by and walk-by systems, phone-based dial-up systems, handheld reading entry devices and touch-based systems etc.	Real-time metering; real-time, on-demand interrogations with metering endpoints; transmit pricing and energy information from the utility company to the consumer; demand response/load management as well as distribution automation.
Supporting infrastructure	One-way communication	Two-way communication
Available information	kWh reading and possibly peak kW demand for the month	Cumulative kWh usage, daily kWh usage, peak kW demand, last interval demand, load profile, voltage, voltage profile, logs of voltage sag and swell events, voltage event flags, phase information, outage counts, outage logs, tamper notification, power factor, and time-of-use kWh and peak kW readings, etc.
Benefited parties	Billing, metering	Billing, metering, customer service, asset management, dispatch, demand management, operation, and planning

Fig. 7. AMR and AMI differences [45]

Smart meters were originally deployed to obtain the operational benefit of AMR, but they rapidly became almost synonymous with the smart grid. It is now widely recognized that the smart grid encompasses a much broader set of technologies that will deliver a much wider range of benefits, including improved reliability, power quality, efficiency, balance of supply and demand, and integration of renewable generation. The

possibility of achieving those benefits will depend on the use of information technologies and the collection of data from smart meters and other sensors in the grid. This requires much more intensive data processing than just automated meter readings.

In a smart grid, following data must be provided to better serve for end customers:

- Broadcast data.
- Billing interval data.
- Detailed consumption data.
- Aggregate statistical data.

The requirement for **broadcast data** arise from the need to balance the grid. Data concerning grid status need to be communicated to market participants, including information such as on price changes, critical peak events, etc. Availability of these data allows consumers to make informed decisions, leading to better allocation and utilization of electricity. To make the market efficient, some form of price signals must be in effect (time of use, critical peak pricing, etc.) so **billing interval data** is needed. A utility needs to take reading at the beginning and end of a period during which a particular price is in effect, so that the utility can bill its customers properly. Moreover let the customers know their current rate of electricity consumption allow them to adjust it, so **detailed consumption data** is needed; they may also use automatic controls to set their preferences so as to avoid having to constantly take actions. Furthermore the customers can take advantage of **aggregated statistical data**. Energy service providers may show customers their consumption by flexible time periods, give them comparisons with neighbours or with historical time series, and other analytic results based on historic usage.

Smart meters in AMI context have the following primary features:

- recording of interval data on energy usage,
- delivery of data to the utility at least daily,
- disconnection switch, which can be remotely commanded,
- power quality sensing. A two-way communication is also enabled with both the utility and the smart appliances and smart equipment in customer homes and businesses.

These features empower consumers with time-based pricing options and detailed energy usage and cost. They also:

- allow smart loads management, at both grid and home level.
- enable utilities to manage better their line voltage and line losses.
- include measurements of surge voltages and harmonic distortion, allowing for diagnosis of power quality problems.
- enable built-in DSO ability to disconnect-reconnect certain loads remotely

- monitor and control the users devices and appliances to manage demands and loads within smart homes and smart-buildings.

Through the integration of multiple technologies (such as smart metering, home area networks, integrated communications, etc.), AMI provides an essential link between the grid, consumers and their loads, and generation and storage resources. The key role of AMI is related to the following aspects:

- Grid interaction with the consumer is enabled by AMI technologies that provide the fundamental link between the consumer and the grid.
- Distributed generation and storage at "prosumer" (producer/consumer) locations can be monitored and controlled through AMI technologies.
- Markets are enabled by connecting the "prosumer" to the grid through AMI and permitting them to actively participate, either as load that is directly responsive to price signals, or as part of load resources that can be bid into various types of markets.
- AMI smart meters equipped with Power Quality (PQ) monitoring capabilities enable more rapid detection, diagnosis and resolution of PQ problems.
- AMI enables a more distributed operating model that reduces the vulnerability of the grid to cyber attacks.

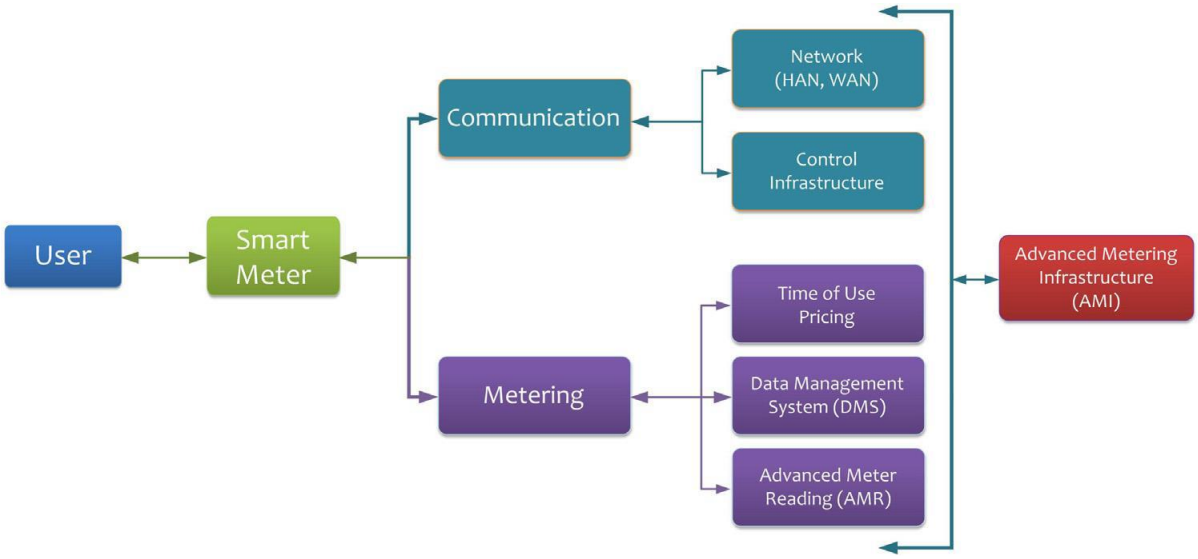

Fig. 8. Smart Meters and AMI main functionalities [36]

The AMI includes software, hardware, communication networks, customer-associated systems and meter data management (MDM) software. A typical AMI system (Fig. 8) consists of the following main components:

- **Smart meters** – The smart meter is the source of metrological data as well as other energy-related information.

- **Customer gateway** – The customer gateway acts as an interface between the AMI network and customer systems and appliances within the customer facilities, such as a home area network (HAN) or building management system (BMS).
- **Communications Network** – This network provides a path for information to flow from the meter to the AMI head-end.
- **AMI Head-end** – This system manages the information exchanges between external systems, such as the meters data management system (MDMS) and the AMI network.
- **MDMS** – Provides utilities with a central data repository between the AMI system and the enterprise application systems to take advantage of the AMI data and transforming into valuable information that can be used by the entire organization to make quality business decisions.

2.4 PROPOSED ARCHITECTURE

The new microgrids paradigm [47–50], in which energy consumers and prosumers (DGs, ESSs, loads, automobiles charging stations, and so on) are aggregated to smartly interact among themselves and with DSOs [19,42–44], accelerates the transformation mentioned in section 2.1. In such cases, DSOs must take deliberate steps to assure network stability and flexible energy exchanges, while maintaining an appropriate level of quality and dependability and preventing an uncontrolled power flow inversion[53–55]. Such issues are more serious in insulated grids, such as those found on Small Islands, which are more susceptible to variations in load and/or generation power. Continuous power flow monitoring, combined with DG and ESS remote control (either directly by the DSO or via information exchanges between the DSO and microgrid aggregators), is critical for reliable network management in such grids [56–58].

In general, a microgrid is a collection of loads, DGs, and ESSs, often at lower voltage levels, that can behave as a single load/generator from the main grid's perspective in both grid-connected and islanded modes. This microgrid vision is seen as the best option for utilising distributed renewable energy sources, particularly at the distribution level. Furthermore, many improved solutions for both generator and load flexible management are proposed at the microgrid level (demand response, demand side management, dynamic energy price, grid-to-vehicle/vehicle-to-grid, virtual power plants, optimal power flow, and so on). In this way, smart distribution networks can be thought of as a collection of more or less self-contained subsystems (i.e., microgrids) that can intelligently communicate with one another and with DSOs [59–63]. However, for true microgrid integration, the impact of RES fluctuation and unpredictability, as well as smart load management, network stability, power supply quality levels, and power flow inversions, must be carefully considered [64]. This is especially true for networks that are not connected to the continental grid, such as those of small islands (or even for rural areas, whose power systems are weakly connected with main grid). The ability of DSOs to communicate with dispatchable resources (DGs, ESSs, and loads) is critical in islanded settings. As shown in

Fig. 9, the microgrid architectural integration for islanded scenarios can be schematized. Microgrids subsystems are at the LV level, downstream secondary MV/LV substations (microgrid aggregators). A set of loads (domestic and/or industrial), DGs, ESSs, vehicle charging stations, and other components may be included in each microgrid subsystem. The aggregated loads/generators are treated as a single controlled load/generator by the DSO. The DSO can manage power flows between the distribution grid and microgrids subsystems at the substation level, allowing intelligent functions like optimal microgrids subsystems operation and management, islanding detection, and DGs/ESSs remote control to be implemented. Users and prosumers can profit from "smart" interactions among themselves at the microgrid subsystem level, allowing full utilisation of distributed RESs [59,60].

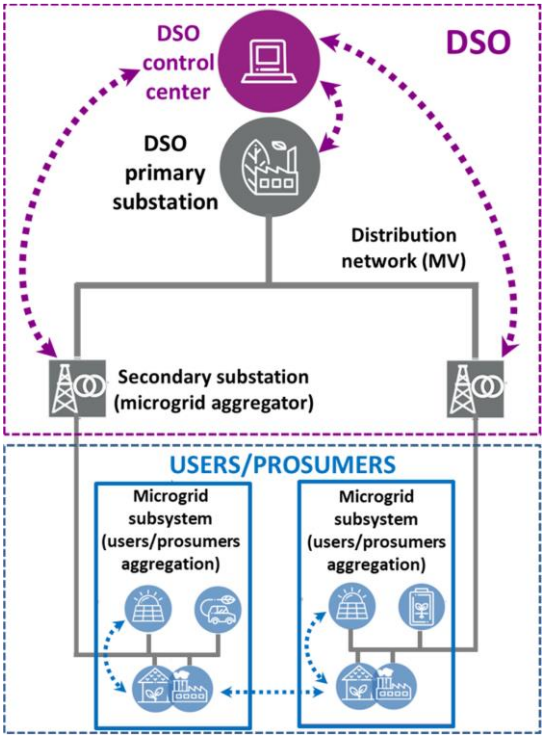

Fig. 9. Microgrids Integration in the distributed network

In this context, the microgrid has primarily been designed to benefit consumers, and various studies in the literature[48,50,65], discuss the perspectives of users/prosumers and the benefits they can derive from microgrid deployment (reliability, resilience, economic benefits, and so on). Such objectives, however, may conflict with DSOs' requirements for network management and stability. On the other hand, the DSO's perspective has not been adequately examined, despite the fact that their position is critical, particularly in islanded scenarios[56–58]. In such cases, DSOs must interact with loads, DGs, and ESSs, allowing for a hierarchical management of users' and prosumers' requests [60], all while adhering to technical restrictions for safe power system operation and stability via real-time Power Flow Monitoring and Control (PFMC) of MV networks [51,66]. Microgrid subsystems can work with the DSO to maintain voltage and frequency regulation

and power quality levels if they are appropriately managed [62,63,67]. Thus, improved information and communication technologies (ICT) are required to allow controllability and observability of the entire grid by a real-time PFMC in order to allow such microgrids incorporation in distribution networks [49]. In this aspect, DSOs currently have partial monitoring and control capabilities of the network and users/prosumers connected to it in today's distribution networks. While distributed monitoring and communication systems for LV networks are currently available, full solutions for a real-time PFMC of MV networks have yet to be developed.
.

General requirements for a real-time PFMC partially match with the general requirements for the smart grid paradigm implementation presented in 2.1 and are: distributed measurement and control systems and devices, a reliable communication infrastructure, and a supervisory centre.

In the literature, various solutions for distributed measurement systems have been offered, most of which are based on the utilisation of a small number of MV measurement points and the development of state estimation and forecasting algorithms [55,68–70]. The algorithmic complexity and MV measurements equipment costs, which include the expenses of MV transducers and measurement instruments (usually expensive phasor measurement units, PMUs) as well as related installation costs, are the main downsides of these solutions. Cataliotti et al. [31] developed a new measuring approach for Load Flow (LF) analysis in the MV smart grid that uses load powers measurements at the LV level. The measures are done at the LV side of the substation MV/LV power transformer, and the equivalent MV loads are used to model the power MV/LV transformers and associated LV loads. The losses of transformers are evaluated starting from the rated data of short circuit and no-load tests. This allows us to achieve a significant cost reduction in the installation; in fact, the installation is simpler and faster because no MV switchboard integration or MV transducers are required; LV current transducers are less expensive than MV ones; and a smaller number of customers would experience energy interruption for their installation (i.e., only those supplied by the secondary substation), resulting in a lower related income loss for the DSO. Even when using a smaller number of measurement points, the method's uncertainty analysis revealed good accuracy in power flow calculation [71]. A control system is necessary in addition to a reliable monitoring method to remotely operate DGs and ESSs, either directly or through microgrid aggregators, to prevent or mitigate over/under voltages or frequency changes. .

DSOs are now deploying communication, control, and measurement infrastructures for AMR and MV network protection and supply restoration in several countries' MV networks. The AMR server is housed in the DSO control centre and communicates with the AMR concentrators of each secondary substation through GSM or GPRS. These lasts are connected to smart meters for both users and DGs via LV PLC. In most DSO control centres, a supervisory control system for MV network protection is also implemented; it may control MV motorised switches directly via GSM or GPRS for protection, fault isolation, or supply restoration purposes. In contrast, several control techniques and architectures for interaction with DGs and ESSs are published in the literature [72–74], but few experimental results on real-world implementation on MV networks are presented. Furthermore, traditional grid-connected DG interface protection systems (IPSs) serve

only as a safety net, disconnecting DGs from the network only when necessary (i.e., when voltage and/or frequency exceed specified thresholds) [19]. DSOs, on the other hand, are unable to regulate DGs and ESSs remotely, owing to a lack of a sufficient communication system with IPSs as well as the deployment of smart interaction methods between prosumers and DSOs or microgrid aggregators.

As regards communications, many solutions for supporting smart grid applications have been proposed in the literature, using various communication infrastructures, such as wireless, PLC, or hybrid solutions, which can also be integrated in an IoT platform [21,37,75–77]. In this regard, DSOs may be faced with heterogeneous communication networks, each with its own set of characteristics in terms of the resources provided by communication links. In such circumstances, depending on the smart grid application needs, the restricted resources provided by some existing communication channels may provide significant challenges in terms of practical implementation. Because of its inherent adaptability for remote control applications, various smart grid functionalities can benefit from the usage of Internet protocol (IP). This can open up new scenarios, but it may have an impact on the limited resources available through existing communication routes like PLC. On the other hand, for IP-based PLCs for last-mile applications with low bitrates, such as DG inverter remote control, such a solution may be practicable, allowing for a favourable trade-off between communication capabilities and costs [75,77]. Redundancy in protection and control, as well as robustness against cyberattacks, are other key considerations. In this regard, there are certain studies in the literature that propose PLC exploitation even at the MV level for applications with modest transmission data rate requirements (for example, when basic commands on network status signals must be provided, or when data must be gathered offline) [21]. In light of the foregoing factors, the development of real-time PFMC solutions with the technological capabilities previously outlined and cheap prices for hardware/software implementation and installation in real systems is still an open topic for efficient microgrid integration in MV networks. .

As already said above, in order to fully implement the microgrid paradigm the DSO must to be equipped with three fundamental components that can add smartness to the grid: a distributed measurement system, a suitable communication system and an enhanced control system based on the architecture that needs to be managed. So with respect to existing infrastructures, the following new elements are introduced:

1. A distributed measurement system for the load powers monitoring over the whole network, based on one PQA installed in each secondary substation.
2. A capillary communication system to connect the DSO control centre to all field PQAs and control devices.
3. A SCADA system, which allows monitoring power flows in each network branch and sending commands to DGs/ESSs for their remote control.

Three types of field devices are used in more detail: commercial PQAs for aggregating the active and reactive powers PL and QL absorbed by the LV loads supplied by the substation power transformer; IPSs for DGs/ESSs connection to the power grid; IED for user device interfaces; communication bridges (named IPS concentrators) between the secondary substations and DSO control centre. To test the feasibility of their

integration on the proposed architecture, PQAs were chosen for system implementation in the Ustica and Favignana networks. This decision was made because PQAs are frequently already placed in secondary substations of existing distribution networks, allowing DSOs to save money when installing a smart system for DGs and ESSs integration in the grid. PQAs, on the other hand, can be a viable and less expensive solution in grids where new equipment must be installed, when compared to other devices such as PMUs. We devised and constructed the IPSs and IPS concentrators, which have been described in prior publications [35,78]. The IPS concentrators and PQAs are installed in each distribution network secondary substation and are linked to the DSO control centre. Furthermore, each substation's IPS concentrator is linked to all IPSs connected to the microgrid, i.e. the LV network component provided by the secondary substation, via LV PLC. All of the protection functions required in [78] for DGs connection are performed by the IPSs. Additionally, they serve as communication hubs between the DSO and the DGs/ESSs. PQA's application on the LV side enables for LF analysis in the MV network utilising measurements of three phase load active and reactive powers taken at the LV level in each secondary substation of the network [79]. Voltage measurements at the MV level VMT at generating substation bus bars are also employed in addition to the LV measurements. The MV transducers and a basic voltmeter can be utilised in this situation; however, by putting a PQA at the feeder's beginning, active and reactive powers at MV bus bars can be measured, and the measured and calculated powers can be compared to validate the PFMC system's accurate operation.

3 MEASUREMENTS FOR SMART GRID

3.1 MEASUREMENTS INSTRUMENTS

Smart grids make use of modern sensing, communication, protection, and control technologies, among others. Generation, transmission, and distribution systems, as well as consumer appliances and equipment, are all covered by these technologies. Equipment is monitored, control techniques are supported, congestion and grid stability are evaluated, and energy theft is prevented using sensing and measurement technology. Measurement instrumentation includes:

- Smart meters;
- Intelligent electronic devices (IEDs);
    - Protection and/or control IEDs
    - Meter and/or recording IEDs
    - IEDs for distributed generation (interface devices, interface protection systems)
- For metering functions, main IEDs are:
    - Power quality analysers (PQAs)
    - Phasor Measurement Units (PMU).

Smart meters have two functions: providing data on energy usage to customers (end-users) to help control cost and consumption; sending data to the utility for load factor control, peak-load requirements, and the development of pricing strategies based on consumption information. A general functional block diagram of a static meter with ADC and fixed-function DSP is shown in Fig. 10. The calculation of the parameters of interest is done with a fixed-function DSP. It can be used in conjunction with ADCs. For the development of smart electricity meters, many integrated circuits and embedded systems for energy metering are available on the market (by Analog Devices, STMicroelectronics, etc.)

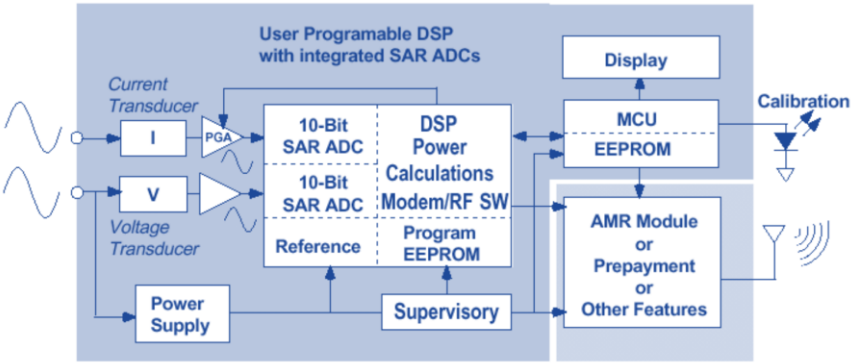

Fig. 10. Functional block diagram of a static meter

The term "intelligent electronic device" (IED) refers to a group of devices that perform protection, measurement, fault recording, and control functions [46]. An IED is made up of a signal processing unit, a microprocessor with input and output devices, and a communication interface. Microprocessor-based voltage regulators, protection relays, circuit breaker controllers, and other serially communicating devices are examples of IEDs. [80]. An IED block diagram is show in Fig. 11.

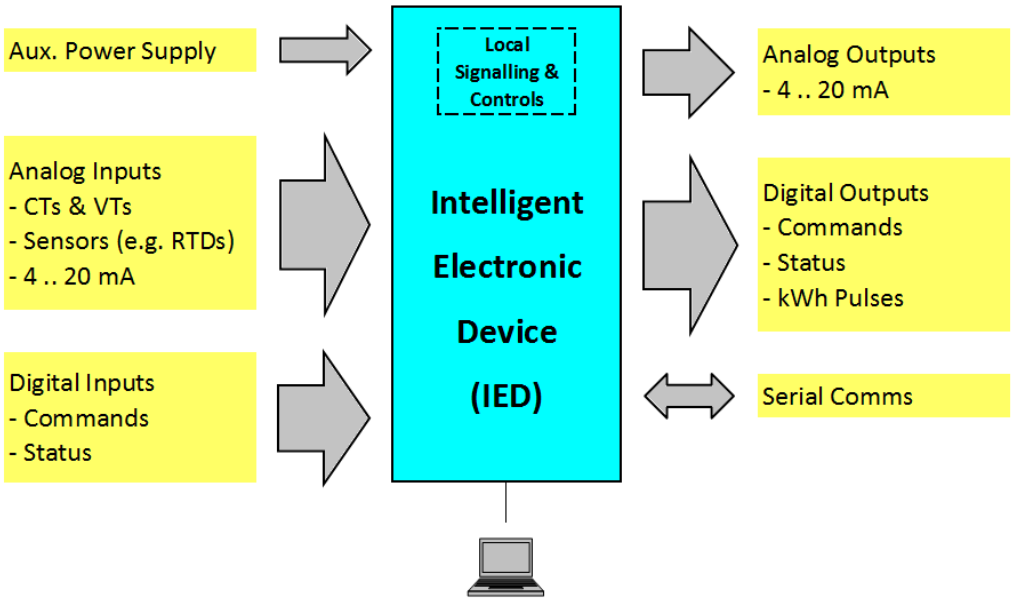

Fig. 11. Intelligent Electronic Device block diagram [80]

The extended functionality of an IED can be separated into the following groups: protection, control, monitoring, metering and communication.

- *Protection*: This functionality covers all protection functions to protect a generator, motor, transformer or feeder.
- *Control functions and logics*: These elements may be control loops in voltage regulators, control logics in circuit breakers, etc.
- *Monitoring*: Each IED should have internal self-supervision and aux. supply monitoring. A “watch-dog” or “healthy” output contact will close if the IED is operating well. Monitoring may also include loss of analogue sensing inputs (e.g. loss of voltage, current, temperature sensors), trip circuit supervision, event recording, etc.
- *Metering*: Most IEDs contain metering values including line voltages (V), phase currents (A) and voltages (V), neutral current (A), residual voltage (V), frequency (Hz), power (MW, MVAR, MVA) and energy (kWh, kVARh), harmonics, disturbance recording, temperatures and analogue channels. Some IEDs are also provided with programmable transducer outputs.

- *Communication*: IEDs could support protocols like Modbus RTU, Modbus TCP, Profibus, etc... In order to enable interoperation of IEDs from different vendors, IEC created the modern IEC 61850 standard.

An example about some IEDs functionalities at HV/MV and MV/LV substations are shown in Fig. 12 [81]

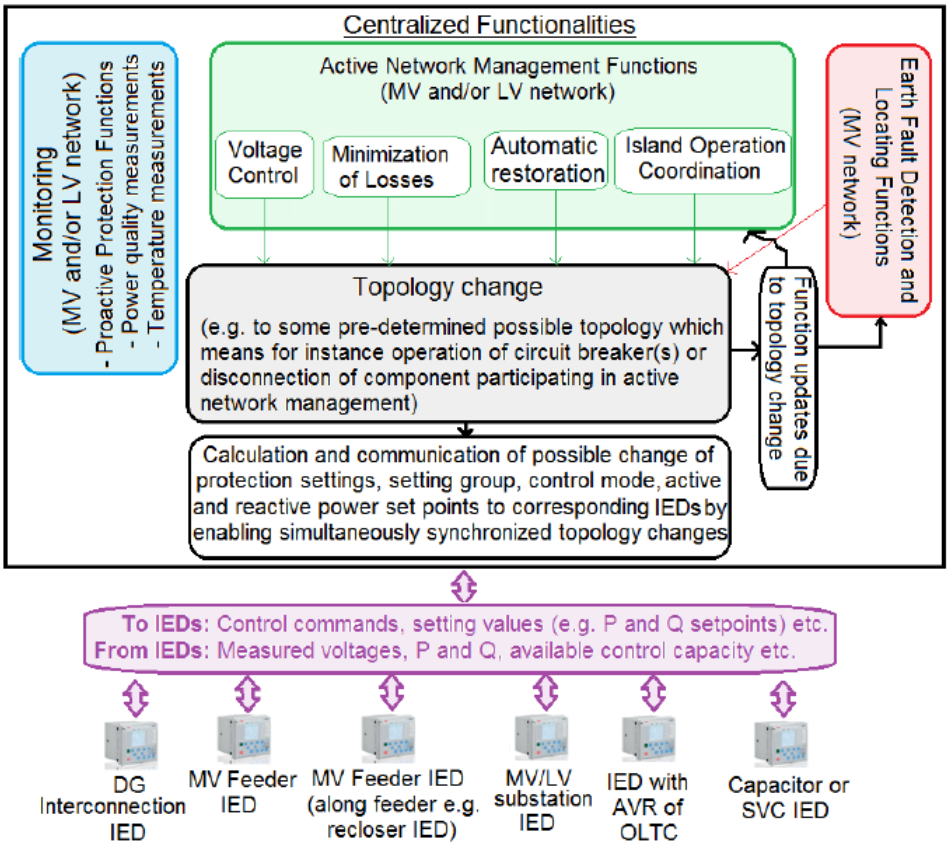

Fig. 12. IED functionalities in smart grid context [81]

IEDs and other grid devices need to communicate securely and, depending on the use case, more or less rapidly between different devices and systems.

Many solutions require extremely precise data time synchronisation. The performance of the time distribution service and the required time accuracy vary depending on the power application requirements; they can range from 100 milliseconds (for substation monitoring) to one millisecond (for IEEE C37.118.1-2011 standard based synchrophasor measurements and IEC 61850-9-2 standard based sampled measured values (SMV)). In smart grids, measurements reliability, precision, speed, and stability, in addition to time synchronisation, are key problems to ensure correct operation in all network disturbances and events, from fast transients to slow continuous changes. For example, frequency measurement and elements using frequency measurement, such

as rate-of-change-of-frequency (ROCOF) i.e. $^{df}/_{dt}$ or utility grid stability supporting functions like frequency dependent load shedding or active power control of DER units, are among the most important measurements in IEDs. In order to obtain the needed response, accurate, rapid, and reliable measurements and signal processing are also required for DG connectivity and MV feeder IED functions. At HV/MV (MV level management by DMS/SCADA or grid automation controller or IED) and MV/LV (LV level management by IED, RTU or MicroSCADA) substations, various active network management functionalities (such as voltage control, island operation coordination, loss minimization, and so on) can be realised through centralised solutions. From a comprehensive idea standpoint, intelligent coordination hierarchy between administration of MV and LV level active zones is also required. From an asset management standpoint, monitoring and earth-fault locating, as well as various event or measurement reporting features, are becoming increasingly crucial. For example, network capacity usage might be maximised without exceeding thermal constraints if real-time cable temperature monitoring was used.

Power Quality Analysers are used to continuously monitor and analyse electricity lines for disturbance which can disrupt the reliable delivery of energy or cause damage to equipment plugged into the grid. Measured power quality disturbances normally include voltage sags and swells, transients, harmonic distortion, and voltage/current imbalance. Multiple parameters are measured simultaneously and displayed in formats that quickly describe overall power quality health. Depending on the instrument and manufacturer, data can be accessed as simple digital values, trend graphs (for fast insight into changes over time), waveforms, or phasor diagrams. The data can also be analysed and organized into tabular formats. Detailed event data allows to see the magnitude, duration and time stamping of anomalies. Communication features can be embedded in order to enable information exchanges in networked connections. PQAs must fulfil relevant Standard requirements, i.e. IEC 61000-4-30, IEC 61000-4-7, and so on (and related European and National standards). Different PQAs are available on the market, both portable, bench or for switchgear installation (for example by Fluke, Janitza, etc.)

The problem of real-time grid monitoring for low-voltage distribution grids with distributed energy resources is addressed in [82,83], where proposed ICT architectures can integrate metering equipment at the user, prosumer, and distribution system operator levels to enable energy management and real-time grid monitoring. A metering and communication system for remote monitoring and control of distributed energy resources connected to low-voltage networks is presented in [40].

PQAs or PMUs can be put in different grid nodes (usually transmission and distribution substations) for grid monitoring and management, including for PQ assessment [84]. This enables the collection of data on the occurrence of PQ disruptions [85]. Several concerns about this type of equipment in this framework have been researched in the literature, including metering characteristics, measurement reliability, and data availability. In [86], for example, a technique to improve distributed PMU availability during wired network failures is proposed. PMU presents new solutions in [87,88], with the goal of achieving a good trade-off between low cost and sufficient accuracy criteria. The accuracy of signal processing techniques for PMU

measurements in the presence of disturbances in power system operating circumstances is investigated in [89]. Based on PMU data and the cloud-based IoT paradigm, [90] presents an upgraded method for distribution system status estimate. PQAs are used to analyse power flows at the distribution level in [71,91,92], with suitably distributed measurement systems and corresponding power flows estimation algorithms that can also deal with partial data availability proposed. PQ meters are incorporated into a heterogeneous communication infrastructure in [93] so that voltage dips in distribution networks may be analysed.

3.2 SMART METERS AND ENERGY RELATED INFORMATION

However, by incorporating PQ meters at the user level in the distributed measurement infrastructure, more complete information about PQ levels across the grid might be obtained. This may, for example, enable the introduction of billing policies based on both energy usage and supply quality. In this context, [94] describes the development of a low-cost microcontroller-based power quality meter that may be used at the user level for real-time monitoring of some PQ parameter. In [95] the development of a prototype electronic power meter that integrates the measurement of typical power quality parameters as well as additional power terms for load assessment is described. In [79] the authors propose a smart sensor network for non-intrusive load and power quality monitoring in residential and industrial settings. Harmonic distortion is a significant PQ disturbance, particularly in distribution grids, where the increasing presence of non-linear loads and power electronics in distributed generation and storage systems can significantly degrade the quality of supplied power, and several electronic appliances and loads (at the home, commercial, and industrial level) are extremely sensitive to supply quality, particularly in terms of harmonic distortion [96].

To enable diffuse PQ measurements, new technologies must be introduced that can deliver appropriate information on the quality of the power supply to both end-users and distribution system operators at reasonable costs. It should be noted that the installation of complex and expensive apparatus is not economically possible in the context of extensive distribution of PQ measurements at the user level. Low-cost devices, on the other hand, have been proposed for implementing PQ measuring duties; in this case, such additional instrumentation should be deployed alongside existing energy meters, or new integrated platforms should replace those presently in use in distribution networks. In [97], we looked into a different approach to the problem, namely, the feasibility of putting PQ measurements on existing smart metering platforms, thereby utilising existing installed instrumentation and hardware architectures by simply changing the firmware and implemented metrics. This permits the installation costs to be zeroed. Integration of PQ measures into existing smart meters could open up new market prospects for both energy traders and manufacturers; also, customers would be able to simply monitor the quality of supplied power without having to deal with multiple metering devices. PQ phenomena measurements and limits are covered by specific standards [98–101]. The main reference is the IEC 61000-4-30, which defines the methods for PQ parameter measurement and the related accuracy requirements; as regards, harmonics (and inter-harmonics) measurements, it refers to IEC 61000-4-

7. The instrument's compliance with such standards is crucial to enable their use for monitoring or even billing purposes. In more detail, IEC 61000-4-30 defines two classes of measurements, i.e., classes A and S (correspondent to classes I and II of IEC 61000-4-7, respectively). Class A instruments are meant to be used for contractual applications or compliance verification with allowed disturbances limits; class S instruments are allowed for statistical applications such as surveys or power quality assessment and they obviously entail processing requirements lower than those of class A.

3.2.1 Commercial Energy Meters Specifications and Standard Requirements. A case study.

The challenges associated to the integration of PQ measures on commercial systems for smart metering have been investigated, starting with the aforementioned standard requirements for PQ and harmonic measurements. In this context the energy meter based on STCOMET platform by STMicroelectronics [102], which is now being used in various countries for energy meter deployment, was used as a case study to verify the possibility to integrate in the meter the PQ measurement, as defined by IEC 61000-4-30.

The evaluation kit for the STCOMET platform, named EVLKSTCOMET10-1 [102], was used as a case study to demonstrate the feasibility of the PQ measurement capability of an electronic board currently used for remote energy metering. The EVLKSTCOMET10-1 is a single device that combines a Cortex™-M4 microcontroller, a metrology section, and a PLC transceiver. The STCOMET device may transmit and receive on the AC mains line utilising Narrow-Band PLC (NB-PLC) modulation, single or multi carrier Orthogonal Frequency-Division Multiplexing (OFDM) up to 500 kHz, allowing it to be used for AMR applications. The PLC modem architecture was created with EN50065, FCC (Federal Communications Commission), and ARIB (Association of Radio Industries and Businesses) in mind. It enables the STCOMET to support PRIME, G1, G3, IEEE 1901.2, and other narrow-band PLC protocol requirements when used in conjunction with the application core. Fig. 13 depicts the device's functional block diagram.

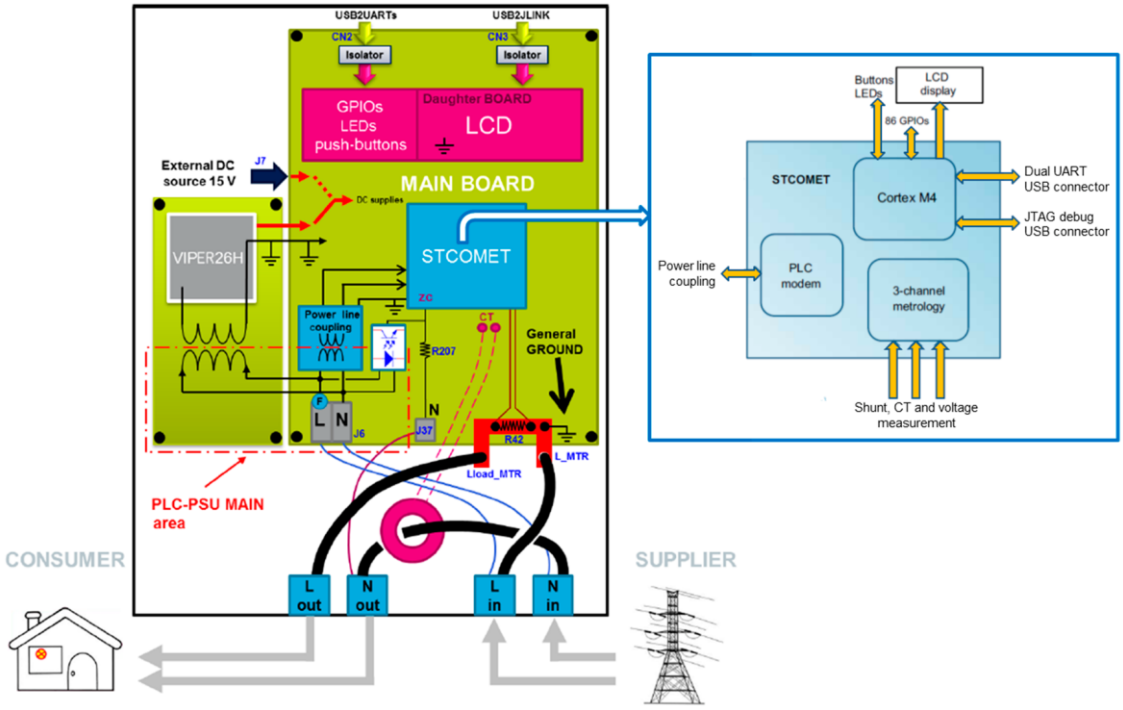

Fig. 13. EVLKSTCOMET10-1 functional block diagram

The metrology sub-system is suitable for EN 50470-1, EN 50470-3, IEC 62053-21, IEC 62053-22 and IEC 62053-23 compliant class 1, class 0.5 and class 0.2 AC metering applications. In more detail, the metrology sub-system mainly consists of two programmable gain low-noise low offset amplifiers (PGA) and three 24-bit ΣΔ ADCs. As regards the measurement transducers, a resistor divider is used as a voltage sensor (Fig. 14), while a shunt and a current transformer are available for current measurement (in the experimental tests the shunt was used).

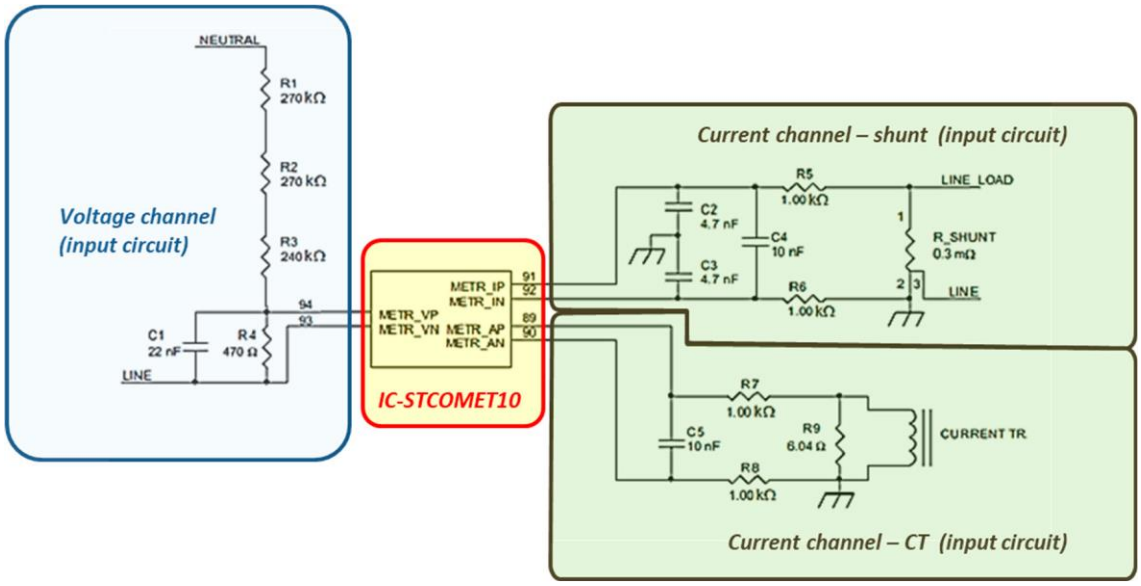

Fig. 14. EVLKSTCOMET10-1 metrology reference application schematic

Low-pass filters are included to prevent aliasing phenomena. The digital section consists of a hardwired DSP and DFE (Digital Front End) to the input modulators and an interconnection bus with the Cortex™-M4 core. Available memories are: 640 kB or 1 MB of embedded Flash; 128 kB of embedded SRAM (static RAM); 8 kB of embedded shared RAM. EVLKSTCOMET10-1 metrological main specifications are summarized in Table 1. In the original implementation, the metrology sub-system calculates instantaneous and RMS voltage and currents, total and fundamental active, reactive and apparent power and energy [97].

Parameter	Value
Nominal Input Voltage	230V
Nominal line Current	5 A
Nominal Input Frequency	50/60 Hz
Sampling Frequency	7.8125 kHz
Bandwith (-3 dB)	0-3,6 kHz
Voltage/Current RMS accuracy	0,5%
Active/Reactive power/energy accuracy Over 1:5000 dynamic range Over 1:10000 dynamic range	 0,1% 0,5%

Table 1. EVLKSTCOMET10-1 metrological main specifications

As mentioned before, IEC 61000-4-30 defines two classes of measurement, A and S [98]. For 50/60 Hz systems, the measurement time interval (t.i.) for supply voltage, harmonics, inter-harmonics, and unbalance is 10/12 cycles (i.e. 200 ms). The base t.i. values for the 10/12 cycles are aggregated over three additional intervals: 150/180 cycles, 10 minutes, and 2 hours (aggregation of twelve 10-min intervals). The t.i. for frequency reading is 10 seconds. Class S has less stringent processing and accuracy criteria than class A. Power frequency, voltage magnitude, flicker, voltage dips/swells and interruptions, unbalance, harmonics and inter-harmonics, mains signalling voltage on supply voltage (below 3 kHz), rapid voltage changes are all covered by the IEC 61000-4-30 standard, which includes detailed requirements for measurement methods, measurement uncertainties, and measuring ranges. Magnitude, imbalance, harmonics, and inter-harmonics are all taken into account while measuring current. The main requirements (measurement uncertainties and ranges) of IEC 61000-4-30 are summarized in Table 2. IEC 61000-4-30 relates to IEC 61000-4-7 and IEC 61000-4-15, respectively, for harmonics/inter-harmonics and flicker measurements. It should be noted that the effect of measurement transducers is not included in the accuracy parameters. In the commercial STCOMET platform, only some IEC 61000-4-30 PQ metrics requirements, are implemented. In the following, the implementation and experimental verification, respect to class S requirements, have been carried out, taking into account the metrological aspects of STCOMET and the IEC 61000-4-30 criteria.

Parameter	Class	Uncertainty	Measuring range
Frequency	A	± 10 mHz	42,5 ÷57,5 Hz 51 ÷ 60 Hz (for 50/60 Hz systems)
	S	± 50 mHz	
Voltage magnitude	A	± 0.1% U_{din}	10 ÷ 150 % U_{din}
	S	± 0.5% U_{din}	20 ÷ 120 % U_{din}
Dips/swells (amplitude and duration)	A	± 0.2% U_{din} ± 1 cycle	Not applicable
	S	± 1% U_{din} ± 1-2 cycles	
Interruptions (duration)	A	± 1 cycle	Not applicable
	S	± 1-2 cycles	
Current	A	± 1%	10 -150 % of full scale
	S	No requirements	

Table 2. IEC 61000-4-30 Requirements Summary (U_{din} is the declared supply voltage)

3.2.2 PQ Metrics implementation on STCOMET

The measurement of power system frequency voltage and current RMS, as well as voltage dips and swells, is already implemented by STCOMET. The comparison between the IEC 61000-4-30 requirements for class S instruments and the STCOMET on-board metrics is reported in Table 3.

Parameter	IEC 61000-4-30			STCOMET Metric Main Features	Correction Algorithms
	Measurement Range	Time Interval (t.i.)	Maximum Error		
Frequency Period	42,5 ÷57,5 Hz (for 50 Hz syst.)	10 s (not overlapping)	- Number of integer cycles during the 10-s t.i. divided by their cumulative duration - Harmonics and inter-harmonics are attenuated	- Measurement from zero-crossing (voltage channel, with a low pass filter). - Frequency range between 32.55 and 81.38 Hz - Resolution of 8 µs - Period is calculated as	- Single frequency value is obtained as period reciprocal (on-board metric) - Frequency measurement is calculated as the mean of the single frequency

				the mean of the last eight Measured periods	values over 10 s
RMS	20 ÷ 120% U_{din}	200 ms (10 cycles for 50 Hz)	- The r.m.s. value includes, by definition, harmonics, inter-harmonics, etc. - Every 10/12-cycle interval shall be contiguous and not overlapping - Not used for dips, swells, voltage interruptions, and transients	- RMS measurement is obtained from voltage / current samples - Voltage / current are not filtered - Integration time is 10 cycles - RMS value is updated every 128 µs	- No modifications of on-board metric - Measurement reading is updated every 10 cycles, in order to have not overlapping t.i.
Dips Swells Interruption	-	-	- The basic measurement shall be the RMS over a half cycle or full cycle ($U_{rms(1/2)}$ or $U_{rms(1)}$) - Measured data are maximum / residual voltage (i.e., the max./min. voltage value during the event) and duration (i.e., the difference between start and end times of the event) - For interruptions only duration is measured	- The fundamental component of voltage (RMS) is compared to a 10-bit threshold - An internal time counter is incremented until the momentary voltage value is below/above the threshold - Maximum / residual voltage is not calculated - Interruptions measurement is not on-board	- ($U_{rms(1)}$) has been implemented - $U_{rms(1)}$ is compared with the event threshold to obtain event start, end, and duration - An internal counter is incremented until $U_{rms(1)}$ value is below / above the threshold - $U_{rms(1)}$ measurement is used to store the residual / max. voltage
Harmonics	10 ÷ 100 % of harmonic limits, up to 40th order	200 ms (gaps allowed) ± 0.03% Max. synchr. error (optional)	- DFT/FFT - t.i. synchronized to the power system frequency - Rectangular window (Hanning in case of loss of synchronization	- Not on-board	- New algorithm

Table 3. STCOMET on-board metrics vs. IEC 61000-4-30 requirements (class S)

In order to improve the measurement capability of the STCOMET platform, a study has been made on its sampling, computation and memory capabilities with respect to the possibility of implementing further PQ

metrics. Starting from this, some correction algorithms have been designed to meet the IEC 61000-4-30 standards for on-board measurements. In brief:

A. Frequency and period

According to IEC 61000-4-30, frequency reading shall be obtained every 10 s, as the ratio of the number of integral cycles counted during the 10-s time clock interval, divided by the cumulative duration of the integer cycles. When a zero crossing (ZRC) method is used for frequency calculation, harmonics and inter-harmonics are required to be filtered, in order to minimize the effects of multiple zero crossings. With respect to these requirements, DSP on STCOMET computes period starting from zero-crossing (ZRC) signal of the voltage channel; it comes from fundamental voltage (through a LPF filter). Resolution of the zero-crossing signal is 8 μs (given by the 125 MHz internal clock); the period value is updated as the average of last eight measured periods. In the implemented metric, frequency measurement is obtained as period reciprocal and it is calculated as the average of frequency values measured over 10 s.

B. Voltage magnitude (RMS)

IEC 61000-4-30 requires that the RMS measurement shall be obtained over a 10/12 cycles t.i. for a 50/60 Hz power system frequency (i.e. 200 ms). Every 10/12-cycle interval shall be contiguous, and not overlapping (with few exceptions, see [98]). RMS DSP block on STCOMET calculates RMS values of current and voltage continuously, every 128 μs, as soon as a new sample is available from the ADC. The integration time is 200 ms. The synchronization error on this observation window is equal to 0.032 % (i.e. 64 μs, equal to half the sampling time $T_s = {}^{1}/_{F_s} = 128\ \mu s$). Non overlapping t.i. is obtained by suitably set the measurement reading update. For dips, swells and interruptions detection, the RMS measurement over 1 cycle has been also implemented (see next section).

C. Dips, swells, interruptions

According to IEC 61000-4-30, on single-phase systems a voltage dip/swell begins when the U_{rms} voltage falls below /rise above the dip/swell threshold, and ends when the U_{rms} voltage is equal to or above/below the dip/swell threshold (plus a hysteresis voltage). A voltage dip/swell is characterized by a pair of data, i.e residual/maximum voltage (i.e. the minimum/maximum voltage value during the event) and dip/swell duration (i.e. the difference between the start time the end time of the event). The interruption is defined similarly to dip (with its own threshold), but the event is characterized only by its duration. To fulfil the IEC 61000-4-30 requirements a proper algorithm has been implemented, based on the measurement of the voltage RMS over 1 cycle of the signal $U_{rms(1)}$. This value is compared with the event (dip/swell/interruption) threshold to obtain the event start, end and duration. An internal counter is incremented until $U_{rms(1)}$value is below/above the threshold (selectable by user, together with the hysteresis voltage, if any [98]). During the event, $U_{rms(1)}$ measurement is used to store the residual or maximum voltage for dip or swell event, respectively. Flowcharts of swell and interruption metrics are reported in Fig. 15 and Fig. 16, respectively (dip

metric implementation is similar to swell one, with the exception of threshold comparison and residual voltage storage).

D. Harmonics

As already mentioned, the EVLKSTCOMET10-1 uses a zero-crossing method for measuring the signal period/frequency, therefore this value can be used for the synchronization of the observation window T_w of 10/12 cycles of the 50/60 Hz input signal, i.e., 200 ms. If the frequency is not 50 Hz, the window would be greater or less than 200 ms. In accordance with [99], DFT/FFT algorithms have been evaluated for harmonic analysis. DFT can be performed with any number of samples N, but it has a higher computational cost ($O(N^2)$); on the other hand, the FFT has a much lower computational cost ($O(N \log N)$, however, it needs a number of samples equal to a power of two to be performed (i.e., N = 1024, 2048, etc). An analysis of the computational time required for the algorithm executions with STCOMET leads to choose FFT (DFT execution time was not compatible with timing requirements for harmonic analysis even considering gaps). To use the FFT, the closest values for N should be 2048. On the other hand, the STCOMET has a fixed sampling frequency of 7812.5 Hz, then the acquisition of 2048 samples would lead to a not synchronous observation window (i.e., $T_w = 2048 * 128\,\mu s \approx 262\,ms \neq 200$). Thus, a time-domain interpolation algorithm has been implemented to obtain N = 2048 samples over the time interval of 10 cycles. Fig. 17 shows a flow chart representing the operations of the algorithm implemented on STCOMET.

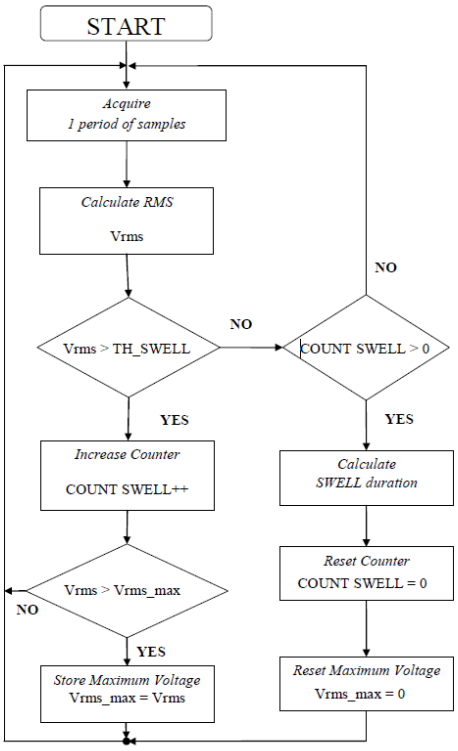

Fig. 15. Flow Chart of voltage swell metric implemented on STCOMET

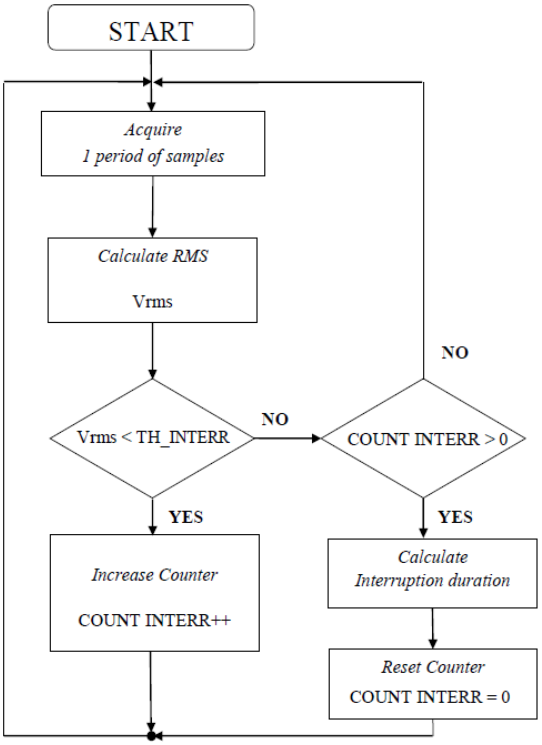

Fig. 16. Flow chart of voltage interruption metric implemented on STCOMET

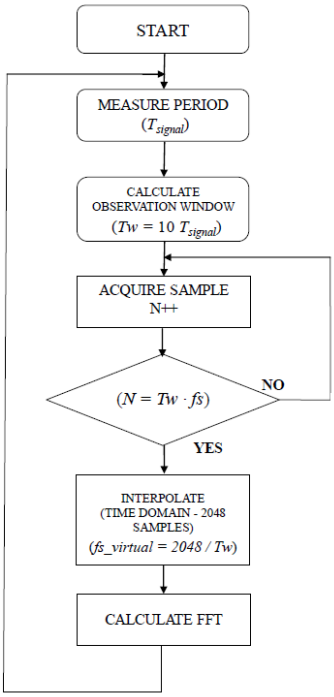

Fig. 17. Flow chart of harmonics analysis implemented on STCOMET

1. Starting from the measurement of the signal period T_{signal} (carried out by STCOMET via zero-crossing, ZRC), an observation window equal to $T_w = 10 * T_{signal}$ is set (for example, in the case of a 50 Hz signal, $T_{signal} = 20\,ms,\ T_w = 200\,ms$).
2. The number of samples to be acquired and used for the algorithm is set: $N = T_w * f_s$, where $f_s = 7812.5\,Hz$ is the STCOMET sampling frequency (M = 1562.5 samples, rounding to the upper integer, i.e., 1563).
3. The time-domain interpolation of the acquired N samples is carried out to obtain 2048 samples for the FFT algorithm (a simple linear interpolation algorithm was used in the implementation, to minimize the computational cost). A virtual sampling frequency is determined, *fs_virtual*, which, in the same observation window Tw, would lead to the acquisition of the aforesaid 2048 samples:

   $$f_{s\_virtual} = {2048}/{T_w}$$

   In the case of $T_w = 200\,ms$, $f_{s\_virtual} = 10240\,Hz$.

4. The FFT is calculated on the 2048 samples.

As regards the memory requirements, in the case of $f = 50\,Hz$, $T_w = 200\,ms$, and $f_s = 7812.5\,Hz$, the number of samples acquired is $M = {T_w}/{f_s} = 1563$, so the number of bytes allocated in the STCOMET memory for samples storage is:

K = 1563 x 32 = 6.252 kB

Considering that for the FFT calculation it is necessary to store 2048 samples (with both real and imaginary part), memory occupation is equal to 2048 x 32 x 2 = 16 kB. Furthermore, to allow the acquisition of samples of the subsequent observation window while performing the FFT calculation, it is necessary to instantiate a second register of 16 kB size. This was made in order to investigate the possibility of harmonic measurements without gaps between the observation windows. In summary, 32 kB are needed for samples storage and the FFT calculation algorithm; this requirement is compliant with STCOMET features, since the device has a RAM of 128 kB.

In this way, the algorithm can virtually synchronise the observation window, minimising the synchronisation error, regardless of the input signal period. Furthermore, the "virtual re-sampling" of the signal allows the FFT to be calculated on 2048 samples in a 10-period observation window, reducing leakage and scallop loss errors. The use of a basic linear interpolation approach allows the harmonic calculation's processing cost (FFT + interpolation) to be limited. To verify this, the time required for FFT computation with and without interpolation was measured experimentally; as shown in Fig. 18, the overall time required for FFT with interpolation is 11.4 ms (a time of 9.6 ms was measured in the case of FFT calculation without interpolation). It should be noted that while the interpolation and FFT algorithms are running, the device is

still collecting samples for the next observation window, which are saved in memory for the next FFT computation.

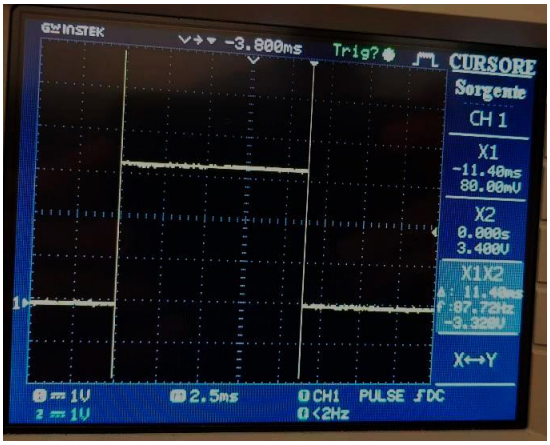

Fig. 18. Time measured for FFT calculation

Fig. 19 shows the plots of the FFT calculated by STCOMET without interpolation (a) and with interpolation (b) (test with sinusoidal voltage, $f = 50\ Hz, V_{rms} = 230\ V$); as expected, the use of interpolation drastically reduces leakage and scallop loss errors.

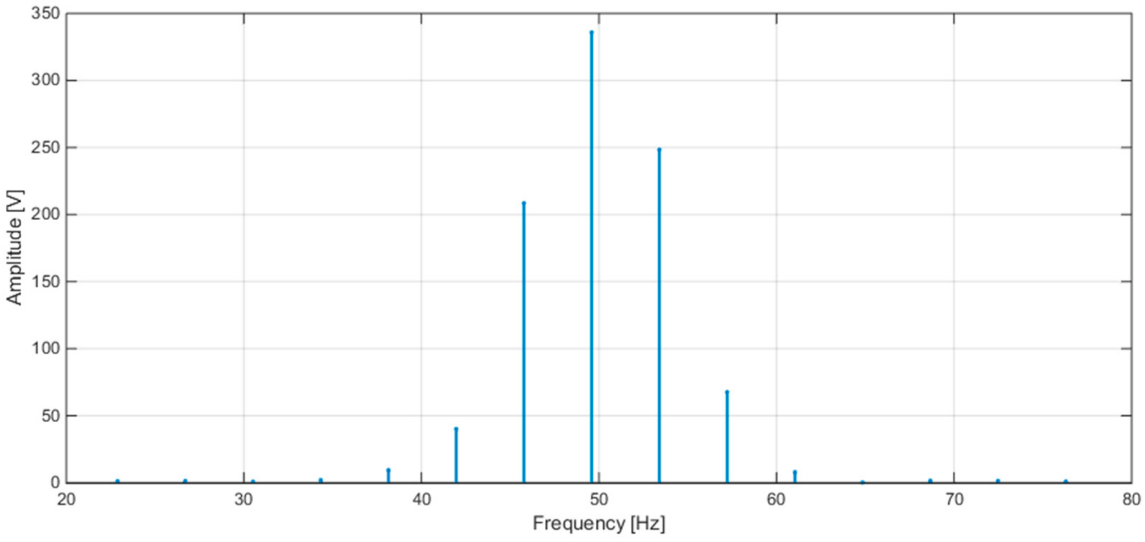

(a)

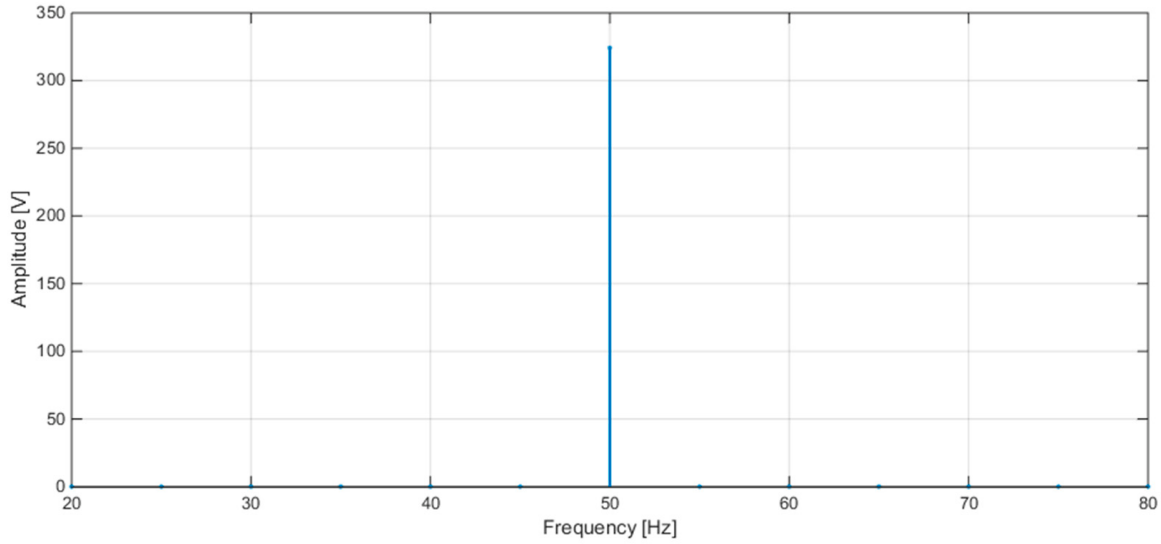

(b)

Fig. 19. (a) FFT without interpolation; (b) FFT with interpolation

3.2.3 PQ Metrics Implementation on STCOMET: Experimental Results

To verify the PQ metrics performances, experimental tests have been carried out by using a Fluke 6100A calibrator (Fig. 20). The USB JTAG J-linkOB was used to connect the EVLKSTCOMET10-1 to a PC. IAR Embedded Workbench was used to programme STCOMET with the established metrics. Different PQ phenomena (harmonics, dips, swells, interruptions) were reproduced in the laboratory for different test signal frequencies (in the range of 42.5 57.5 Hz). Table 4 shows the harmonic composition of test signals. Table 5 - Table 8 summarise some of the results obtained for frequency, RMS, and dips/swells/interruptions measurements. The acquired results and related errors (maximum values) with respect to the power calibrator are compatible with class S requirements, as can be seen. These findings show that the STCOMET hardware platform, when combined with appropriate firmware metrics, may be used to construct a PQ meter that meets IEC 61000-4-30 class S criteria without altering the hardware platform or adding other modules.

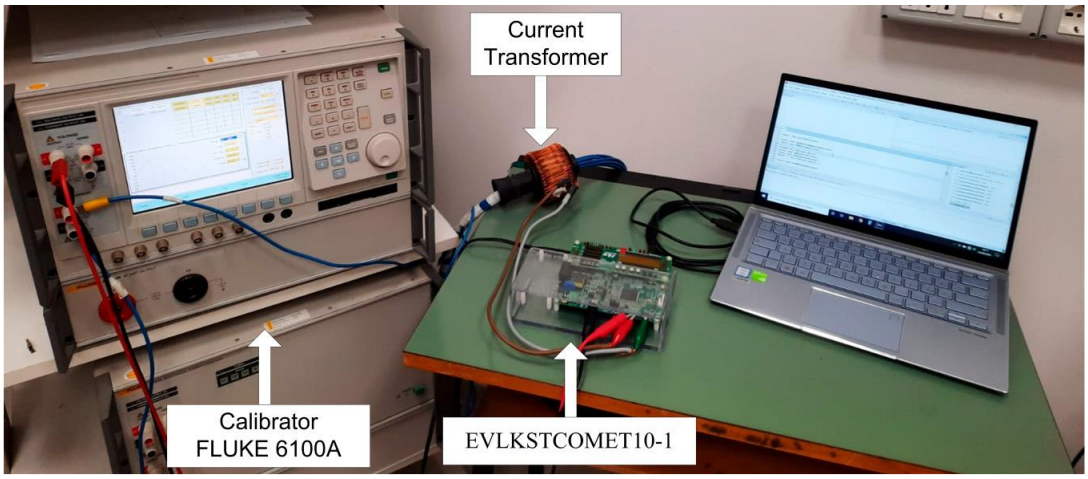

Fig. 20. Test Bench

Signal	RMS (fundamental/total)	Harmonic order	Harmonics RMS
Voltage	V1 = 230 V V = 238.90 V	3	20% V1
		5	15% V1
		7	10% V1
		9	8% V1
Current	I1 = 5 A I = 5.194 A	3	20% I1
		5	15% I1
		7	10% I1
		9	8% I1

Table 4. Non-sinusoidal signals harmonic content

Test conditions	Generated frequency	Measurements and errors (referred to calibrator)		
		Period (s)	Frequency (Hz)	E (mHz)
230 V (RMS, sinusoidal)	42.5	0.023528	42.5025	2.5
	47.5	0.021048	47.510	10
	49.5	0.020200	49.5050	5.0
	50	0.020000	50.000	0.0
	50.5	0.019800	50.5050	5.0
	52.5	0.019040	52.521	21
	57.5	0.017384	57.524	24
231,90 V (RMS, distorted)	42.5	0.023528	42.5025	2.5
	47.5	0.021048	47.510	10
	49.5	0.020200	49.5050	5.0
	50	0.020000	50.000	0.0
	50.5	0.019800	50.5050	5.1
	52.5	0.019040	52.521	21
	57.5	0.017384	57.524	24

Table 5. Period/Frequency Measurements

Test conditions	Signal frequency	Measurements and errors (referred to calibrator)	
		RMS (V)	e%
Vrms 230 V	42.5	229.97	0.011
	47.5	229.83	0.072
	49.5	229.97	0.011
	50	229.87	0.057
	50.5	229.93	0.026
	52.5	229.94	0.026
	57.5	229.90	0.042
Irms 5 A	42.5	4.987	0.25
	47.5	4.987	0.25
	49.5	4.987	0.25
	50	4.996	0.08
	50.5	4.987	0.25
	52.5	4.987	0.25
	57.5	4.987	0.25

Table 6. RMS Measurements – Sinusoidal Test Signal (voltages and currents)

Test conditions	Signal frequency	Measurements and errors (referred to calibrator)	
		RMS (V)	e%
Vrms 238.90 V	42.5	238.49	0.17
	47.5	238.42	0.20
	49.5	238.42	0.20
	50	238.45	0.19
	50.5	238.45	0.19
	52.5	238.45	0.19
	57.5	238.35	0.19
Irms 5.14 A	42.5	5.171	0.38
	47.5	5.179	0.21
	49.5	5.171	0.38
	50	5.171	0.38
	50.5	5.179	0.21
	52.5	5.171	0.38
	57.5	5.171	0.38

Table 7. RMS Measurements – NON-Sinusoidal Test Signals (voltages and Currents)

Event type	Event severity (% of RMS)	Event duration (s)	Measurements and errors (referred to calibrator)	
			Residual/maximum voltage [V] (and e%)	Duration (s) *
Dip	80%	2.000000	184.83 (0.45%)	2.000
Swell	110%	2.000000	253.91 (0.89%)	2.000
Interr.	2%	2.000000	--	2.000
* measurement resolution: 1 period (20 ms)				

Table 8. Dips, Swells and Interruption Measurements – Test Signal V=230v, f=50Hz

It should be noted that, even if some improvements have been achieved on the measurement capabilities of the STCOMET device, its main features in terms of sampling frequency do not allow to reach the possibility of developing a IEC-6100-4-30/4-7 Class A meter. Indeed some accuracy specification have been improved so to match the Class A requirements. However the synchronization error on sampling cannot be adjusted so to obtain a Class A meter, some hardware modification should be made on the platform.

3.3 CONTROL CENTRE MEASUREMENTS INTEGRATION

To achieve the features outlined in Section 2.4, we propose an upgraded PFMC system that builds on current communication, control, and measurement infrastructures for AMR and supply protection and restoration. The improved PFMC system incorporates several methods given in literature, which have been improved further to improve system efficiency, robustness, and dependability. In greater depth, the PFMC system architecture incorporates some commercial measurement equipment as well as [35,40] innovative IPSs solutions. In terms of monitoring and control methods, the LF calculation is implemented using the method described in [31]. A B/F power summing method (rather than the B/F current summation method provided in [31]) is employed to obtain a more efficient solution for SCADA deployment without worsening power flow calculation errors. The PFMC algorithm includes the loads estimation method presented in [103] and a real-time LF results verification for detecting the occurrence of one or more field device unavailability or malfunction to improve system robustness and reliability even in the case of some load measurements unavailability.

3.3.1 Load Flow Calculation at SCADA

The proposed architecture is presented in Section 2.4 and it is schematized in Fig. 21. As shown in Fig. 22 the SCADA system calculates power flows in each branch of the network using the algorithm given in the flow chart. The SCADA system can also send control commands to DSOs so that they can communicate with DGs and ESSs.

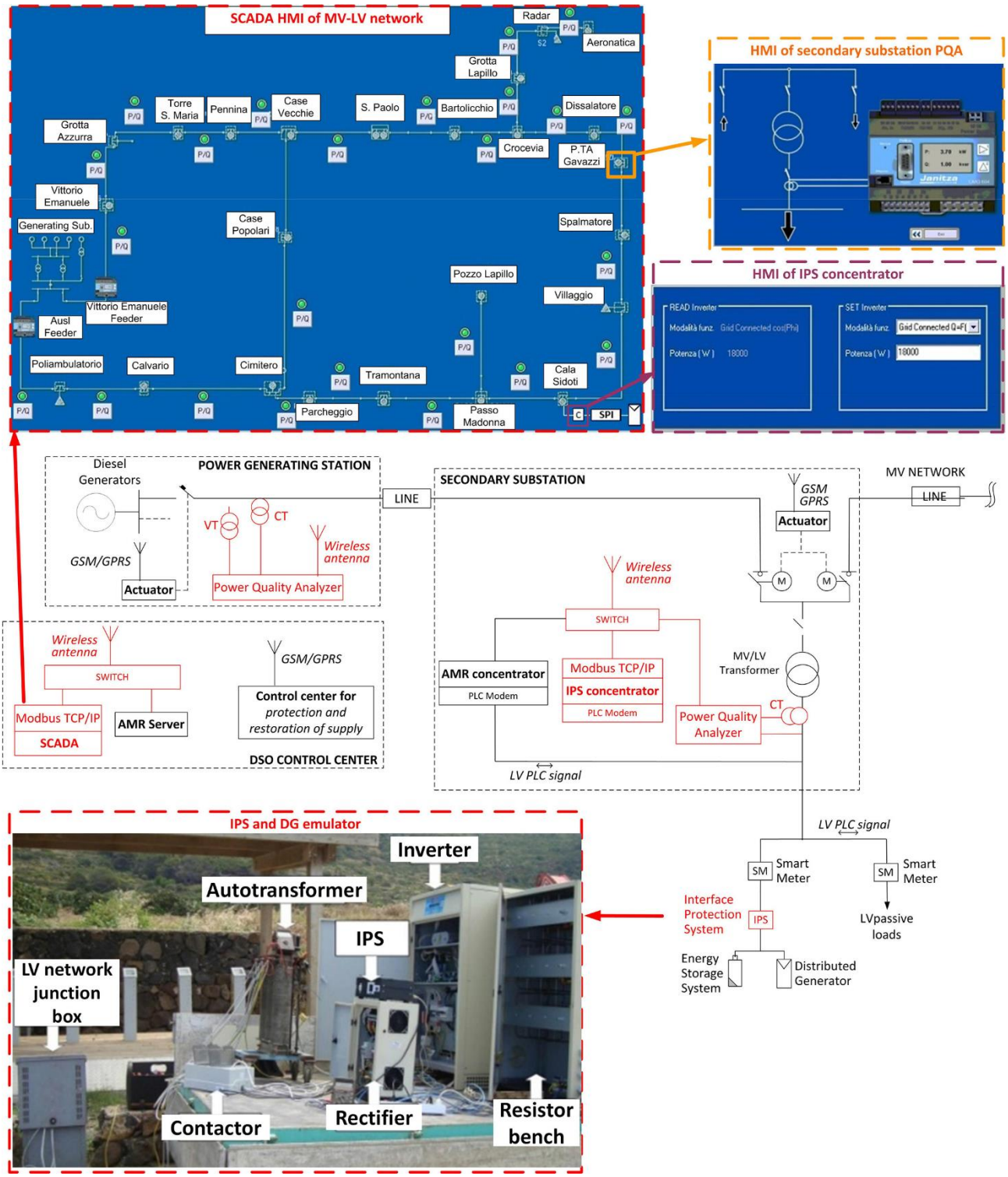

Fig. 21. Enhanced architecture for real-time power flow monitoring based on existing communication, control, and measurement infrastructures for AMR and supply protection and restoration. The additional pieces are shown in red in relation to the current infrastructure.

The method starts with the control centre asking all of the network's measurement sensors. If some of these instruments are temporarily unavailable (due to a communication system failure or instrument malfunction, for example), the missing load power values are calculated using the approach given by[103]. It trains artificial

neural networks using past data from load power measurements and uses real-time observations to estimate load. The LF algorithm can calculate the MV network state variables based on the measured/estimated load powers. Iterative B/F power summing is used [104,105], which is particularly efficient for radial networks. Data from measurements and estimations are fed into an iteration process that updates branch active and reactive power flows (P_i and Q_i) in backward sweeps and bus voltages (V_i) in forward sweeps until a convergence condition is reached. The details and the math of the algorithm has been published in [106]

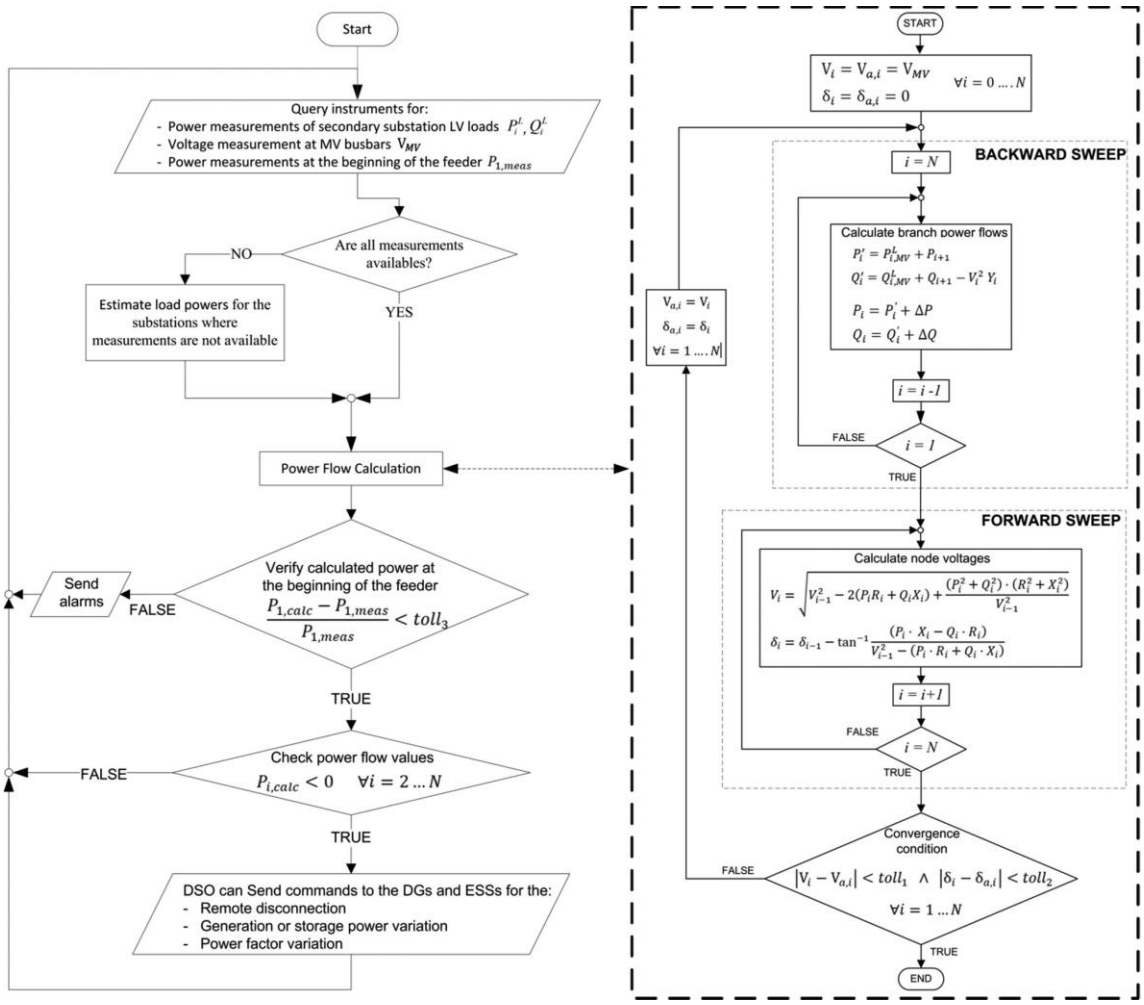

Fig. 22. Flowchart of the monitoring and control algorithms

Following the calculation of power flows, the algorithm checks the calculated power flows at the feeder's beginning by comparing them to the measurements of the PQA installed at the slack bus. If the difference exceeds a certain threshold, the calculated values are marked and a warning signal is issued to the DSO; this can also aid in the detection of potential SCADA faults or cyberattacks. If the difference is less than the threshold, computed values can be accepted instead. If negative values of active power flows are detected in this case, the DSO can send control commands to the DGs/ESSs IPSs to change their inverter operative

conditions, i.e., to vary their power productions or power factors, or, if necessary, to disconnect them from the grid to avoid potential instabilities.

3.3.1.1 Real-Time Implementation and Experimental Tests

Thanks to collaboration with the local DSO, the suggested PFMC was implemented in the test case of the Ustica MV-LV distribution network. As detailed in the following, a separate SCADA system was designed for the PFMC implementation. A first series of experiments were performed utilising a mobile station that emulated a photovoltaic generator and its connection equipment, including the inverter and the IPS, to verify the PFMC performances in different scenarios of DG connections in the microgrid downstream secondary substation. Various scenarios of the microgrid operation downstream of a secondary substation aggregator, as well as its integration and interaction modalities with the DSO, were thus emulated. The PFMC performances were further validated via a one-year test campaign, which included periods with varying load circumstances;

Ustica's electricity is generated by a diesel power station, which has five generating units with a total installed capacity of about 6 MVA. The electricity is distributed using an MV network with 23 secondary substations that feed LV users. The network is often divided into two radial MV feeders, *AUSL (AU)* and *Vittorio Emanuele (VE)*. To connect the DSO supervisory control centre to each secondary substation, a HiperLAN communication system using the Modbus TCP/IP protocol is implemented. To link the inverter to the LV network for the PFMC system development, a new IPS prototype was used. The IPs was implemented on a ST Microelectronics STEVAL-IPP001V2 platform. Both the inverter and the IPS meet the CEI-0-21 standard standards [19]. Furthermore, the new IPS enables real-time interaction between the DSO and inverter to change its operating mode, i.e., selecting the maximum power output and power factor, and, if necessary, remotely disconnecting the power plant from the LV network [19,40]. In order to establish communication between the DSO SCADA control centre and IPS, an IPS concentrator built on the same hardware platform was placed in the secondary substation upstream the LV line. To that, the prototypes incorporate a ST7580 PLC modem capable of transmitting n-phase-shift keying PLC signals in the CENELEC band. The IPS communicates with the inverter via Modbus/RTU over RS232. The DSO supervisory control centre is linked to the devices installed in each secondary substation via a HiperLAN communication system using the Modbus TCP/IP protocol (PQAs and IPS concentrators). The MV bus bar voltages at the producing substation and load powers at each secondary substation's LV bus bar are measured using Janitza UMG 507 and 604 PQAs, respectively. The UMG 507 PQAs are linked at the start of each MV feeder via the MV and current transformers. In addition to the MV, each UMG 507 PQA includes a measurement of the MV feeder power flow, which is used as a comparative value for the LF algorithm validation. The LV current transformers connect the UMG 604 PQAs to the LV bus bars of each secondary substation. To keep all devices synced, a network time protocol (NTP) system running over an Ethernet network was employed. The SCADA software collects all PQA measurements and processes them using the previously defined LF method. The network

characteristics used for LF method implementation were derived from Ustica DSO's rated data of power transformers, cables, and overhead power lines. When MV power flow inversions are discovered, warning circumstances are indicated and the MV power flows are calculated for each branch. In this situation, the SCADA control centre sends appropriate commands to the DGs and ESSs, IPSs, and inverters in order to regulate their power flow injection/absorption into/from the network based on a set DSO strategy. Fig. 21 show the SCADA HMI of the MV-LV network. The SCADA HMI IPS panel can remotely control each LV DG, selecting the inverter operating mode and the DG maximum power production. A PQA is utilised in each secondary substation to measure the load power at the LV bus bar. It can be accessed remotely via the SCADA HMI PQA panel.

As previously stated, during the measurement campaign, a preliminary series of tests was carried out by positioning the DG emulator at various positions on the grid. The DG emulator was linked to an LV line departing from an MV/LV substation for each test site, and the PFMC performances were examined in various cases of power flow inversions (involving different MV branches). An adjustable ac supply was produced for the DG emulator by connecting an autotransformer to the LV network or a diesel generator. The autotransformer was used to alter the power generated by the mobile station. The autotransformer output was linked to a rectifier and resistor bench to simulate the working curve of a solar power plant, allowing the inverter maximum power point tracking system to operate. In [106] the details of two of the aforesaid test are presented.

A one-year monitoring test campaign was carried out to further validate the PFMC performance in diverse load circumstances, including times of low and high loads, corresponding to the winter and summer seasons, respectively. Every 15 seconds, the measured and computed power flow values were kept. The active power flows measured and computed at the beginning of the two feeders in two days of the year are presented in Fig. 23 - Fig. 26 as an example. The following has been calculated:

- In Fig. 23 a medium error of 0.23%, a standard deviation of 0.17%, and a maximum error of 2.0% were measured throughout the day.
- In Fig. 24 a medium error of 0.52%, a standard deviation of 0.56%, and a maximum error of 7.6% were measured throughout the day.
- In Fig. 25 a medium error of 1.3%, a standard deviation of 0.97%, and a maximum error of 7.8% were measured throughout the day.
- In Fig. 26 a medium error of 1.4%, a standard deviation of 0.70%, and a maximum error of 6.5% were measured throughout the day.

As can be observed, the power flow estimation trend matches the measured one, with a middle error of less than 1.5 percent and a maximum error of less than 8%. Concerning the variability of errors, it should be emphasised that the one-year results cover operating conditions under both measured and estimated conditions, depending on the genuine availability of meter information throughout system operation (the PFMC algorithm automatically use estimations when one or more measurements are not available). In this regard, [103] studied

the impact of uncertainty in load power prediction on power flow calculation accuracy. The power flow uncertainties rise, as expected, in the presence of the estimated loads, although this increase is limited (below 3 percent and 6 percent for the active and reactive powers, respectively, for the tests reported in [103]).

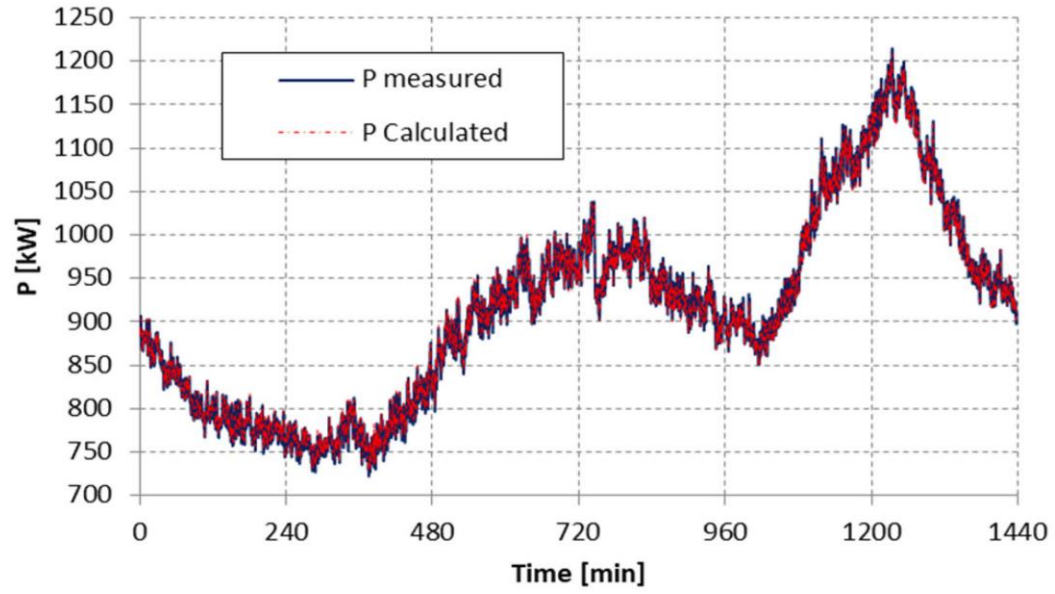

Fig. 23. Measured and calculated active power flow at the beginning of VE feeder the 15th of August 2016.

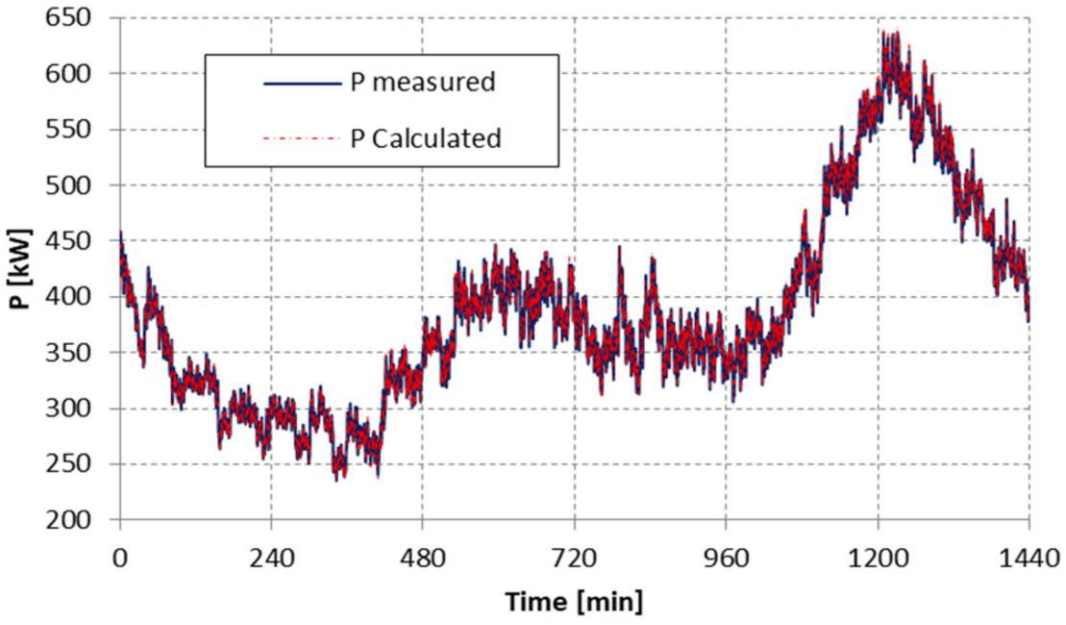

Fig. 24. Measured and calculated active power flow at the beginning of AU feeder the 15th of August 2016

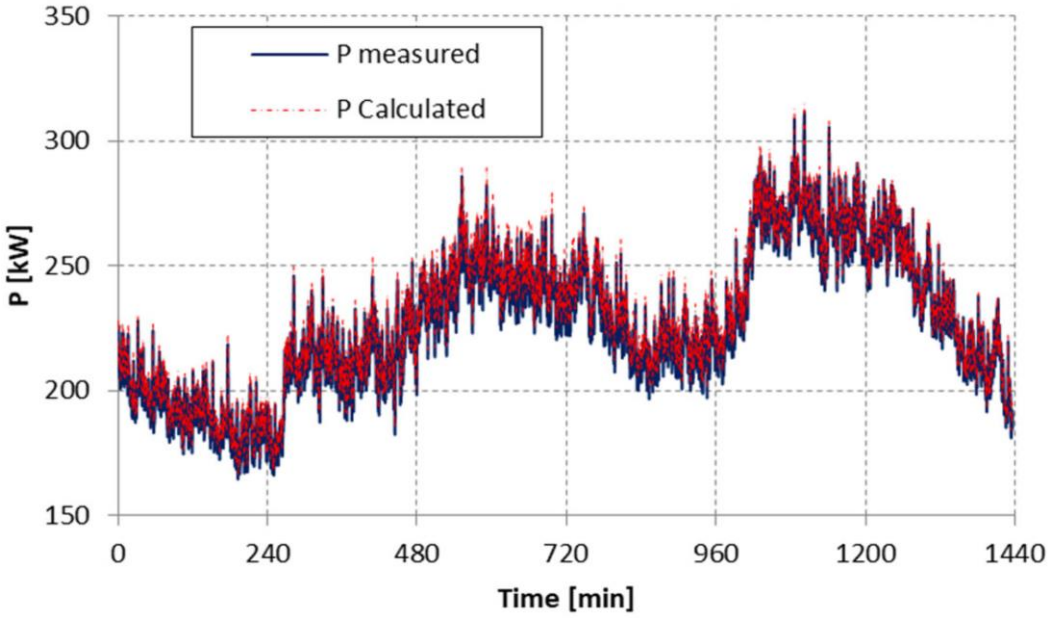

Fig. 25. Measured and calculated active power flow at the beginning of VE feeder the 27th of November 2016

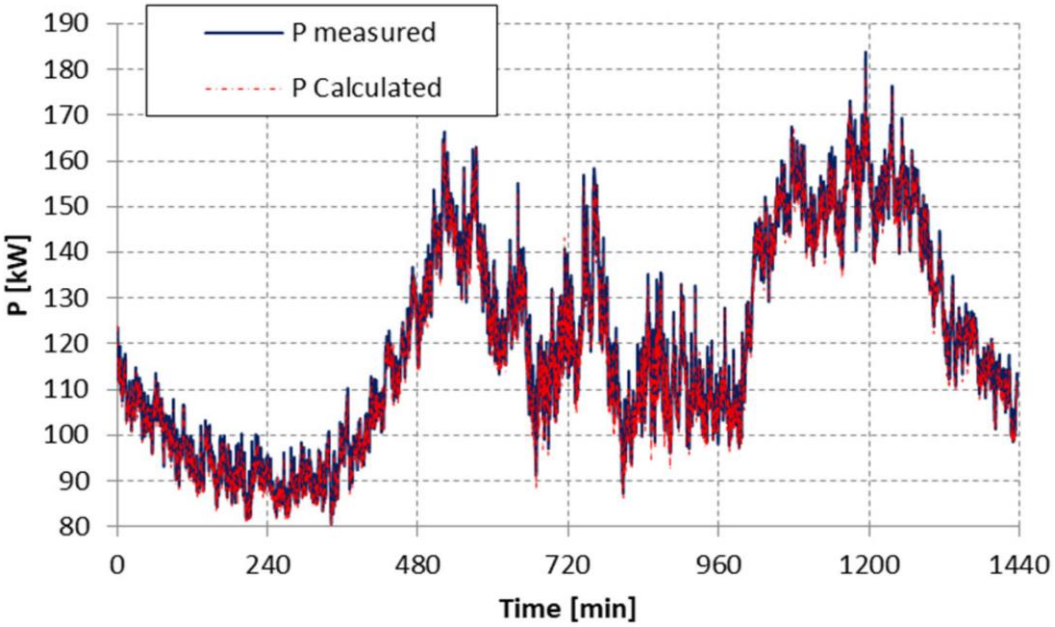

Fig. 26. Measured and calculated active power flow at the beginning of AU feeder the 27th of November 2016

Fig. 27 and Fig. 28 illustrate the mean value and standard deviation of errors estimated on data from November 2015 to October 2016. As can be observed, the mean error and standard deviation were always less than 2%, validating the PFMC algorithm's reliability under various load situations. When compared to the data obtained for the active power flows, the reactive power flows revealed greater variability. Fig. 29 and Fig. 30 illustrate the mean value and standard deviation of the errors found for the reactive powers. As illustrated in the figures, percentage mean errors and standard deviations have

higher values but are always less than 5%. This is owing to increased uncertainties imposed by PQAs in reactive power measurements, as well as increased uncertainties in cable line shunt admittances.

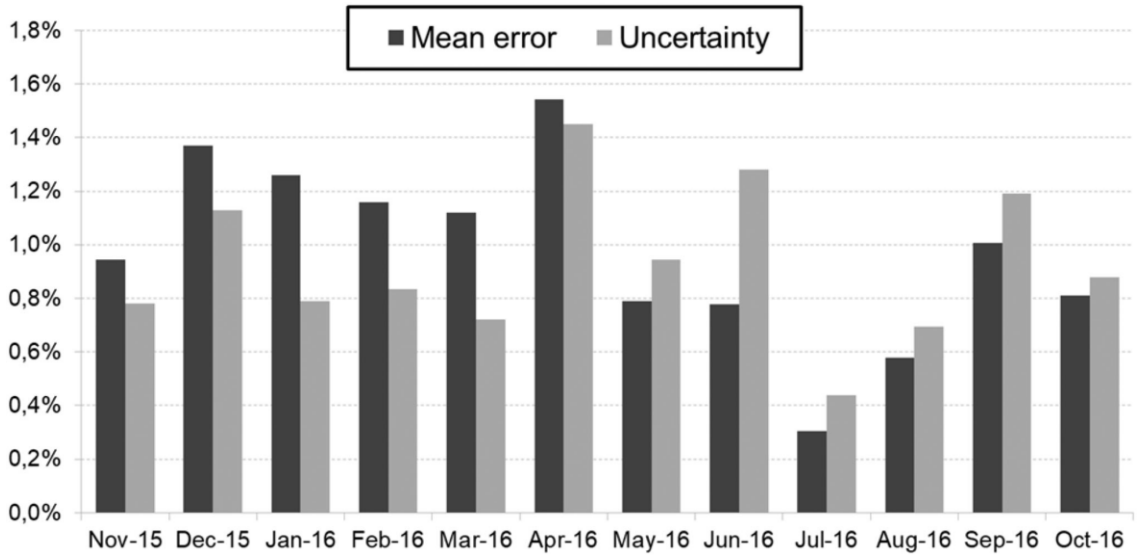

Fig. 27. Mean value and standard deviation of errors between the measured and calculated active power flow at the beginning of VE feeder in one year

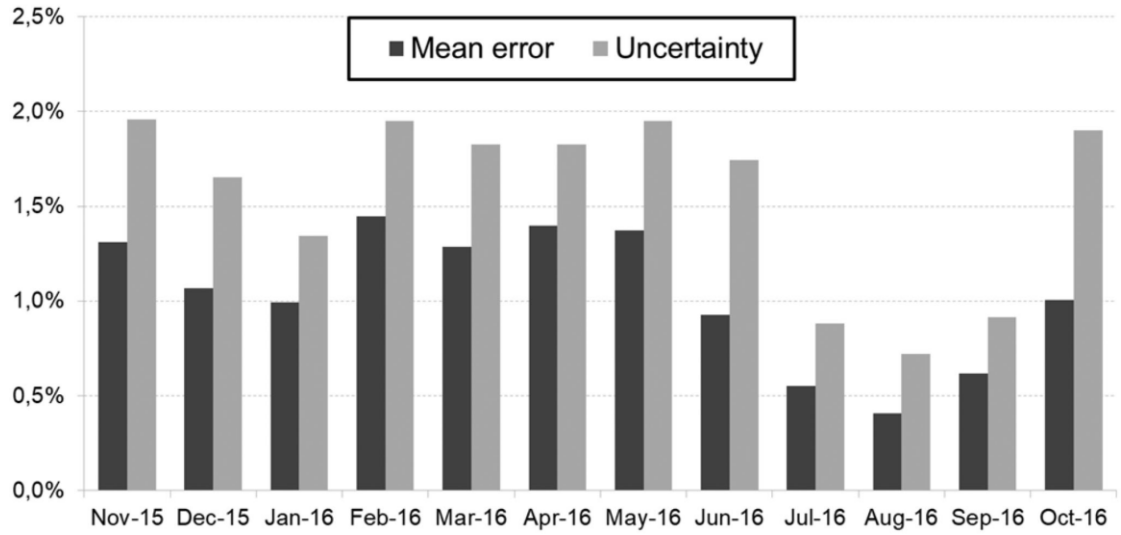

Fig. 28. Mean value and standard deviation of errors between the measured and calculated active power flow at the beginning of AU feeder in one year.

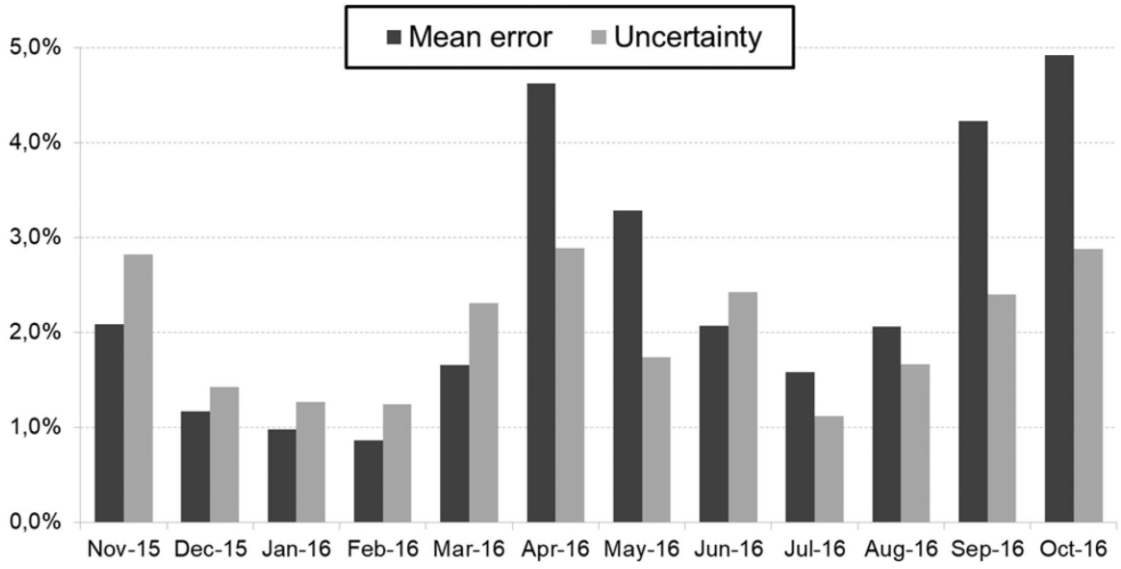

Fig. 29. Mean value and standard deviation of errors between the measured and calculated reactive power flow at the beginning of VE feeder in one year.

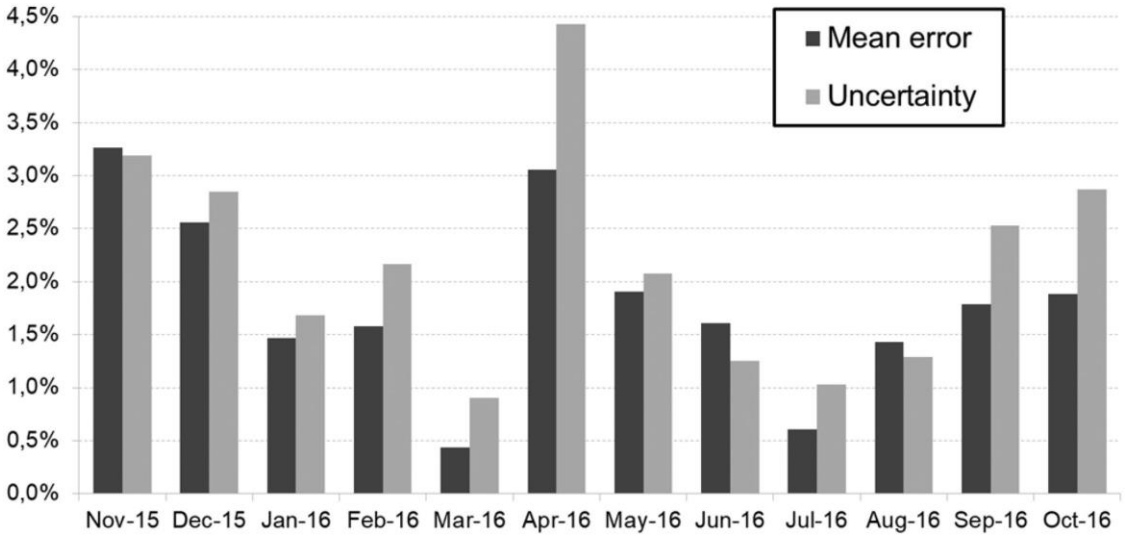

Fig. 30. Mean value and standard deviation of errors between the measured and calculated reactive power flow at the beginning of AU feeder in one year

The experimental results demonstrate that the developed PFMC can effectively monitor the network in real time in all test circumstances. They also confirmed the accuracy of the estimating method and its incorporation into the PFMC system for distribution network management. The DSO can manage power flows by delivering commands to the DGs/ESSs via the created devices. DSOs can regulate power flows between the main grid and the microgrid subsystems' downstream substations in this manner, enabling for the introduction of smarter functions such as optimal microgrid operation and management, islanding detection, and DGs/ESSs remote control. In this regard, improved logics should be created to facilitate interaction between the DSO and prosumers. Proper strategies, for example, could be implemented in the

future to satisfy both prosumers' economic interests and the DSO's network management needs, by introducing economic incentive strategies for optimising prosumers' benefits while providing the DSO with the ability to request variations in power exchanges profiles between DGs/ESSs and the grid.

3.3.2 From SCADA enhanced features to Hyperion Software

The approach described in the preceding section calls for the LF algorithm to be built in a new SCADA system that will be implemented alongside the SCADA system already in use at the DSO control centre. Another way would be to incorporate the LF algorithm into the DSO's SCADA system. The issue is that the system in use at the control centre often runs the power plant controls and systems, which is classed as critical infrastructure for the DSO. Even if the improvements would have been made by highly qualified individuals, the distributors we worked with were hesitant to disrupt their crucial infrastructure. Another problem of the implemented SCADA system for the LF calculation was its flexibility with respect to the real power grid. In fact, the grid topology can deeply altered if the DSO acts on the MV switches in the secondary substations and makes re-closures as needed by the grid. This significant change must be reflected in both the graphical interface and the SCADA's backend business logic. This level of adaptability is not afforded by the used SCADA framework. To address the issues raised above, a new approach has been developed to add features to the DSO control system. In fact, instead of using the DSO's SCADA or developing a new SCADA, a new software has been developed, called Hyperion, that acts as an oracle to the DSO control system side by side.

Hyperion is software that models, monitors, analyses, and studies the electrical grid in order to assist the grid's operator with decision-making and forecasting. Using Hyperion, it’s possible to create a network model and analyse the evolution of parameters like as voltages, currents, powers, power flows, transformer and line losses, distributed generation plant production, state of charge, and storage system behaviour over time. Adoption of the Hyperion software allows the operator to create a digital twin of the distribution network, allowing them to not only monitor the parameters of interest, but also receive recommendations on the optimal operation of both traditional generation plants, such as diesel groups, and renewable generation plants.

The software was developed as a Software as a Service (SaaS) to interface with the operator's existing software, eliminating the need to acquire and maintain new software or demand functionality upgrades of old legacy products. To meet needs that may vary depending on the network or the operator, the software was designed with a foundation (core or nucleus) onto which modules implementing certain macro functions are grafted. The network modelling and computation of the Load Flow on medium voltage network lines constitute the core, which is shared by all. In contrast, the input and output production vary depending on the module that the distributor choose to incorporate into his information system.

3.3.2.1 Network Modelling

The digital representation of the network is initially created based on the description files of the network that contains information provided by the DSO. 4 different files are used:

- bus or node file
- lines file
- switches file
- transformers file

The information contained in these files (Network description files) are the only ones necessary to create a network model and all its possible and possible reconfigurations. It is in fact very simple, by acting on the state of the switches, to create a new network configuration that reflects the current one or to simulate new configurations to test their effectiveness. Automatic network reconstruction is handled by a process that can be prompted directly or that can, at regular intervals, check the network definition files for changes. The network topology is automatically derived from the information on the lines and switches. Hyperion implements the digital representation of the most common configurations that can actually be found in the MV cabin. It is in fact possible to model the following cases:

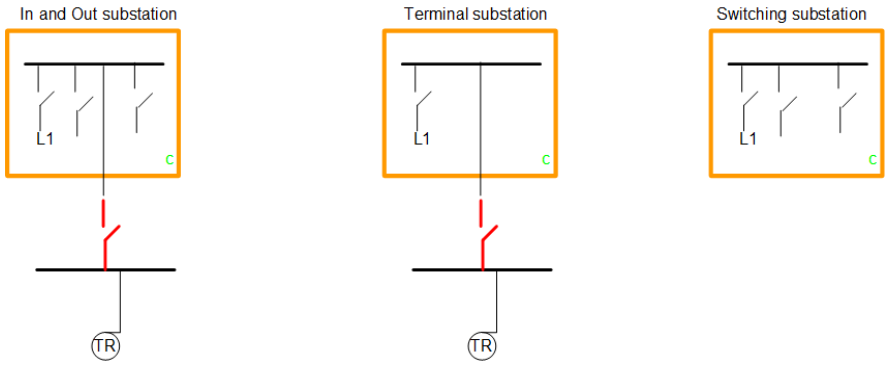

Fig. 31. (a) In and out substation (b) terminal substation (c) switching substation

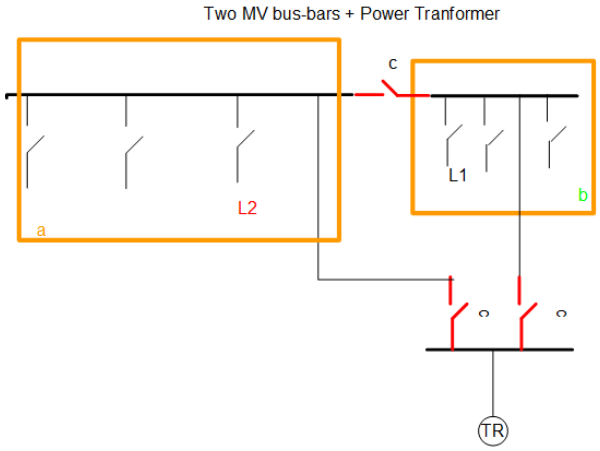

Fig. 32. Two MV bus-bars plus a power transformer

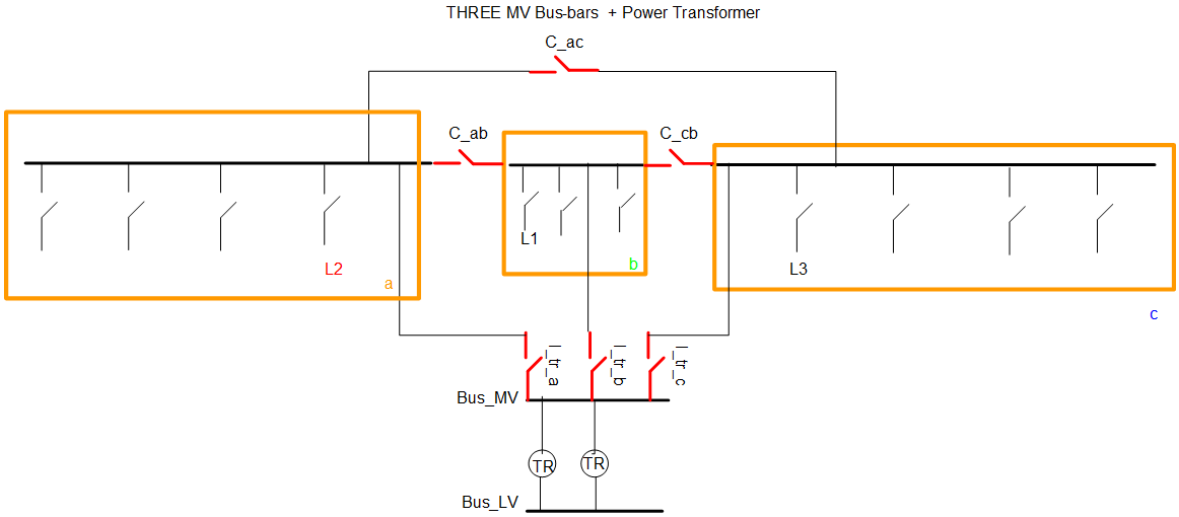

Fig. 33. Three MV bus-bars plus a power transformer

All the elements represented in Fig. 31, Fig. 32 and Fig. 33 are instantiated in the software and are controllable. It is therefore possible to manage maintenance cycles, temporary reconfigurations, commissioning of auxiliary transformers or load overturning between one line and another. Furthermore, thanks to the possibility of entering the geographical coordinates for each node of the network, a georeferenced map (Fig. 34) can be generated in which the nodes are grouped by colour, revealing the line to which they belong, also highlighting the lines not in service and any sections of mains not powered.

Fig. 34. Georeferenced map of the Favignana MV network

At each node of the network, if connected to a transformer, can be assigned a load (active power P and reactive power Q, voltages V), which will assume historical, current or expected values, depending on the module that is using the network. In the same way it is possible to manage distributed generation or storage plants. These values are, once assigned to the corresponding nodes, used by the Load Flow calculation process which, as a

main result, will return the power flows on the medium voltage lines that connect the secondary substations. Hyperion calculates flux using different algorithms from the literature but it is also possible to implement custom algorithms.

3.3.2.2 Simulation module

The Hyperion simulation module is used to validate network setups and test stability in the presence of distributed generation and simulated storage systems. Historical data from MV meters or meters is utilised to recreate the status of the base network before simulating GD and ESS systems with defined features.

The historical data from the meters in the MV substation and the MV meters are used to rebuild the network's state. These are frequently provided in non-standard formats, and their structure may vary over time. As a result, each network object in the simulation must have its own data ingestion phase.

The data used are usually provided at 15-minute intervals, although the time interval can be customized:

- Datetime
- Active Power
- Reactive Power
- Voltages (if available)

The values loaded from files are saved on a relational database that already has the network topology, allowing each cabin to be linked to its own historical measurements. Through this module, Hyperion can support large simulation studies with the goal of determining the network's stability under various operating scenarios. As a result, the module loads a "control file" in which all of the data about the plants to be simulated, as well as the parameters that condition the software and the simulation outputs, are defined for each simulation. The simulation will take care of instantiating the base network and causing it to evolve during the specified time (*date from - date to*) while taking into consideration the plant information specified in the file. An example of the simulation file is showed in Fig. 35

The simulation of GD facilities can take place in two ways:

- By loading historical data for reference
- By loading ideal data provided by reference simulation studies

```
{
 "simulation": [
        {
        "name": "Scenario Base MaxProd PV 1800kW ES 530kW_3000kWh",
        "desc": "Rete %s Massima Produzione",
        "date_from":    "7/04/2019 00:00:00",
        "date_to":      "8/04/2019 23:45:00",
        "time_mins": 15,
        "switches":[],
          "PV": [
            {"name": "Bue Marino",          "id_DSO": 1,    "p":   0.013743119    , "side":"l"},
            {"name": "Punta Marsala",       "id_DSO": 2,    "p":   0.054035446    , "side":"l"},
            {"name": "Motta",               "id_DSO": 3,    "p":   0.037918515    , "side":"l"},
            {"name": "Punta Fanfalo",       "id_DSO": 4,    "p":   0.124937448    , "side":"m"},
            {"name": "Grotta Perciata",     "id_DSO": 5,    "p":   0.037481234    , "side":"l"},
            {"name": "Gen. Di Vita",        "id_DSO": 6,    "p":   0.033733111    , "side":"l"},
            {"name": "Torretta",            "id_DSO": 7,    "p":   0.045277331    , "side":"l"},
            {"name": "Burrone",             "id_DSO": 8,    "p":   0.056171877    , "side":"l"},
            {"name": "4 Vanelle",           "id_DSO": 9,    "p":   0.084645121    , "side":"l"},
            {"name": "Cavallo",             "id_DSO": 10,   "p":   0.020164904    , "side":"l"},
            {"name": "Centrale Elettrica",  "id_DSO": 11,   "p":   0.037481234    , "side":"l"},
            {"name": "Camaro",              "id_DSO": 12,   "p":   0.029185388    , "side":"l"},
            {"name": "Calamoni",            "id_DSO": 13,   "p":   0.034557698    , "side":"l"},
            {"name": "S. Francesco",        "id_DSO": 15,   "p":   0.094084145    , "side":"l"},
            {"name": "Suore Canossiane",    "id_DSO": 17,   "p":   0.012493745    , "side":"l"},
            {"name": "Tempo di Mare",       "id_DSO": 18,   "p":   0.043253344    , "side":"l"},
            {"name": "S. Leonardo",         "id_DSO": 19,   "p":   0.07076457     , "side":"l"},
            {"name": "Vallone",             "id_DSO": 20,   "p":   0.006246872    , "side":"l"},
            {"name": "Cimabue",             "id_DSO": 21,   "p":   0.029547706    , "side":"l"},
            {"name": "Tre Croci",           "id_DSO": 22,   "p":   0.066029441    , "side":"l"},
            {"name": "Campo Sportivo",      "id_DSO": 23,   "p":   0.018740617    , "side":"l"},
            {"name": "Egadi Turismo",       "id_DSO": 24,   "p":   0              , "side":"m"},
            {"name": "Case Canino",         "id_DSO": 25,   "p":   0.014399041    , "side":"l"},
            {"name": "Carrubbo",            "id_DSO": 26,   "p":   0.0293603      , "side":"l"},
            {"name": "Faraglione",          "id_DSO": 27,   "p":   0.025687139    , "side":"l"},
            {"name": "Discesa Approdo",     "id_DSO": 28,   "p":   0.039723862    , "side":"l"},
            {"name": "Approdo Ulisse",      "id_DSO": 29,   "p":   0.062468724    , "side":"m"},
            {"name": "S.P. Punta Sottile",  "id_DSO": 31,   "p":   0.040048699    , "side":"l"},
            {"name": "Faro Punta Sottile",  "id_DSO": 32,   "p":   0              , "side":"m"},
            {"name": "Via Roma",            "id_DSO": 33,   "p":   0.052473728    , "side":"l"},
            {"name": "Chianazzo",           "id_DSO": 34,   "p":   0.016291843    , "side":"l"},
            {"name": "P.zza Matrice",       "id_DSO": 36,   "p":   0.0293603      , "side":"l"},
            {"name": "Egadi Factory",       "id_DSO": 37,   "p":   0.012493745    , "side":"m"},
            {"name": "Badia",               "id_DSO": 38,   "p":   0.015304837    , "side":"l"},
            {"name": "Cala La Luna",        "id_DSO": 39,   "p":   0.012493745    , "side":"m"},
            {"name": "Tonnara Florio",      "id_DSO": 40,   "p":   0              , "side":"m"},
            {"name": "Torregrossa",         "id_DSO": 41,   "p":   0.172413678    , "side":"l"},
            {"name": "Nuovo Carcere",       "id_DSO": 42,   "p":   0.02498749     , "side":"m"}

        ],
        "storage": [
            {"name": "Bue Marino",          "id_DSO": 1,    "size": 0.1325, "capacity": 0.750, "soc":  20,"side":"l"},
            {"name": "Gen. Di Vita",        "id_DSO": 6,    "size": 0.1325, "capacity": 0.750, "soc":  20,"side":"l"},
            {"name": "Torretta",            "id_DSO": 7,    "size": 0.1325, "capacity": 0.750, "soc":  20,"side":"l"},
            {"name": "4 Vanelle",           "id_DSO": 9,    "size": 0.1325, "capacity": 0.750, "soc":  20,"side":"l"}
        ],
        "controller_type": "hybrid",
        "plot": ["active power flow","line_losses","storage","storage_soc","storage_energy"],
        "mins_apf_on": ["SlackBus L1 - Cavallo", "SlackBus L2 - Suore Canossiane A", "SlackBus L3 - Centrale Elettrica"]
    }
  ]
}
```


Fig. 35. Hyperion simulation file

The first way consist in importing historical data from GD plant meters and using them as a reference for other plants to be simulated. Knowing the size of the reference system and the one to be emulated, it is possible to compute what the output might be. Fig. 36 shows a plot of a real PV profile. The second technique, on the other hand, is based on the use of PVGIS from European Commission Science Hub [107] production statistics and hourly data of dawn and sunset, on which an ideal parabola is generated and used to balance the output of the plant to be simulated. Fig. 37 show a plot where all the PV facility profile of a given simulation are overlapped.

Regardless of the calculation method, the output values of the plants are employed as static generators that feed power into the network in the node where the plant is installed in the control file at each step of time.

The ESS plants are simulated by modelling an accumulation for each node where storage is desired and a controller that supervises all of the plants. A fuzzy logic control technique was created for optimal storage system management, as well as a simpler control (at time intervals with flow inversion control on the feeders) for a more direct analysis of their behaviour. The type of management algorithm can be selected using an appropriate parameter in the simulation control file.

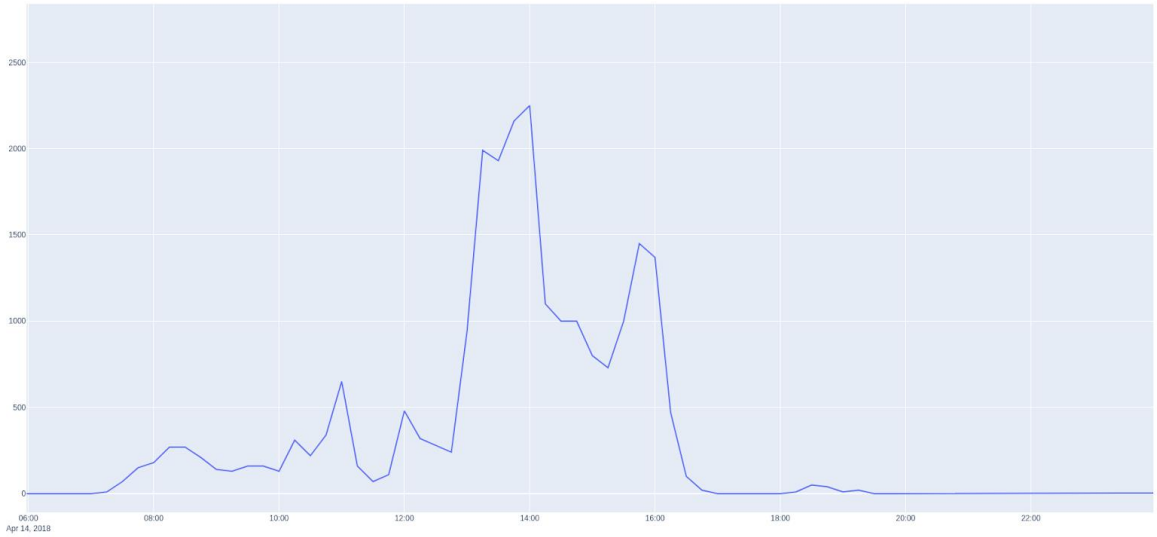

Fig. 36. Real production for the simulation of the GD (Photovoltaic) facility for 14 April 2018

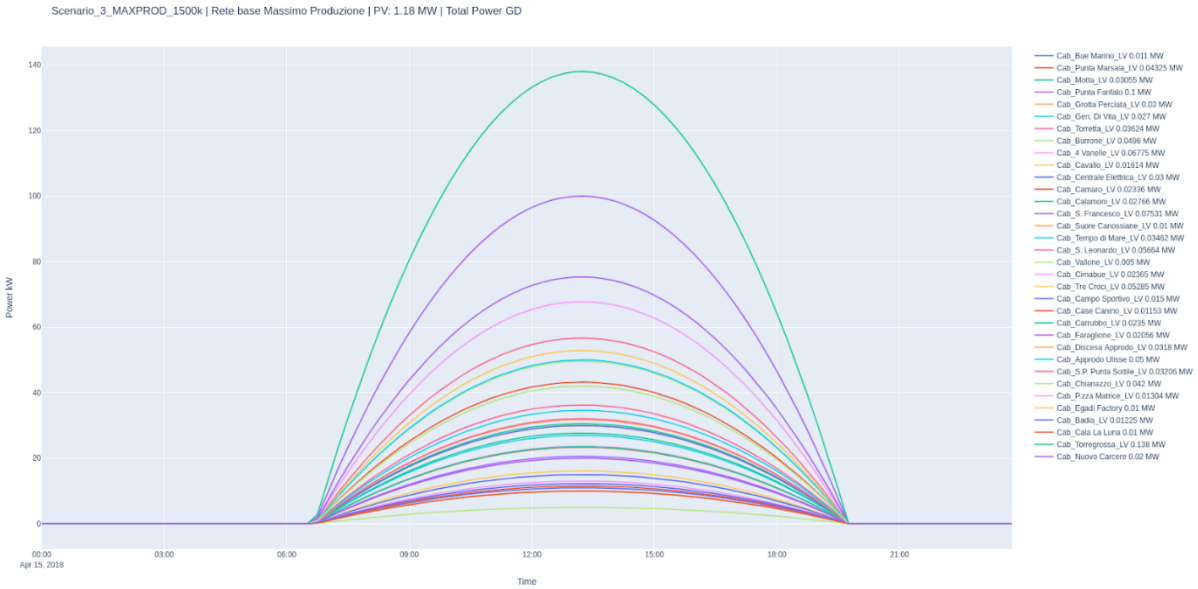

Fig. 37. Simulated production for each GD facility (Photovoltaic) on an ideal basis April 15, 2018

Within the control file (Fig. 35) there is a section dedicated to the choice of information to be displayed as output. In fact, the module, in addition to creating an excel file for an analytical display of the outputs, generates interactive graphics on html files which can then be viewed on a regular browser without the need for special programs. The following plots are currently available:

Plot	**Data**
active power flow	Lines active power flow
feeder sum	Feeders sum
reactive power flow	Line reactive power flow
loading percent	Percentage load of the lines with respect to their capacity
voltages	Voltage profile for each substation
voltages angle	Voltages angle
pv	Active power generated by GD facilities
storage	Active power generated/absorbed by ESS systems
storage energy	Energy generated/absorbed by ESS systems
storage soc	State of Charge of the ESS systems
line losses	Leaks on the line
trafo losses	Leaks on the transformers
currents	Line currents

Table 9. HTML output plot available

Some charts generated by the simulation are provided as examples. In Fig. 38 all the MV branches flux are showed as result of the simulation of the Favignana network for 13 and 14 August 2019.

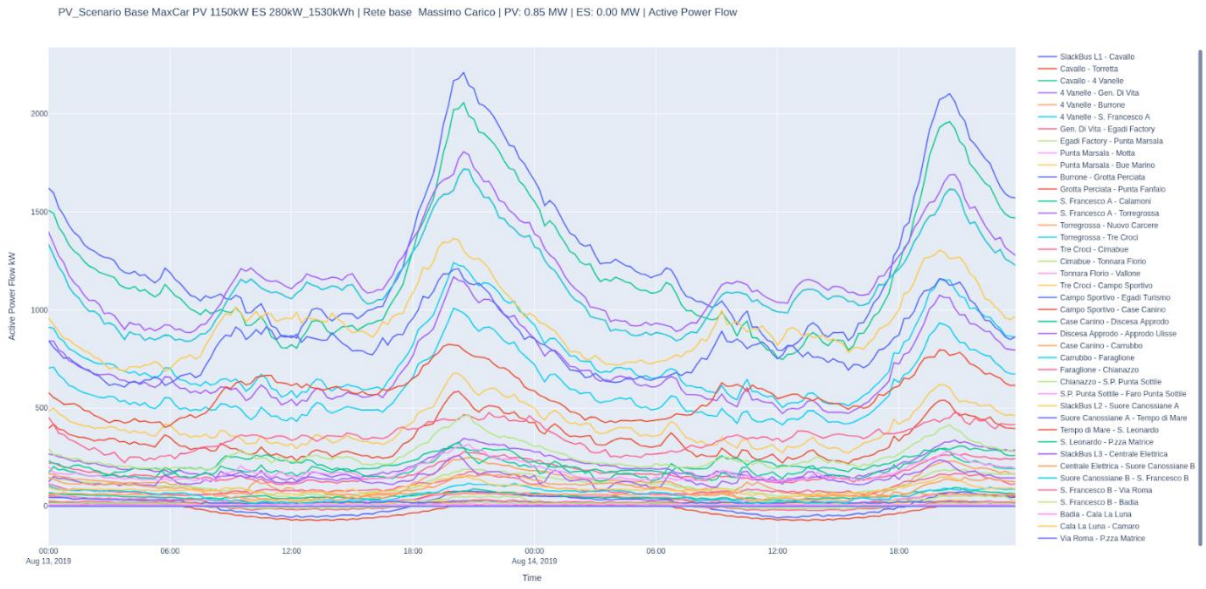

Fig. 38. Active Power Flux for each MV branch

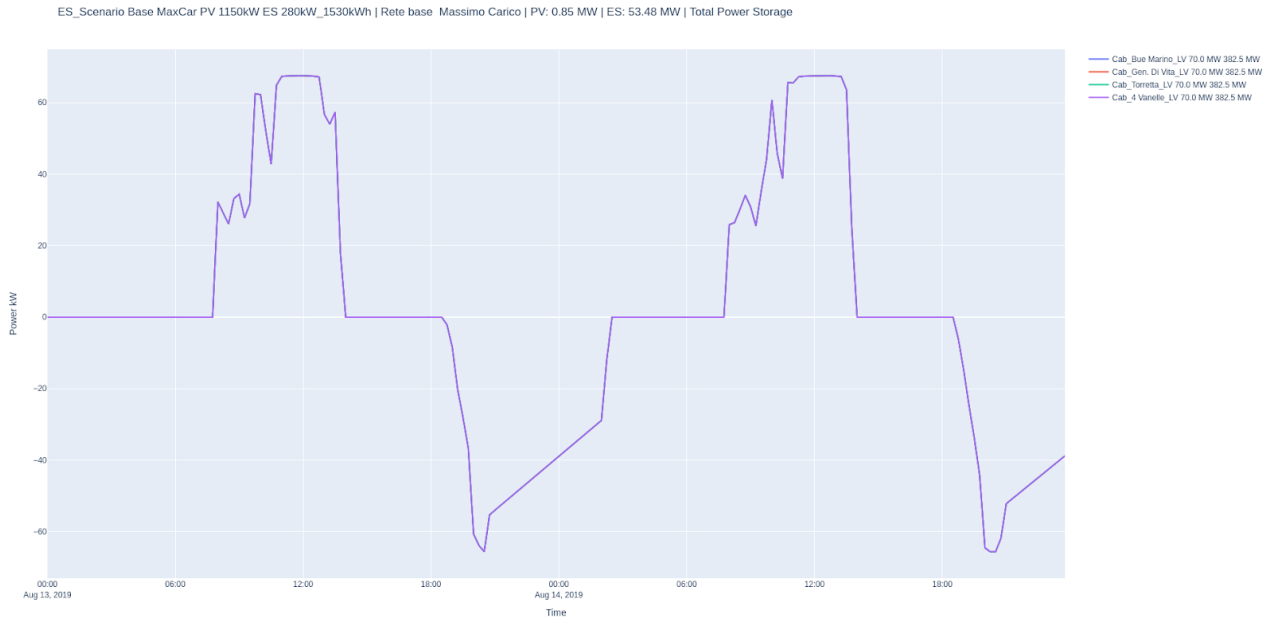

Fig. 39. Power generated / absorbed (load convention) by 4 Vanelle ESS system

In Fig. 39 the result of the simulation for 13 and 14 August of ESS 70kW 382kWh systems installed under 4 Vanelle substation in the Favignana grid is showed. In Fig. 40 the State of Charge of the same facility is showed.

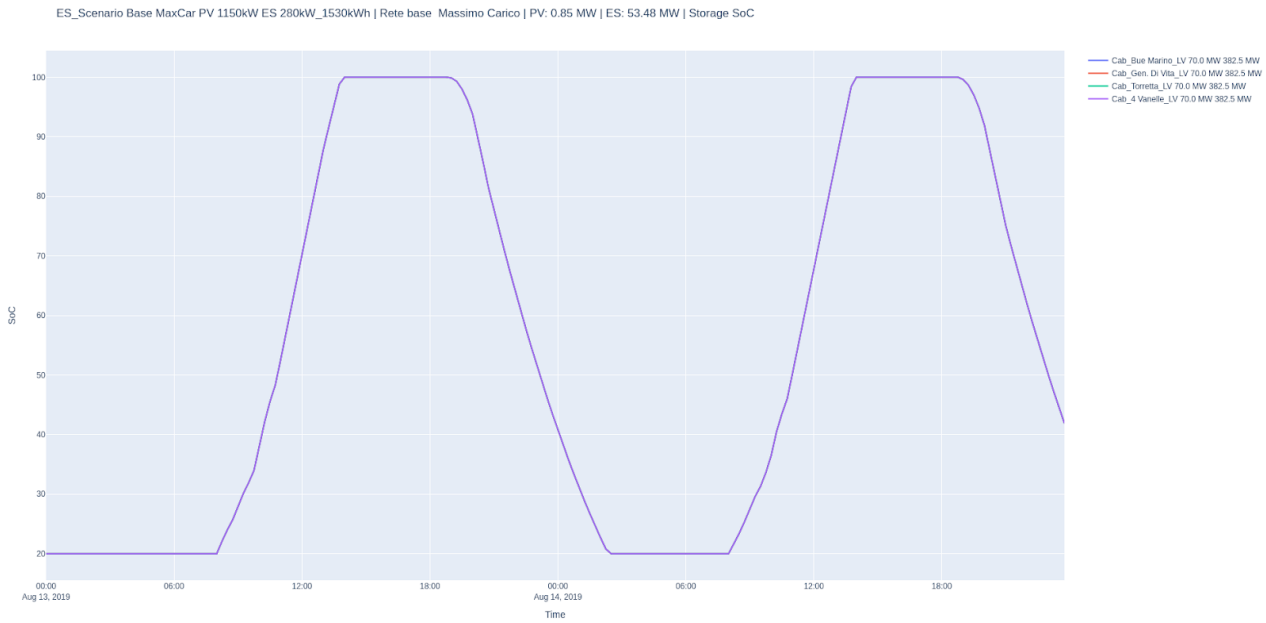

Fig. 40. State of Charge of 4 Vanelle ESS system

3.3.2.3 Real-time module

This module gives real-time access to Hyperion's basic functions. That is, it enables the DSO to process MV substation measurement data in real time, generating values for power flows on MV lines and, in the presence of distributed generation or storage systems, also suggestions for which systems to control and how. The information gained on the flux can, in fact, be used to regulate generations facilities. The information about the upstream flux, in particular, can be used as suggestions for regulating the diesel groups at the main power plant. Unlike the simulation module, the real-time module ingests data by providing a set of APIs that are accessed by SCADA applications. For example, measurements are submitted to Hyperion via an HTTP POST call that includes the data required for processing in the body. The results of the call will be returned to the caller. The OPC standard is also being explored for adoption in industrial areas that require it. The measurements received throughout the data intake process are subsequently recorded to a relational database and used by the core to calculate load flow.

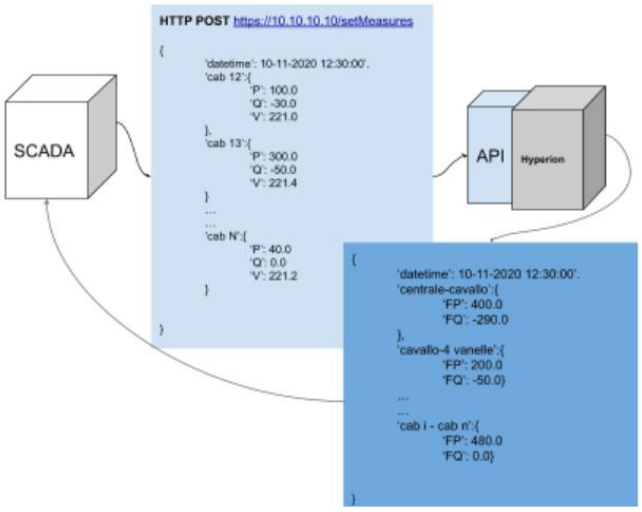

Fig. 41. Hyperion SCADA Integration

As previously stated, calculated values of power flux on MV lines are returned in response to an API call. Furthermore, control files can be generated in the same way that they are in the simulation module. In particular, xlsx files for analytical control of derived values and interactive html plots that display the instantaneous or time-consuming trends of the parameters to be monitored can be generated.

4 POWERLINE COMMUNICATION FOR SMART GRID PARADIGM

4.1 COMMUNICATION REQUIREMENTS

A reliable real-time flow of information between different components of the grid is a crucial and integral need of the smart grid vision. As a result, the establishment of a smart grid requires a specialised and secure communication medium. Because there are just a few sensors deployed in the grid, the traditional power grid only has a limited communication infrastructure. Furthermore, most of the data these sensors are designed to convey is not in real time. The smart grid, on the other hand, will necessitate a vast deployment of sensors at various levels across the system, as stated in the previous section. A reliable and strong communication infrastructure is necessary in the smart grid to accommodate such a large amount of data flow. Apart from improved power grid monitoring and control, communication infrastructure is necessary to support several new but distinct smart grid functions. Some examples of such applications include data flow from household appliances to smart meters and communication between smart meters and data concentration centres.

Because two-way communication will be adopted at most levels, the communication system in the smart grid will be sophisticated. Furthermore, communication systems are required for the use of appliances such as smart meters. In order to develop reliable and robust communication, such a complicated communication system will encounter a number of issues that must be resolved. Some of these issues are covered farther down.

- Interference

  The implementation of smart meters in consumers' homes is a critical component of the smart grid. In today's world, a normal household contains a large number of electrical and electronic equipment, and this number is growing every day. In today's houses, a home area network (HAN) is a reality. Interference between home area networks and smart meters may occur as a result of this widespread implementation. It could also lead to the transmission of faulty signals from smart meters, compromising the system's security. Harmonics emitted from electricity lines can also cause interference with the smart grid's communication system.
- Data Transmission Rate

  The communication system in a smart grid is critical for data gathering, processing, and transmission of control actions to the smart grid's components and devices. However, the smart grid's requirement for a large number of smart meters and real-time sensors will generate a large volume of data that must be transferred in a fast and secure manner. Furthermore, the need for two-way communication must be met. As a result, communication devices capable of conveying large amounts of data in a secure and timely manner are a must for the smart grid.
- Standardization

The power grid is made up of many different components. As an integral part of the grid, the smart grid necessitates two-way communication among many of these disparate components. Implementing such a system necessitates the use of an integrated communication system. .

Distributed control and measurement systems, as described in chapter 2, have become critical for network monitoring and management, as well as the implementation of various intelligent functions such as system state knowledge, remote control of DG, real-time analysis of energy flows, AMR, DSM, network diagnostics, fault detection, and so on [108,109]. Typical electrical quantities (such as power, voltage, current, switch status, electricity production, and remote controls) as well as environmental and other characteristics are among the data collected by the network (monitoring and warning on temperature, safety or security, etc.). These data must be shared throughout the smart grid's various actors, including DSOs, active consumers, and prosumers. As a result, developing a capillary communication system that is reliable, cost-effective, and simple to install for both MV and LV distribution networks becomes a vital necessity of smart grids. Wireless communication infrastructures (mostly GPRS) and PLCs are the most often utilised solutions in electrical networks.

Power line communication (PLC) is a generic term for any technology that uses the power line as a communication channel. The idea of using power lines also for communication purposes has already been around at the beginning of the last century. The use of PLC technology has several advantages, the most important of which is the low cost of installation and the fact that the communication network already exists under the control of the DSO, requiring no additional wiring beyond the pre-existing power lines, limiting deployment costs to the cost of connecting modems to the existing electrical grid. One of the most significant criteria for PLC applications is that all of the components must be connected reliably at all times, in any environment, and must be resistant to interference. Because electricity lines are shared media, there is a lot of interference that makes it difficult to communicate data reliably. As a result, particular consideration must be given to making PLCs perform in severe settings [110]. It has been common practice to distinguish power line communication scenarios according to operation voltages of the power lines [111].

High-voltage (HV) lines, with voltages ranging from 110 kV to 380 kV, consist of long overhead lines with few or no branches, and are used for state-wide or even international power transfer. As a result, they have lower attenuation per line length than their medium and low-voltage equivalents, making them ideal wave guides. However, their ability to provide broadband SG communication services has been limited to this point. The practicalities and costs of coupling communication signals in and out of these lines have been a concern due to time-varying high-voltage arcing and corona noise with noise power swings in the order of several tens of dBs. Furthermore, fibre optical networks are in strong rivalry. These links may be spliced together with the HV system's ground conductor in some circumstances[112,113]. Nonetheless, [114–116] reports on some successful experiments using HV lines.

Medium-Voltage (MV) lines through primary transformer substations, with voltages ranging from 10 kV to 30 kV, are connected to the HV lines. Power is distributed between cities, towns, and bigger industrial users via MV lines. They can take the form of above-ground or underground lines. They also have few branches and connect directly to intelligent electronic devices (IEDs) such reclosers, sectionalizers, capacitor banks, and phasor measurement units. Monitoring and controlling IEDs requires only a small amount of data, and NB-PLC can provide cost-effective communication solutions for these activities. [31,44,103,117,118] contains MV-related studies and trials.

Low-voltage (LV) lines, secondary transformer substations link to the MV lines with voltages ranging from 110V to 400V. However, a communication signal on an MV line can flow through the secondary transformer to the LV line with a significant attenuation of 55 to 75 dB [119,120]. If one wants to construct a high data rate communications path, a specific coupling device (inductive, capacitive) or a PLC repeater is typically necessary. The LV lines connect directly to the end customers' premises or via street cabinets. It should be noted that there is a significant regional topological variance. A smaller secondary transformer on a utility pole in the United States, for example, might serve a single house or a small group of houses. In Europe, however, it is more common for a single secondary transformer substation to service up to 100 households. The electrical grid usually enters the customers' premises through a house access point (HAP), which is followed by an electricity meter and a distribution board (fuse box). PLC systems that have been in operation up to this point are commonly referred to as Access systems. Because low voltage networks only reach a few hundred meters between the transformer unit and the customers, PLC provides an alternate approach for achieving "last mile" access.

Three main type of PLC technologies exists:

Ultra Narrow Band (UNB): Technology in the ultra-low frequency range (0.3–3 kHz) or the upper portion of the super low frequency band (30–300 Hz) that operate at very low data rates (less than 100 bps). The UNB-PLC has a wide operating range (150 km or more). Despite the low data throughput per link, the systems employed leverage a variety of parallelization techniques and efficient addressing to provide good scalability. Despite the fact that these UNB solutions are proprietary, they are very mature technologies that have been in use by hundreds of public utility agencies for at least two decades.

Narrowband (NB): technologies operating in the VLF/LF/MF bands (3–500 kHz), which include the European CENELEC bands, the US FCC band, the Japanese ARIB band and the Chinese band. Specifically, we have the following:

- Low Data Rate (LDR): single carrier technologies able of data rates of few kilobits per second. Some typical examples of LDR NB-PLC technologies are: LonWorks, IEC 61334, X10, HomePlug C&C, SITRED, etc.

- High Data Rate (HDR): multicarrier technologies capable of data rates ranging between tens of kilobits per second and up to 500 kbs. Typical examples of HDR NB-PLC technologies are: ITU-T G.hnem, IEEE 1901, PRIME and G3-PLC.

Broadband (BB): technologies operating in the HF/VHF bands (1.8–250 MHz) and having a PHY rate ranging from several megabits per second to several hundred megabits per second. Typical examples of BB-PLC technologies are: HomePlug 1.0 (and following version), IEEE 1901, ITU-T G.hn, etc.

To gain access and control over energy meters in private houses, AMR systems typically used ultra-narrowband power line communication (UNB-PLC) technologies like in [121] and [122,123]. UNB-PLC systems are often built to communicate over long distances using LV/MV transformers to transmit their signals. This helps to minimise the number of modems and repeaters required to a minimum. Low data speeds of 0.001 bit/s and 60 bit/s for in [121] and [109,110], respectively, are disadvantages, as are often constraints to unidirectional connections. These UNB-PLC technologies are included because they are pioneers in the field of AMR and distribution automation. However, with many planned Smart Grid installations, communication infrastructure requirements are substantially higher, for example, to enable demand response, distributed generation control, and demand side management applications. These applications, among others, are thought to be supported by PLC-based AMI. To meet rising AMI demands, UNB-PLC solutions were pushed to the background in favour of more contemporary narrowband PLC (NB-PLC) technologies like Power line-Related Intelligent Metering Evolution (PRIME) [124] and G3-PLC [125]. Bidirectional data speeds for NB-PLC are in the hundreds of kbit/s range, while yet keeping the ability to communicate across long distances and through transformers.

4.2 POWER LINE-RELATED INTELLIGENT METERING EVOLUTION – PRIME PROTOCOL

The PRIME (PoweRline Intelligent Metering Evolution) PLC technology (ITU G.9904) is an OFDM (Orthogonal Frequency Division Multiplexing) -based technology for coping with the challenges of smart grids in existing low-voltage and medium-voltage networks [124]. PRIME technology was developed within the PRIME Alliance and is now approved as the international ITU G.9904 standard. The PRIME Alliance (http://www.prime-alliance.org/) is an ecosystem of companies that focuses on the development of a new open, public and non-proprietary telecommunications solution that not only includes the smart metering functionalities, but also supports progress towards the smart grid. Iberdrola was one of the first utilities to use PRIME on a large scale to demonstrate the high performance of PRIME systems on the Spanish network and in other countries. Other supply companies worldwide (Energa-Operator, EDP, Gas Natural Fenosa, etc.) have PRIME operations in operation today (15+ from November 2014). The PRIME specification was the greatest achievement of the PRIME Alliance. This means that more than 26 different providers are able to offer

PRIME-certified products. PRIME v1.3.6 is the protocol version that is used successfully in millions of smart meters in the field today. In any case, within the active PRIME Technical Working Group, the PRIME specification has undergone an important advancement to improve system performance with two important features, robust modes and FCC / ARIB band expansion. PRIME v1.4 will [126] introduce a number of new modes called “robust modes” (as an example within CENELEC---A band, the addition of robust modes provides more reliable communications up to 14.5 dB gain compared to PRIME v1.3.6 but lower data rates with 5kbps and 10kbps) and will extend the frequency coverage up to 500 kHz to achieve higher data rates in environments where such extended frequencies can be used. These developments would not have been possible without extensive channel measurements by the PRIME Technical Working Group to validate the performance of the robust PRIME modes. The two new transmission modes are Robust DBPSK and Robust DQPSK, which add four OFDM symbol repetitions after the already existing PRIME v1.3.6 convolutional encoder. Headers with increased robustness are combined with longer preambles (= 8,192 ms) to protect against power line impulse noise. These robust modes enable communication in low signal-to-noise ratio environments and enhance the excellent results achieved in PRIME deployments around the world. One of the unique features of the robust PRIME modes is that repetition occurs at the OFDM symbol level rather than the bit level, so that more time domain diversity can be achieved. The bandwidth expansion to 500 kHz is intended to offer higher data rates of up to 1 Mbit / s for applications and areas in which other frequency bands can be used (America and Asia, other applications such as automotive communication). The PRIME bandwidth extension also includes the robust modes and longer preambles for reliable communication. All of these improvements come along with the necessary Media Access Control (MAC) layer adjustments. The MAC layer is a fundamental part of the PRIME specification. The MAC layer enhancements allow full backward compatibility of any development that is PRIME v1.3.6 compliant and ensure full support for the sound solutions provided by the multiple active vendors in the PRIME ecosystem. Most of the new functions in the MAC layer of the PRIME specification are also the result of the experience gained over the past four years in global field use analysing a large number of PRIME networks. Apart from the features resulting from the new physical layer (PHY) requirements, the main new features of the MAC layer in the PRIME specification v1.4 are aimed at reducing the overhead of the channel by increasing the size and flexibility of the Reduce the framework and reduce the number of control packets. For example, data packets and ALIVE packets are used to inform about the quality of each connection and decisions about the modulation scheme are made with this information in mind. In this article we describe some important features of the robust modes and FCC / ARIB band expansion.

4.2.1 PRIME System Architecture

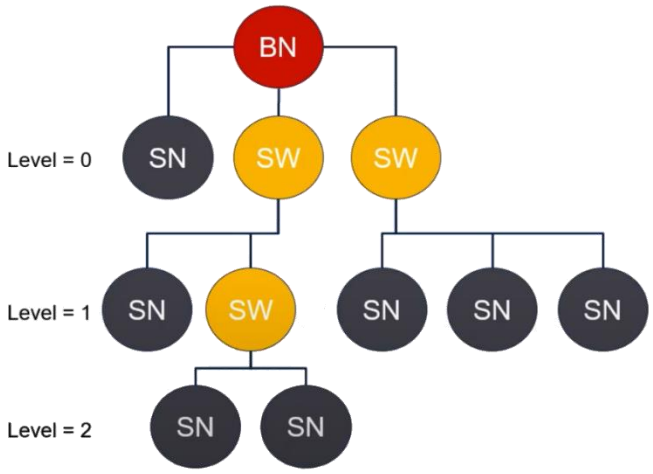

Fig. 42. PRIME Subnetwork tree architecture

PRIME devices, called service nodes (SN), automatically form a “tree” type network topology when plugged into the power line and are managed by a centralized “root” of the “tree” called a base node (BN). It transmits network synchronization beacons (BCN) and conducts key management operations such as Service Node registration, connection setup and management, resource allocation, and encryption, among other things. Connecting to the subnetwork to convey their own information and, if necessary, relaying information from neighbour Service Nodes are the two roles of Service Nodes. When a Service Node transmits solely its own data, it is referred to as a Terminal, however when it additionally relays data from neighbouring nodes, it is referred to as a Switch. The Base Node dynamically manages node promotion (from Terminal to Switch) and demotion (from Switch to Terminal). So basically PRIME systems forms subnets, with each subnet having a base node and several service nodes (Fig. 42).

There is a competition-free and a competition-based access mechanism, the usage time and duration of which are determined by the base node. Contention-based access uses CSMA / CA [88, 92]. To ensure data protection, authentication and data integrity, a security profile 1 is defined that uses 128-bit AES encryption [93]. The specification also defines a security profile 0, which does not correspond to any encryption, and leaves room for the definition of two further security profiles in future versions. In order to connect the MAC and the application layer, PRIME defines a convergence layer (CL) between the two. The CL can be divided into a Common Part Convergence Sublayer (CPCS) and a Service Specific Convergence Sublayer (SSCS). The CPCS takes on the tasks of data segmentation and assembly and is adapted to the respective application. Three SSCSs are currently defined: The NULL Convergence Sublayer offers the MAC layer a transparent way to use it, which is as simple as possible and minimizes overhead. It is intended for applications that do not

require any special convergence capability. The overall architecture is shown in Fig. 42

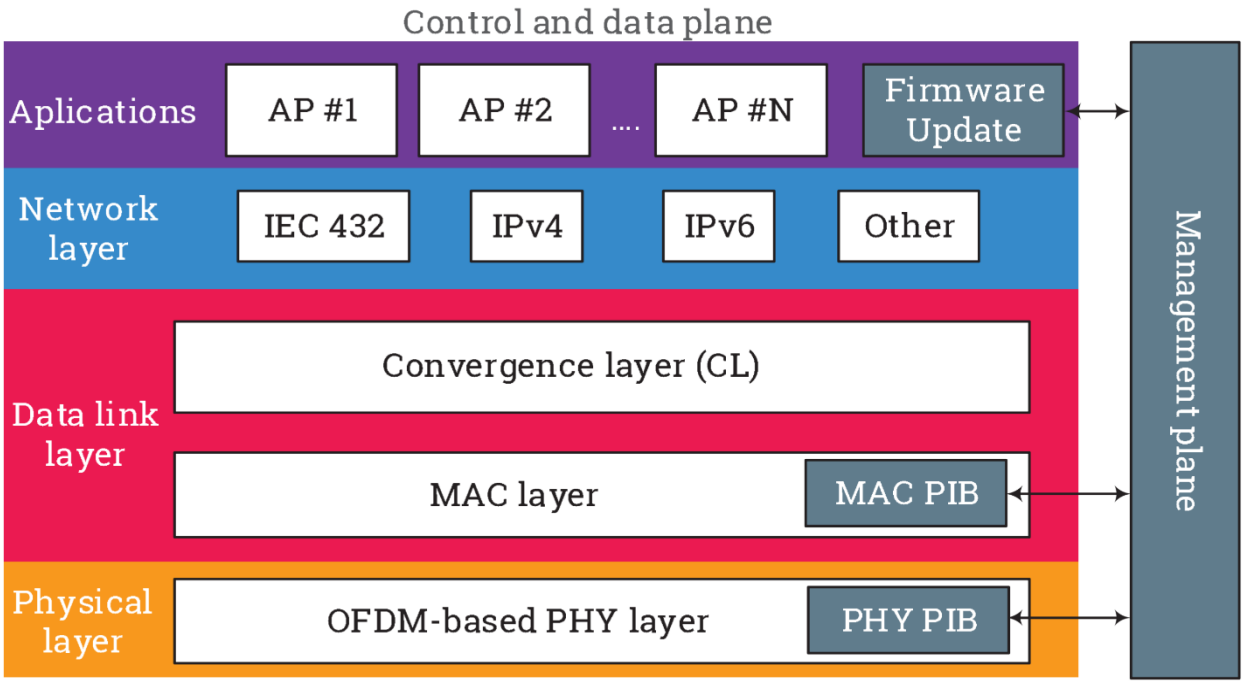

Fig. 42. PRIME system architecture [127]

4.2.2 PRIME Specifications

Fig. 43 below shows the communication layers and focuses on the data, control and administration level.

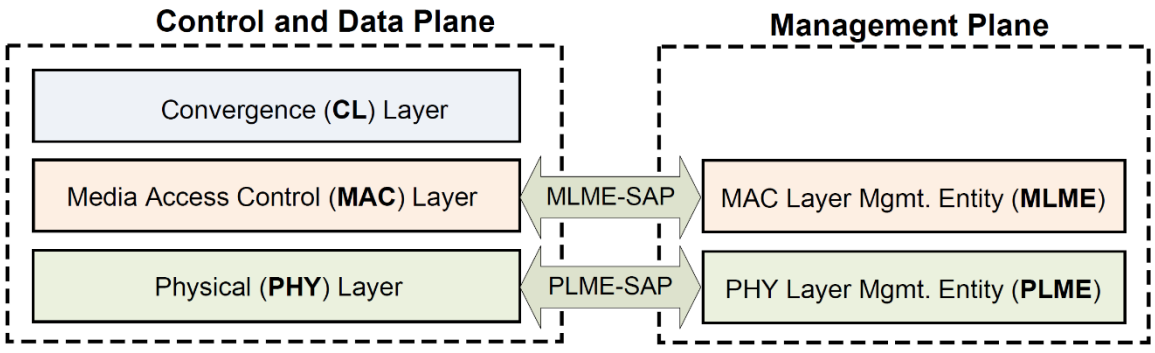

Fig. 43. Reference model of protocol layers used in the PRIME specification [124]

The Convergence Layer (CL) classifies the traffic by assigning it to its correct MAC connection; this layer does the mapping of each type of traffic to be properly included in MPDUs. It can also contain header compression functions. Multiple SSCSs are defined to accommodate different types of traffic in MPDUs. The MAC layer provides the core MAC functionalities of system access, bandwidth allocation, connection

establishment / maintenance and topology resolution. The PHY layer sends and receives MPDUs between neighbouring nodes using OFDM. OFDM is chosen as the modulation technique because of:

- its inherent adaptability in the presence of frequency selective channels (which are frequent but unpredictable due to narrowband interference or unintentional interference);
- its robustness to impulse noise resulting from the extended symbol duration and the use of FEC;
- its ability to achieve high spectral efficiencies with simple transceiver implementations.

The PHY specification described in 4.2.2.1 also uses a flexible coding scheme. The MAC can adapt the PHY data rates to the channel and noise conditions.

4.2.2.1 PHY Layer

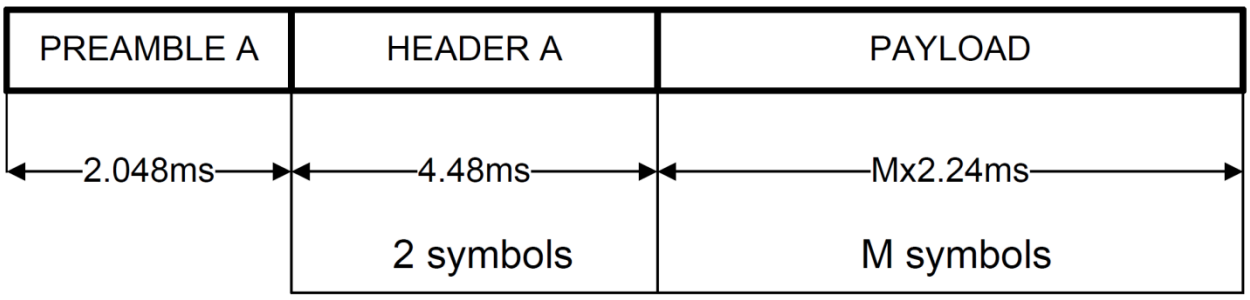

Fig. 44. PHY Frame of type A [124]

The PRIME specification v1.4 defines two types of PHY frames called Frame of Type A and Type B. The structure of the PRIME PHY frame of Type A is shown in Fig. 44. Each Type A PHY frame begins with a preamble of 2.048 ms, followed by 2 + M OFDM symbols, each 2.24 ms. The first two OFDM symbols carry the PHY frame header, while the remaining M OFDM symbols carry the user data. The value of M is signaled in the header and is at most equal to 63.

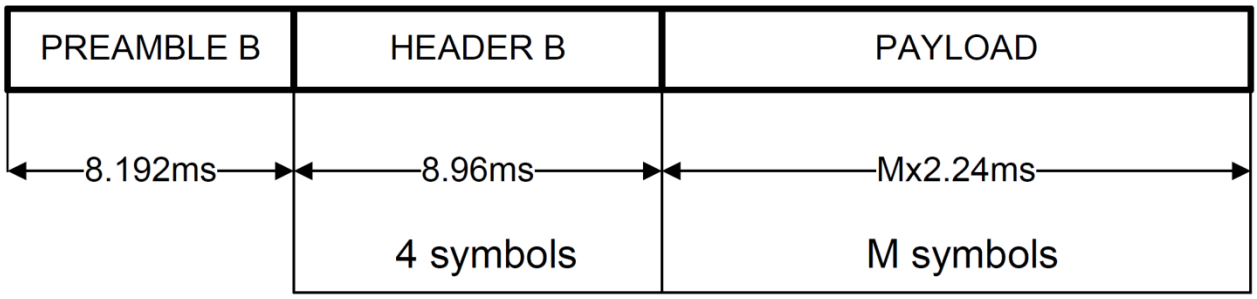

Fig. 42. PHY frame of type B [124]

The structure of the Type B PHY frame is shown in Fig. 42. Each type B PHY frame begins with a robust preamble of 8.192 ms, followed by 4 + M OFDM symbols of 2.24 ms each. The first four OFDM symbols

carry the PHY frame header, while the remaining M OFDM symbols carry the user data. The value of M is signaled in the header and is at most equal to 252.

The type A frame corresponds to the Physical Layer Protocol Data Unit (PPDU) defined in PRIME v1.3.6. The Type B frame is a new type of PPDU and contains a more efficient header specially designed to support the robust transmission modes. In addition, the Type B PHY header has several advantages:

1. It can signal four times more symbols than a Type A header because robust PPDUs are expected to be longer.
2. It offers up to 8 times more padding than Type-A headers.
3. Its CRC is 12 bits instead of 8 bits, which reduces the possibility of false positives in the PHY layer by 16 times.
4. It is smaller than type A header by reducing the MAC layer information so that it can be encoded in 4 symbols after repetition (1 symbol before repetition). The type A header uses 2 symbols with no repetition mechanism.

Depending on the channel conditions, the transmitter can use the type B frame to benefit from its greater robustness, or the type A frame which has a reduced overhead, whereby higher transmission efficiency can be achieved. Both the type A and type B PHY frames defined by PRIME v1.4 support the FCC / ARIB band expansion, i.e. robust modes are available in combination with frequency band expansion.

4.2.2.1.1 Robust Modes

In order to cope to the very harsh environments that can be found in certain countries and operating conditions, additional optional robust transmission modes have been introduced in the PRIME specification v1.4. These modes were developed to improve the robustness of the system against impulse noise and interfering noise. In particular, all parts (preamble, header and payload) of the Type B PHY frame have been improved by introducing a repetition factor of four.

4.2.2.1.2 Preamble Extension

The PRIME v1.4 preamble is based on a linear chirp signal that has three important characteristics:

1. Constant signal envelope. The preamble can provide a higher level of energy compared to the OFDM signal that forms the remainder of the frame.
2. Flexible frequency definition. The preamble can be defined in different frequency intervals.
3. Excellent autocorrelation properties.

In order to give the preamble of type B additional robustness against impulsive noise, the chirp sequence forming a preamble symbol $S_{PS}(t)$ is repeated four times, which leads to a preamble length of approximately 8.192 ms. The last preamble symbol has a phase inversion that can be used by the receiver for accurate frame synchronization. In the case of several channel bands, each preamble symbol $S_{PS}(t)$ consists of the

concatenation of two or more sub-symbols $S_{SS}(t)$. The number of sub-symbols corresponds to the number of active channels used at the same time. Each sub-symbol contains a chirp signal that is defined on the frequencies of one of the active channels. In order to reduce spurious spectral emissions and avoid signal distortion due to frequency discontinuities, the top and bottom samples of each sub-symbol are shaped and overlapped with the neighbouring sub-symbol. This approach gives maximum freedom in defining the channel assignment, while maintaining the constant signal envelope and the good autocorrelation properties of the single-channel preamble.

4.2.2.1.3 Repetition Encoding

The forward error correction mechanism (FEC) of the robust transmission modes of PRIME v1.4 consists of the concatenation of convolutional coding and repetitive coding, as shown in Fig. 47.

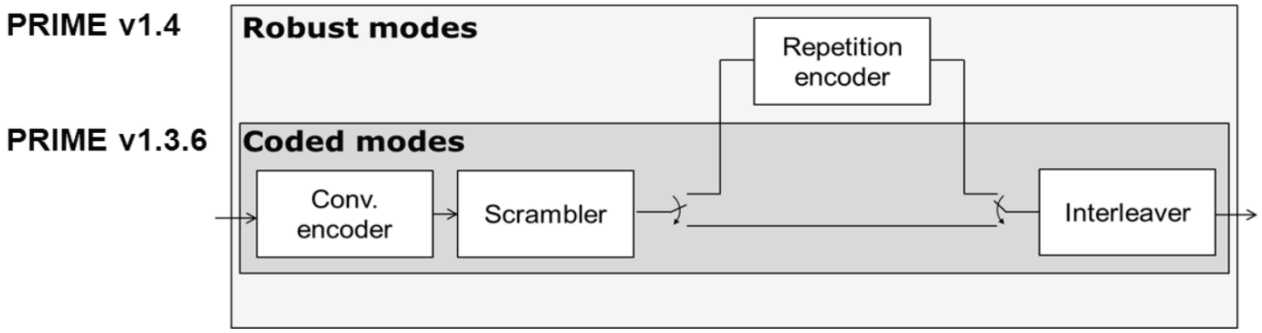

Fig. 47. Block scheme of the PRME v.1.4 robust FEC mechanism [124]

The PRIME v1.4 repeater block repeats the convolutional encoded bit sequence assigned to an OFDM symbol by a factor of four. Since each repeated sequence is placed on a different OFDM symbol, the time diversity of the system increases with a consequent improvement in the resistance to impulsive noise bursts. In addition, thanks to a cyclical shift in the repeated sequences, each bit replica is placed on a different frequency, which gives the system a frequency diversity. This leads to a strong improvement in system performance in the case of narrow-band interferers and channel notches. A pictorial description of the PRIME v1.4 repeat coding is given in Fig. 47.

The specially developed repeat coding of the PRIME v1.4 makes it possible to obtain the above improvements (time and frequency diversity) while maintaining a symbol-based interleaver. This solution has three important advantages over the alternative solution of increasing the interleaver block size:

1. it has less complexity, less memory footprint and less cost;
2. It facilitates PRIME v1.3.6 backward compatibility as the same interleaver can be reused to decode PRIME v1.3.6 and PRIME v1.4 frames;
3. It does not increase the decoding latency as any OFDM symbol can be processed instantly.

In order to enable the choice of the best compromise between robustness and throughput, both DBPSK and DQPSK modulations are supported in the robust transmission modes. In fact, using DQPSK modulation

reduces the throughput loss due to repetition coding while maintaining the benefit of both time and frequency diversity.

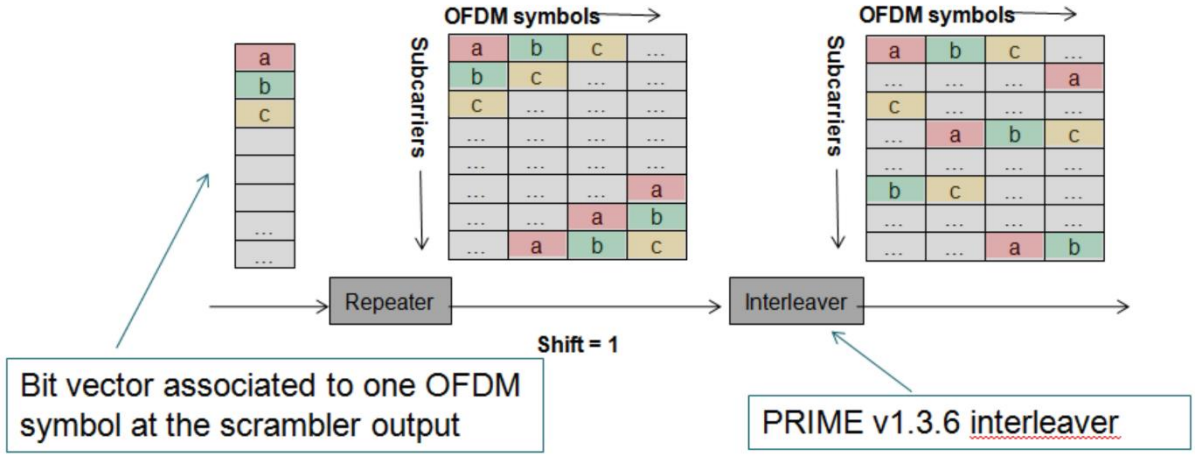

Fig. 47. Repetition encoding description [124]

According to the simulation results carried out by the members of the PRIME Technical Working Group during the specification definition, the robust DBPSK mode enables an improvement in system performance of around 4 dB in the case of additive white Gaussian noise, which enables reliable communication with a signal-to-signal - Noise enables a power ratio of 0 dB (1% of the image error rate with a payload of 256 bytes). The increase in performance is much higher in more disruptive scenarios. For example, a notched channel showed an increase in performance of more than 6 dB and a maximum gain of 14.5 dB was achieved for impulsive noises. These results are based on the measured channels in the power grids of the PRIME Technical Working Group.

4.2.2.1.4 FCC/ARIB frequency band extension

The PRIME PHY originally specified an OFDM modulation scheme in the CENELEC A band (3 kHz to 95 kHz), which is intended for distribution network operation in accordance with EN 50065-1. The successful introduction of PRIME technology in many of the countries regulated by CENELEC has led to increasing demand outside of Europe with the consistent further development of the specification. PRIME v1.4 extends the system band up to 500 kHz, eight times the originally available bandwidth. The use of this extended frequency range is subject to the applicable local regulations, e. EN 50065-1 in Europe or FCC Part 15 in the USA. The PRIME v1.4 PHY specification uses the frequency band from 41.992 kHz to 471.6796875 kHz. This area is divided into eight channels that can be used either as individual independent channels or NCH of

them simultaneously as a unique transmit / receive band. Fig. 49 shows the channel assignment of PRIME v1.4.

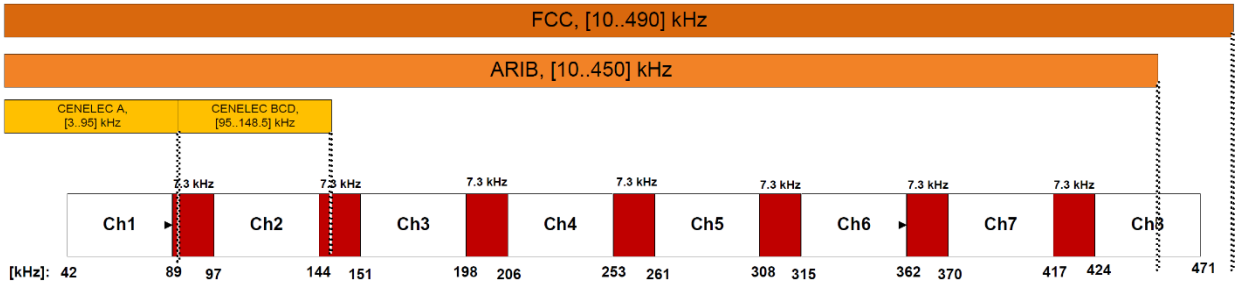

Fig. 49. PRIME v1.4 FCC / ARIB frequency band extension [124]

OFDM modulation is specified in each channel with the data signal loaded on 97 equally spaced sub-carriers and transmitted in symbols of 2240 µs, 192 µs of which is a short cyclic prefix. Adjacent channels are always separated by guard intervals of fifteen sub-carriers (7.3 kHz). The new PRIME v1.4 PHY Layer designates the PRIME v1.3.6 header as type A and extends the concept of this header for band expansion by more MPDU bytes in the two header symbols that are transmitted in the additionally available channels.

PRIME v1.4 offers extremely high flexibility as the eight available channels can be combined in many different ways to form “bands”. The number of supported bands and their configuration is called the “band plan” and is managed by the MAC layer. By combining several channels into one band, PRIME v1.4 can achieve baud rates of at least 5.4 kbps (one channel in the most robust mode) to a maximum of 1028.8 kbps (eight channels in the less robust mode). These baud rates are listed in Table 10

Sub-carrier modulation scheme	DBPSK			DQPSK			D8PSK	
Convolutional code (1/2)	✓	✓	✗	✓	✓	✗	✓	✗
Repetition Code	✓	✗	✗	✓	✗	✗	✗	✗
Raw data (kbps)	$N_{CH} * 5.4$	$N_{CH} * 21.4$	$N_{CH} * 42.9$	$N_{CH} * 10.7$	$N_{CH} * 42.9$	$N_{CH} * 85.7$	$N_{CH} * 64.3$	$N_{CH} * 128.6$

Table 10. PRIME v1.4 data rates where $1 \leq N_{CH} \leq 8$ *is the number of active channels*

The typical noise behaviour in a standard Powerline channel favours transmission in higher channels. A possible application, the e.g. three upper channels (Ch5, Ch6 and Ch7) in DQPSK_CC would provide a raw baud rate of 128 kbps. The service nodes contain a set of specific pre-configured bands. This so-called band plan is deployment-specific. The PRIME compliance tests define which bands are mandatory for a service node. The MAC section of the PRIME v1.4 specification lists some basic rules for how service nodes should search the various bands of the plan to automatically determine which band to operate.

4.2.2.2 MAC Layer

The new robust PHY frames (type B) are longer and therefore imply a different use of the channel. Beacons with robust modulation are up to four times longer than beacons with non-robust modulation. To maintain throughput, the MAC introduces two new features:

- The MAC frame (Fig. 50) length is flexible and can be 276, 552, 828 or 1104 symbols long. The frame length is commanded by the base node. The longer frames reduce the amount of time that is used for beacon transmission, thus increasing throughput at the expense of slower network convergence. Base nodes choose an optimal policy based on the extent of the robust mode transmission on the network.
- The beacon slot concept has been revised to support the different beacon lengths. Beacon slots and conflict-free zone (CFP) are merged in PRIME v1.4 into a single CFP at the beginning of the MAC frame. Beacon positions have been defined in symbols since the start of the frame. The base node is responsible for reserving a contest-free period for the beacons from the MAC-CFP area. This specification improvement enables base nodes to optimally plan beacons and thereby minimize the time reserved for beacon transmission.

Changes to the frame structure and the beacons can be initiated by the base node with the help of control messages.

The robust type B PHY frames use a longer preamble. The length of the preamble has an important influence on the determination of the channel occupancy. It was necessary to adapt the parameters used in the CSMA-CA algorithm. To maintain efficiency in networks that do not use robust modulations, two sets of parameters are defined. Depending on whether robust mode transmissions are used in a PRIME network, the base node commands the service node to use one or the other set of parameters. The information about which parameter set a service node should use is disseminated through the network as part of the beacons.

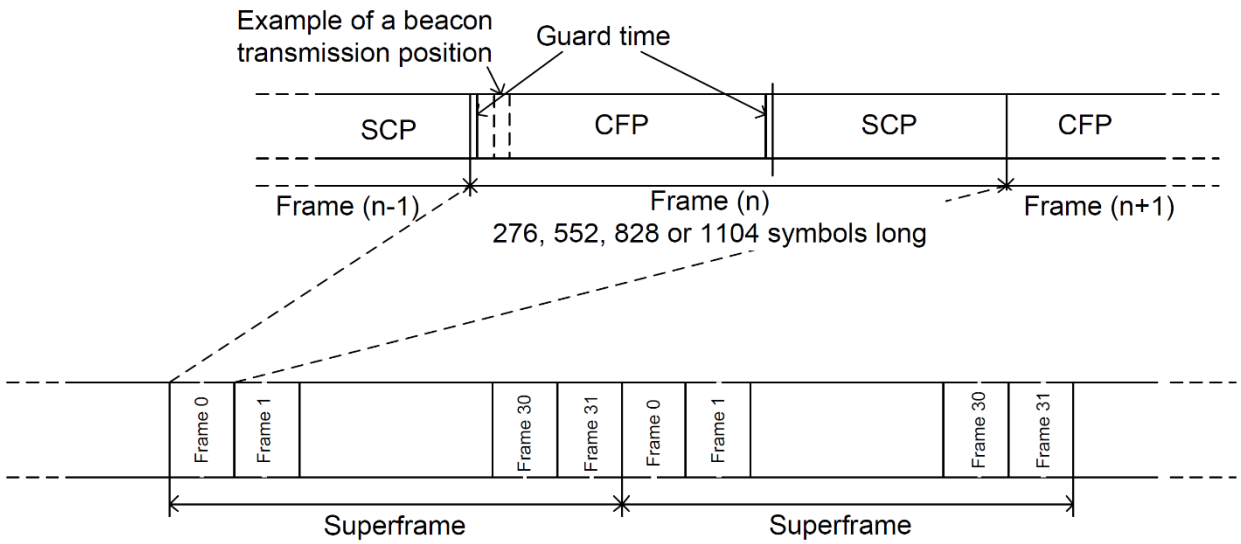

Fig. 50. MAC Frame Format [124]

4.2.2.2.1 Modulation Selection

The robustness management (RM) mechanism has been revised to support the new robust mode modulations. It is designed to select the most suitable transmission scheme from the eight available (Robust DBPSK, Robust DQPSK, DBPSK_CC, DBPSK, DQPSK_CC, DQPSK, D8PSK_CC and D8PSK). Depending on the transmission channel conditions, the nodes should decide either to increase the robustness or to select faster transmission modes for generic DATA packets. MAC control packets are not subject to this mechanism and are transmitted in Robust DBPSK, Robust DQPSK or DBPSK_CC.

By default, the decision about the applicable transfer mode is made locally. That is, a dynamic adaptation of the transmission mode is carried out taking into account channel information at the connection level that is exchanged between any pair of nodes in direct view (parent and child). As an exception to this rule, a base node can decide to deactivate dynamic robustness management and to force a certain transmission mode in the service node (s). This static configuration is set during registration. The robustness management mechanism has two main features:

- Link quality information, which is embedded in the packet header of all generic packets.
- Link level ACK-ed ALIVE mechanism.

4.2.2.2.2 Link quality information embedded in the packet header

All generic packets transmit connection quality-related information. Four bits in the packet header are used by the sending device to inform the other peer of the weakest modulation scheme that the sender assumes it could receive from that specific peer. The sending device calculates this value by processing the received packets sent by the other peer. Whenever a node receives a generic packet from a peer, it should update some information regarding the sending peer. Basically the modulation scheme that the sender considers possible (4-bit value contained in the transmitted header) and at the same time the receiving node should reset a time stamp that is used to check whether this information is valid or not.

Whenever a node wishes to transmit DATA to an existing peer, it must check the validity of the robustness management information it stores in relation to that peer:

- If the robustness management information is out of date: The node must transmit using the most robust modulation scheme for the PHY frame type used available. Note: The first time a node sends DATA to a peer, the RM information is automatically considered to be “out of date” and therefore the most robust modulation scheme available should be used.
- If robustness management information is valid: The modulation scheme previously saved by this node can be used for transmission.

4.2.2.2.3 Link level ACK-ed ALIVE mechanism

The ALIVE procedure has been modified to work hand in hand with the new RM mechanism. It defines repetitions that are carried out in each hop, both in the downlink and in the uplink. A device that sends ALIVE packets must use this fact to accept a delivery error if it does not receive the corresponding ACK packet. In this case, the sending device should retransmit the packet: The first repetition should be carried out with the same robustness that is successively increased after each repetition at the link level. Once the maximum number of repetitions is reached, the least robust modulation in which the node can transmit could be stored, even if the repetitions are due to the ACK packets, should the robustness management information correct a change to a more robust modulation than required. The device that receives the ALIVE packets must send the ACK packet with at least the same robustness as the received packet when it receives a packet that is sent more than twice. The ALIVE packets should be transmitted in one of the following encoding: DBPSK_CC, Robust DQPSK and Robust DBPSK. The robustness increase should be carried out in this order. In addition to supporting RM, the new ALIVE procedure has other advantages. The new ALIVE package contains information about the quality of each link. This information provides the base node with precise information about the entire network.

- All of these new features have some bandwidth costs that are lower than independent robustness management packages. To reduce these costs even more, some optimizations have been added. The

maximum ALIVE time has been increased by 8 so that a network can manage more devices than a PRIME v1.3.6 network. If all nodes were robust, they could hold twice as many nodes as they do today with the same ALIVE bandwidth.

- Switch nodes update their ALIVE time every time they switch an ALIVE on nodes that are dependent on them, reducing the need to perform ALIVE operations on them, while being more robust to collisions and making the networks more stable.
- When ARQ data packets or some control packets are received from the base node, the receiving terminal node updates the timer for the ALIVE sequence.

4.2.2.3 Convergence Layer

There are two sublayers in the Convergence layer. A collection of generic services is provided by the Common Part Convergence Sublayer (CPCS). The Service Specific Convergence Sublayer (SSCS) is a collection of services that are tailored to a single communication profile. There are multiple SSCSs, one for each communication profile, but only one CPCS. The utilisation of CPCS services is optional, in the sense that a given SSCS will use the services it requires from the CPCS while ignoring those it does not. The structure of the Convergence Layer is show in Fig. 51

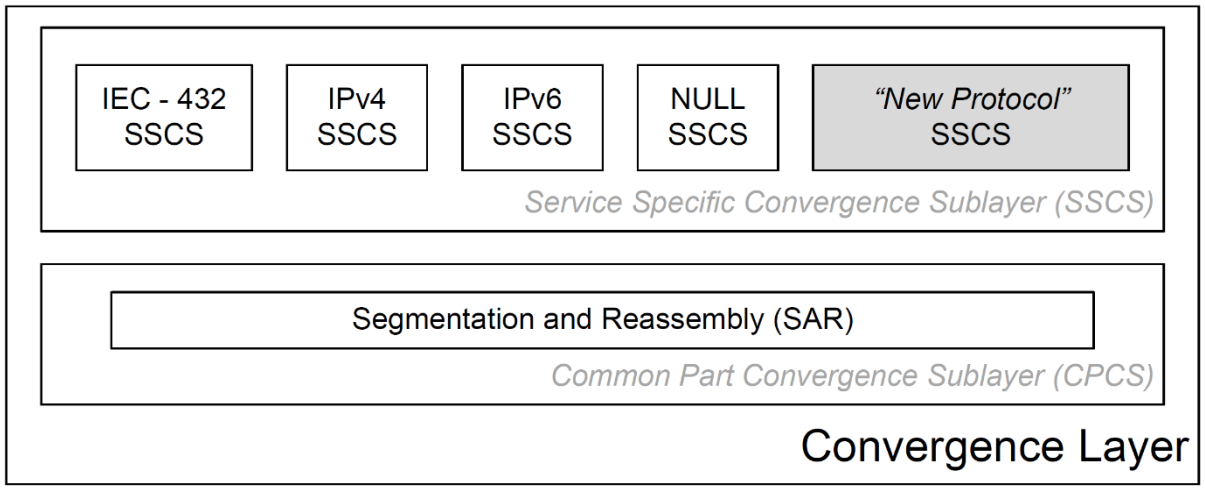

Fig. 51. Structure of Convergence Layer

Only the Segmentation and Reassembly service is defined in the CPCS (SAR). At the CPCS, CPCS SDUs that are greater than'macSARSize-1' bytes are segmented. CPCS SDUs that are equal to or less than *'macSARSize -1'* bytes may be segmented as well. Segmentation is the process of breaking down a CPCS SDU into smaller parts so that the MAC layer can transfer them. The smaller parts (segments) are reunited

(reassembled) at the peer CPCS to construct the entire CPCS SDU. All segments of a segmented SDU, save the last, must be the same size and have a maximum length of *macSARSize* bytes. When the channel is bad, segments may be decided to be smaller than *'macSARSize -1'* bytes. Of course, the last segment could be smaller than *'macSARSize -1'* bytes. The *macSARSize* is a constant value for all conceivable modulation/coding combinations at the PHY layer to keep SAR functionality simple. The value of *macSARSize* is such that it is always possible to transmit a single segment in a single PPDU with any modulation/coding combination. As a result, there's no need to find a unique MTU between peer CPCSs or update the SAR setup for each change in modulation/coding combination. When connecting with its peer, a Service Node that supports packet aggregation can combine numerous segments into one PPDU to boost efficiency.

Null SSCS (aka CL NULL) provides a transparent path to upper levels for the MAC layer, keeping things as simple as possible and minimising overhead. It's designed for applications that do not need any special convergence capability. The SAR service, as defined above, will be used by this SSCS's unicast and multicast connections. Even if they do not require the SAR service, the SAR heading must be included (notifying just one segment). Null SSCS primitives are just a direct mapping of the MAC primitives. Because the mapping is direct and they will work like the ones in the MAC layer, a complete explanation of each primitive is avoided and can be found in [128]. The directly mapped primitives have the same parameters and execute the same functions as those in the MAC layer. Below in Fig. 52 is a list of the primitives that are directly mapped.

Null SSCS mapped to …	**… a MAC primitive**
CL_NULL_ESTABLISH.request	MAC_ESTABLISH.request
CL_NULL_ESTABLISH.indication	MAC_ESTABLISH.indication
CL_NULL_ESTABLISH.response	MAC_ESTABLISH.response
CL_NULL_ESTABLISH.confirm	MAC_ESTABLISH.confirm
CL_NULL_RELEASE.request	MAC_RELEASE.request
CL_NULL_RELEASE.indication	MAC_RELEASE.indication
CL_NULL_RELEASE.response	MAC_RELEASE.response
CL_NULL_RELEASE.confirm	MAC_RELEASE.confirm
CL_NULL_JOIN.request	MAC_JOIN.request
CL_NULL_JOIN.indication	MAC_JOIN.indication
CL_NULL_JOIN.response	MAC_JOIN.response
CL_NULL_JOIN.confirm	MAC_JOIN.confirm
CL_NULL_LEAVE.request	MAC_LEAVE.request
CL_NULL_LEAVE.indication	MAC_LEAVE.indication
CL_NULL_LEAVE.response	MAC_LEAVE.response
CL_NULL_LEAVE.confirm	MAC_LEAVE.confirm
CL_NULL_DATA.request	MAC_DATA.request
CL_NULL_DATA.indication	MAC_DATA.indication
CL_NULL_DATA.confirm	MAC_DATA.confirm
CL_NULL_SEND.request	MAC_SEND.request
CL_NULL_SEND.indication	MAC_SEND.indication
CL_NULL_SEND.confirm	MAC_SEND.confirm

Fig. 52. Primitive mapping between the CL NULL and the MAC layer primitives [124]

4.3 PLC PROPOSED ARCHITECTURE

Several research on the use of this technology for communications in Smart Grids have been presented in recent years. We looked into the use of PLC on both LV and MV networks in particular. For example, in compliance with CEI 0-21, the usage of Narrow Band PLC as a communication link for monitoring and controlling the DG connected in the LV network was examined in [40]. A new interface protection system (IPS) and a data concentrator were proposed as part of the solution. The developed IPS included communication capabilities via a PLC modem in the CENELEC A band. Apart from supporting the same PLC communication features for information exchange with the IPS connected to the LV network, the concentrator also included an Ethernet interface for connection with the DSO. The application of PLC technology in MV networks was also examined by authors in [21,78,129]. The authors published the results of a patented PLC coupler in [78] and [129], which can overcome the restrictions of employing PLC at the MV level by requiring cheap installation costs and no changes to MV switchboards. We developed an intelligent measurement, control, and communication architecture for Smart Grids in [21], based on the usage of PLC technology at both the LV and MV levels. Experiments on the field, specifically on the power distribution network on the Italian island of Favignana [21], were conducted to verify the practicality of this intelligent architecture. The ST7580 modulator was used for both the MV and LV PLC links. Single carrier nPSK modulations were used to perform various physical transmission experiments (PHY) in the frequency range from 62 to 200 kHz. Here, a communication system for smart grids is proposed, still based on PLC technology, but offering better performances and new capabilities. These are achieved by implementing the PRIME communication protocols that were not present in the previous version and that can increase efficiency, robustness and security in the management and control of the DG connected to the DSO network. In order to implement the PRIME protocol, it was also necessary to change the hardware used. More specifically, the concentrator was redesigned using new hardware for new protocols and implementation of new functions. In addition, a new device was developed to act as a communication bridge to the inverters of the DG and ESS power plants, with the possibility of being connected to the commercial IPS. Unlike the previous study, in this case the communication bridge can be installed without replacing the IPS of an already connected DG or ESS. In this way, the solution is more general and can be used in all countries by using the IPS that comply with the relevant standards.

4.3.1 Standards for DG Connection on LV networks

The standard CEI 0-21 contains for Italy the technical reference rules for the connection of active and passive users to the electricity networks of LV [130]. The aim of this standard is to define the technical criteria for the connection of users with a nominal voltage AC of up to 1 kV. In addition, this rule for active users is intended to:

- define the commissioning, operation and shutdown of production equipment;
- prevent production facilities from operating in an undesirable islanded mode on portions of the LV networks;
- To define requirements for production facilities to operate in desired islanded mode on the utility's network.

From the above aspects, it is important to define the characteristics of static converters for connecting DG and ESS equipment to the grid via inverters. CEI 0-21 defines standard capability curves that must be met by both DGs and ESSs. Specifically, the following inverter operating modes are defined:

- Grid-connected $\cos(\varphi) = 1$: The inverter must generate active power only;
- Grid-connected $\cos(\varphi) = f(P)$: the power factor of the inverter should follow a standard curve depending on the active power generated;
- Grid-connected$Q = f(V)$: the reactive power delivered by the inverter should follow a standard curve as a function of the measured voltage. This curve is defined for power plants with a generated power higher than 11.08 kW;
- Stand Alone: a contactor is opened to disconnect the DG and the ESS from the grid, but some privileged loads downstream of the contactor can still be supplied so that their electrical supply is guaranteed.

Under normal operating conditions, the inverters must operate with a power factor of 1 or supply active power only. Operation at a power factor other than 1 may be requested by the DSO to better control the operation of the distribution system. Normally, the DSOs only specify which mode to implement when a new plant is connected to the power grid LV. On the other hand, given the evolution of the distribution networks towards a smart grid, the CEI 0-21 standard (see Appendix D of [130]) proposes the possibility to define a set of signals for the control of the distribution network. This also means reconfiguring the operating modes of the inverters of active users in order to adapt the distribution network to the different load conditions and make it efficient. These signals enable the provision of grid services through appropriate active and reactive power settings according to the distribution system requirements; the disconnection of generators when a remote disconnection signal is received; the activation/inhibition of IPS frequency thresholds; the provision of DSO voltage, active and reactive power measurements at the DG and ESS connection point. In this framework, our work aims to propose a new architecture and new equipment to implement this solution. In other countries, different from Italy, other standards regulate the connection of active users, but there are similar approaches. For example, VDE-AR -N 4105, used in Germany but adopted also in other countries, proposes power control curves very similar to CEI 0-21. The proposed architecture could therefore also be usefully applied to inverters and protection systems that comply with these standards by adapting the corresponding control commands.

4.3.2 Power Grid Mapping over PLC-PRIME Network

The physical power grid can now be mapped to a new scheme using the PRIME protocol, in which all DSO MV substations and end users, including consumers and prosumers, are PRIME nodes (Fig. 53). This digital representation of the network is a critical step toward the introduction of current smart grid services, frameworks, and business models. One of the most recent applications in Italy is the possibility of meeting the needs of the emerging paradigm of "renewable energy communities". In 2020, Italy introduced the possibility to "share" energy between different subjects that decide to join together as a community and be recognized by the DSO or a third aggregator operator. The implementation of the PRIME protocol proposed

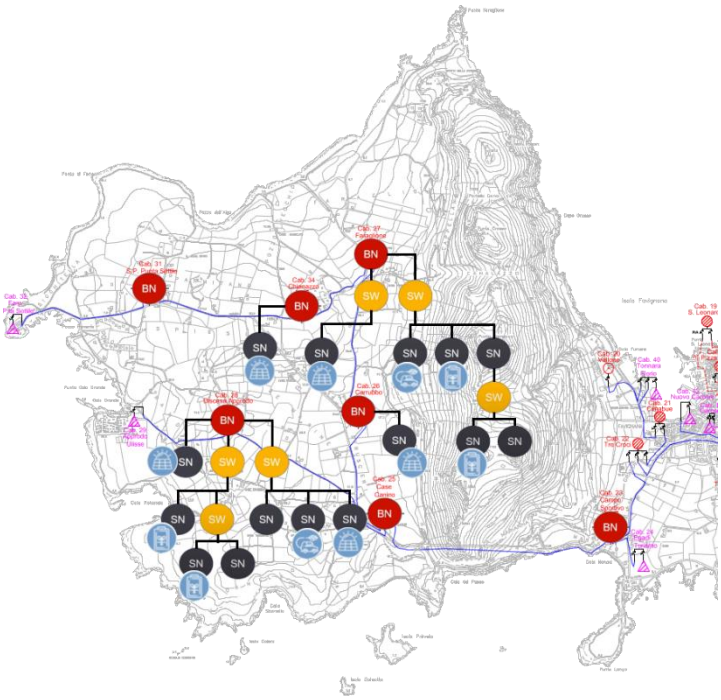

Fig. 53. Power grid mapped as PLC-PRIME network

in this work goes exactly in this direction, since each end node (PRIME service node) can be configured to belong to a specific community or organization. Any information exchanged with the DSO is tagged with the membership information and the data can be aggregated by the DSO for billing purposes. The detailed architecture for the new PLC communication link on LV networks is shown in Fig. 54. This new architecture includes the use of two devices: a concentrator, installed in a secondary substation, and a PLC communication bridge to be connected to a commercial IPS for the generation/storage system. The concentrator now covers more functions than the traditional concentrator in AMR systems, where it was responsible for periodically polling users' meters and collecting and storing all consumption data for billing purposes over long periods of time. Taking advantage of the capabilities of the PRIME protocol, the concentrator in this architecture manages the PRIME subnet under a secondary substation and is responsible

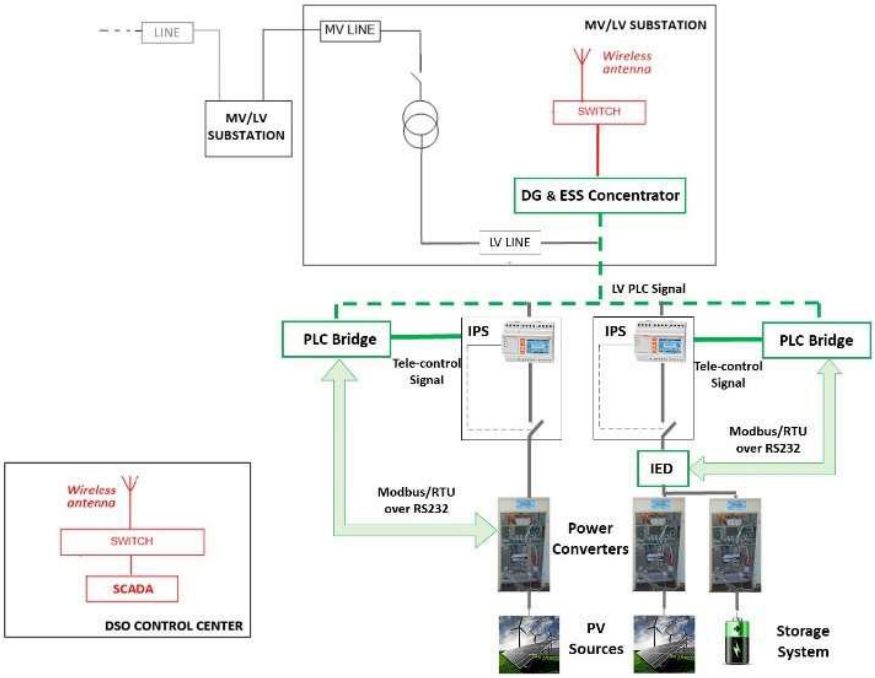

Fig. 54. Proposed PC communication link for DG and ESS connection to LV network

for handling all connections between the control centre and the end-user node. The data flow, concerning control, monitoring and configuration signals for distributed generation and storage systems is bi-directional and runs on a hybrid PLC and Modbus - RS232 communication link. More in detail, the PLC bridge can be connected to a generic interface protection system through digital pins to remotely disconnect the source from the LV network. Moreover, it can be connected directly to an inverter of a PV source or to an Interface Electronic Device. This IED is a communication interface to which a generic inverter of a PV source and/or a bidirectional power converter of a storage system can be connected.

4.3.3 PLC developed devices on LV Networks

4.3.3.1 Concentrator Prototype

The concentrator's primary job in the proposed architecture is to serve as a communication bridge between the DSO and the generation/storage systems. The following are the specific functions that will be performed by the concentrator, broken down further:

- Polling inverters connected to the DG or ESS in order to monitor and feed the SCADA system to regulate generation plants;
- Parsing, wrapper and router of control and management messages to and from DGs and ESSs
- Control the PRIME sub network, handle the communication link to each service/ switch node

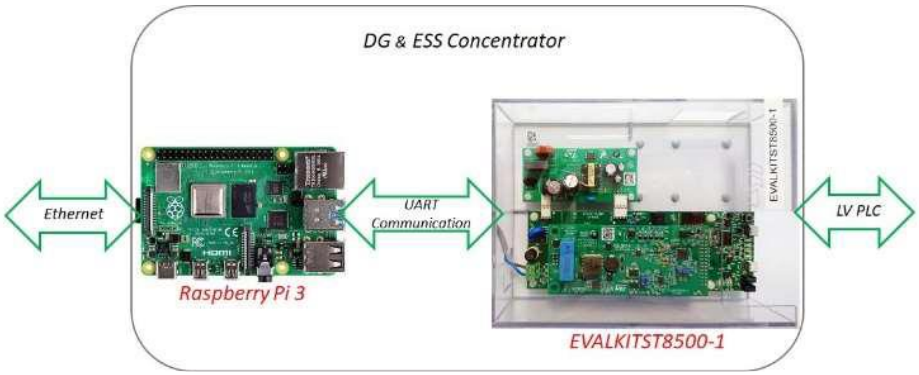

Fig. 55. Connection Block Diagram of DG and ESS Concentrator Prototype

These features were developed and implemented on the concentrator using two evaluation boards: the EVALKIST8500-1 and the Raspberry Pi 3. The EVALKIST8500-1, already used and described by us in [131], is an evaluation board that exploits a PLC transceiver, the ST8500, widely used for smart metering applications. The board acts, for the concentrator, as a PLC communication bridge on the LV network by forwarding the commands coming from the DSO and receiving the information coming from the PLC bridges of DG and ESS control systems. The Raspberry Pi3 acts as the controller of the LV PRIME sub-network and the related PLC bridges. Through an Ethernet interface it allows the concentrator to be connected via LAN/WAN to the DSO. The commands from the DSO are parsed and wrapped before being sent to the EVALKIST8500-1 through serial UART communication. The same operations are performed for the data coming from the PLC bridges of IPSs before being forwarded to the DSO. Moreover, the Raspberry Pi3, using the same UART serial communication and acting as an external host, is able to configure the PLC communication features of the EVALKIST8500-1 (i.e. modulation and frequency band), thus allowing the transmission parameters to be adapted to the communication channel conditions. The block diagram showing the connections between the two boards is shown in Fig. 55.

The concentrator software is based on a C reference application and a binary library for modem management provided by ST Microelectronics as part of the I-Sole and Sinert projects, on which CNR, UNIPA, and ST are still working together. A new Python application was created to implement all of the capabilities requested for the concentrator during the design process. Python was chosen because of its adaptability, efficiency, and reliability, all of which are seen to be beneficial during the prototype process. Furthermore, the availability of numerous frameworks and libraries relieves the developer of the need to write additional code and lets him to concentrate on the application's key features.

The binary library from ST was loaded using the *ctypes* library. *Ctypes* is a Python foreign function library. It supports C data types and allows you to invoke functions from DLLs or shared libraries. These libraries can be wrapped in pure Python [132]. By loading the library in this way, the main programme can access all of the functions implemented in the binary library, thereby allowing the developer to programme the modem.

Three major parts make up the concentrator software. The first is the main programme, which fires the other modules as threads during the initialization process. The first is the modem interfacing module, which is divided into two threads, one for operating the finite state machine (FSM) and the other for interacting with the PRIME 1.14 Protocol's CL NULL Layer. The Web Server Module is the second (WSM). To allow the DSO to interact with the concentrator, this module exposes a set of Representational State Transfer (REST) Application Programming Interface (API).

In order to exchange messages between the modules, a set of priority queues has been implemented. A priority queue is a variant of a classical queue that retrieves open entries in priority order (lowest first). Both the CL NULL and the WSM thread handles two queues one for incoming messages and one for outgoing messages and acts both as producer and consumer handling the queues with respect to the roles they assume at each interaction.

Once initialized, the main module runs an infinite loop where the outgoing queues of the CL NULL and WSM threads are polled. The block diagram of the developed application at thread level is show in Fig. 56.

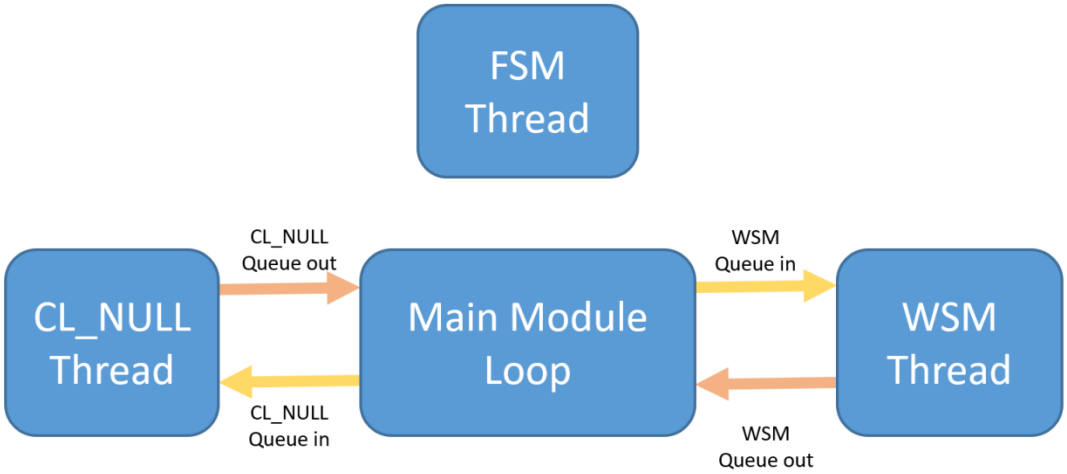

Fig. 56. Thread level block diagram of the developed application

4.3.3.1.1 Registration Phase

The main application keeps track of all the nodes successfully registered to the base-node binding the CL_NULL_ESTABLISH_INDICATION event fired by the FSM. When the event is notified, the base-node starts a rude and dirty clock synchronization phase. The goal of this technique is to determine the overall system latency in order to establish and adjust the clock on the remote node. A ping-like protocol has been implemented to accomplish this, and the round trip time is determined at the base node. The average latency is communicated to the remote device along with the clock information after a variable number of

transmissions. As a result, the service node will set and change its own clock. This method makes a number of simplifications and isn't appropriate for many applications that require great timing precision. The results of the tests illustrate how the implementation of software on platforms with an operating system, and in any case not real-time, is a major limit for the correct estimation of the system's latency, which is made up of processing times, channel access, and channel latency. After a successful synchronisation phase, the concentrator will update its own network map, which will contain all of the information about the connected service nodes.


```
"nodes":[
   {
      "ConHandle":"0x3f4f00",
      "EUI48":"0x80e192f780",
      "Nominal Data":{
         "energy_es":3000,
         "power_es":6000,
         "power_pv":15000
      },
      "ES_info":{
         "function_es":"inject",
         "power_es":3000,
         "soc":20
      },
      "PV_info":{
         "power":12000,
         "status":"GcQ"
      },
      "date":"09/06/2021 11:48:44.022000",
      "end_probe":1623231344.50315,
      "latency":0.21772170066833496,
      "start_probe":1623231344.0677066,
      "update_time":"09/06/2021 11:48:44.164711"
   }
]
```


Fig. 57. Network json representation with nodes information stored at the concentrator

In Fig. 57 illustrates a json representation of the network map after the full registration of one service node. In detail the service nodes basic information are:

- *ConHandle*: is a unique identifier interchanged to uniquely identify the connection being indicated. It has a valid meaning only in the MAC SAP, used to have a reference to this connection between different primitives. Comes from CL_NULL_ESTABLISH_INDICATION.
- *EUI84*: indicates which device on the subnetwork wishes to establish a connection. Comes from CL_NULL_ESTABLISH_INDICATION.

- *Nominal Data*: rated values of the distributed generation/storage connected to the service node. It is derived from data acquired by the service node after the inverter's connection. .
    - *power_pv*: nominal power in watts for the photovoltaic facility
    - *power_es*: nominal power of the storage system
    - *energy_es*: nominal energy of the storage system
- *ES_info*: set of information about the actual behaviour of the storage system
    - *function_es*: *inject* if ESS act as a generator, *store* if ESS act as storage
    - *power*: instant power in W
    - *soc*: actual State of Charge info in %
- *PV_info*: set of information about the actual behaviour of the photovoltaic system
    - *power*: instant power produced in W
    - *status*: operating mode of the inverter as described in 4.3.1
        - *Gcq*: Grid-connected $Q = f(V)$
        - *Pfc:* Grid-connected $\cos(\varphi) = f(P)$
        - *Gccosphi:* Grid-connected $\cos(\varphi) = 1$
        - *Standalone: Standalone*
- *date:* when the service node registration has occurred
- *start_probe / end_probe:* start and end in unix timestamp of the synchronization phase
- *latency:* calculated latency in seconds during the synchronization phase
- *update_time:* when an update on these records occur

The concentrator is now ready to exchange messages with the newly registered service node following the clock synchronisation phase.

4.3.3.1.2 HTTP Application Programming Interface

When queried after a successful synchronisation phase, the concentrator can send information about the production/storage facility connected to the service node to the SCADA system. The SCADA can use the concentrator's API to poll the devices connected to the LV network under an MV secondary substation. When a new API call is detected, the request is parsed, and a new message to send to the modem is prepared and sent over the PLC interface. APIs that have been implemented use authorization to ensure that client requests access data in a secure manner. This entails authenticating the sender of a request and confirming that they have the authority to access or manipulate the relevant data. To make a system-compliant call, the sender must include the authentication data, a key-value pair, in the request header. Fig. 58 show the x-api-key along with his value inside the header of a valid request.

Fig. 58. Valid request header with api-key authentication method

If the request is not system-compliant, a 401 HTTP code (Unauthorized) is returned; otherwise, the call can be processed. The DSO is responsible for selecting the API-key distribution system. The POST HTTP method has been chosen for all the implemented endpoint, and all the data to be passed are specified into the body of the request.

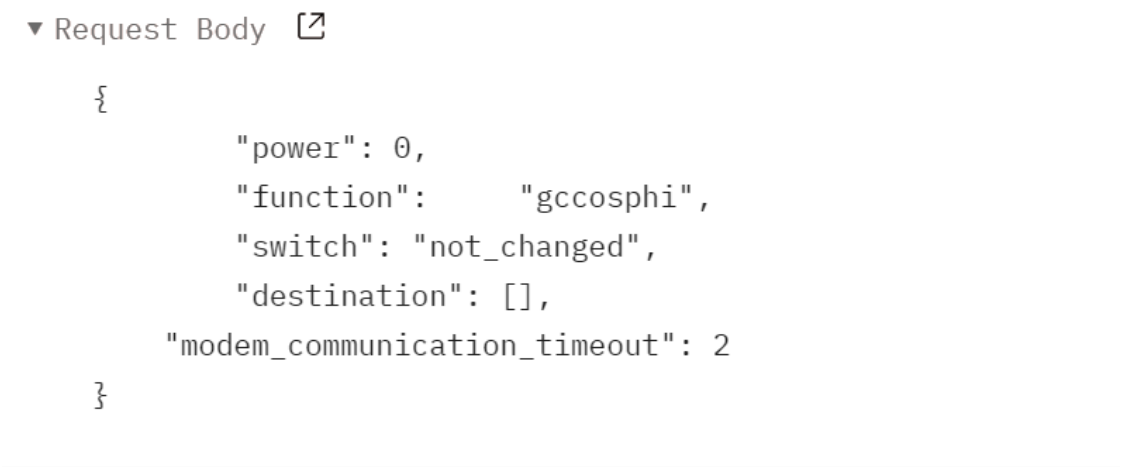

Fig. 59. API call request body

Fig. 59 depicts a valid request body. It includes two mandatory fields that are shared by all endpoints and have an impact on communications after the concentrator:

- *destination*: if empty, the PLC modem have to send a broadcast message, otherwise the field have to specify one or more valid ConHandle values
- *modem_communication_timeout*: a value in seconds to hang on for a valid communication

The set of API implemented includes 4 POST endpoints that, along with the mandatory fields, needs the following:

- /setValuesPV set the functional parameters of the remote generator facility. It has the following mandatory parameters:
  - *power*: set the power to generate. Value in watt
  - *function*: set the operating mode of the inverter as described in *PV_info* in 4.3.3.1.1
  - *switch*: specify the status of the remote contactor.
    - 'open' the facility is disconnected from the grid
    - 'closed' the facility is connected to the grid
- /setValuesES set the functional parameters of the remote storage system. In addition to the parameters of /setValuePV, it needs:
  - *function*: set the operating mode of the ESS
    - "store" the system acts as a load to the grid
    - "inject" the system acts as a generator to the grid
- /setChannel is used to change the communication channel of the PRIME subnet between the 8 channels available:
  - *channel*: the channel to set. It is a number between 1 and 8
  - *nowait*: tells the concentrator if it has to wait for the remote acknowledgement packet from remote node(s) before switch channel locally.
    - 0: change channel locally after the ack packet is received
    - 1: change channel locally immediately
- /getValues: is used to get the status of the subnet along with all the information about connected facilities collected by the concentrator. It is the only endpoint that can get rid of the destination mandatory field, because the default setting is "broadcast"

A HTTP 400 code (Bad request) is returned and the request is discarded if some mandatory parameters are missing in the request body. Otherwise if the request passes the sanity check, a RFC4122 UUID [133] is produced for the request and glue to it. The request is forwarded to the queue out from the WSM and it is added to a list of pending requests. A timer thread is started at the same time with the *modem_communication_timeout* value given. If the requests have not received a response from the PLC modem before the timer has expired, an HTTP 504 code (Timeout) is returned and the request is deleted from the pending list. Otherwise, if the response arrives before the timer expires, a HTTP 200 (Success) code is returned along with the response data. If some error occurs during the elaboration, a HTTP 500 code (Internal server error) is returned. In the time space of the timer launched by the WSM module, within the main application loop, the WSM out queue is checked in order to get the new incoming requests. If a new request is identified, the data are parsed in the correct form to be sent to the service node(s) and a new message is put in the CL_NULL queue in. It means that the new message will be passed to the modem and sent via PLC link.

In the main module application loop, the CL_NULL queue out is checked and the CL_NULL_DATAINDICATIONPRESENT event is bound in order to get the response from the remote service node(s). The data acquired are parsed and wrapped and the response is deposited into the WSM queue in. The WSM check is own queue in and if the response has the same UUID of a pending request it means that the timer for that requests is still on and the response is sent via HTTP along the success code.

4.3.3.2 Remote PLC Bridge

The PLC bridge prototype's key functions are as follows:

- to be able to communicate with the concentrator and receive distributor commands through the PLC link in order to monitor, control, and manage the inverters connected to DG or ESS
- to be able to receive distributor commands from to operate as a communication interface with the DG and ESS inverter management and control systems;
- to route the DSO's remote disconnection signal to the IPS's digital input, which can open the contactor and disconnect the power plant from the network.

On an EVALKIST8500-1 board, these functions were created and implemented. The IPS, DG, and ESS inverters can receive DSO directives provided by the concentrator via a PLC signal in the LV network in this way. The commands and data exchanged with the DG and ESS inverters are sent over a serial connection on RS232 using the Modbus/RTU protocol. The IPS receives the remote disconnection signal via an EVALKIST8500 digital output pin, whose logical level is matched by a suitable voltage conditioning circuit. Fig. 60 depicts the functional diagram of the PLC bridge prototype.

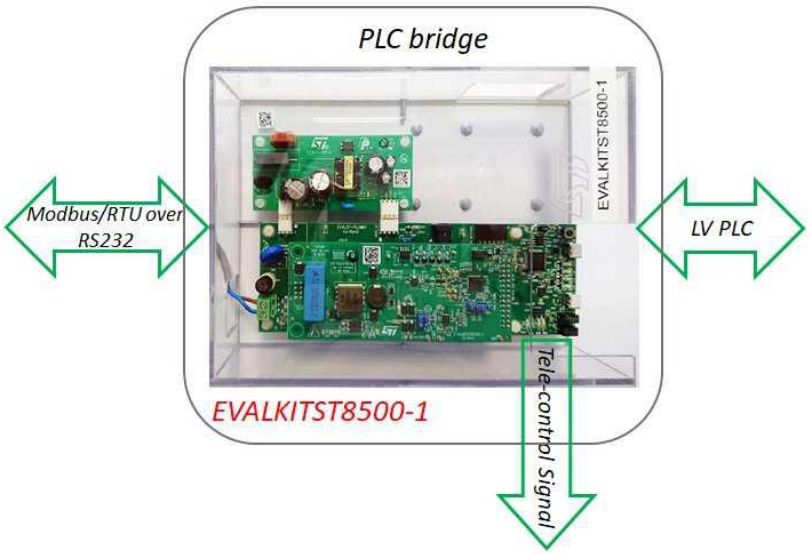

Fig. 60. Functional diagram of remote PLC bridge prototype

4.3.3.2.1 PLC Bridge frames

The PLC bridge prototype can manage various PLC frames forwarded by the concentrator and perform the necessary activities based on them. The following PLC frames are managed by the PLC bridge:

- *Sync* frame
- *Sync Set Time Stamp* frame
- *Channel Configuration* frame
- *Contactor command* frame
- *Set Status* frame
- *Get Status* frame

The *Sync* frame is sent from the concentrator to the PLC bridge to notify the start of clock synchronisation operations. The *Sync* frame format is described Table 10:

Byte	Description	Value
0	Identifier	0x30
1	reserved	0x00
2	reserved	0x00
3	reserved	0x00

Table 10. Sync frame format

When this frame is received, the PLC bridge responds by sending a frame starting with the hex 0x31 identifier. In this way the concentrator will be able to determine the average latency of the communication channel according to the process described in 4.3.3.1.1.

The *Sync Set Time Stamp* frame, sent from the concentrator to the PLC bridge, contains the clock setting that must be set on the PLC bridge taking into account the latency of the channel. The *Sync Set Time Stamp* frame format is show in Table 11:

Byte	Description	Value
0	Identifier	0x32
1	Week Day	0x01 (Monday) to 0x07 (Sunday)
2	Number of Day	0x01 to 0x1F (BIN format)
3	Month	0x01 ÷ 0x0C (BIN format)
4	Year	0x00 ÷ 0x63 (BIN format)
5	Minutes	0x00 ÷ 0x3B (BIN format)
6	Seconds	0x00 ÷ 0x3B (BIN format)
7	Millisecond = (1-(byte7/256))	0x00 ÷ 0xFF

Table 11. Sync Set Time Stamp frame format

On receipt of the *Sync Set Time Stamp* frame, the PLC bridge sets its own internal clock to synchronise with the main clock of the concentrator. The resolution of clock equals 3.9 ms (1-(255/256)).

The *Channel Configuration* frame is sent from the concentrator to the PLC bridge to change the communication channel on which PLC transmissions occurs. The channel can be chosen from the eight available according to the frequency range defined for the PRIME protocol. Table 12 describe the *Channel Configuration* frame format.

Byte	Description	Value
0	Identifier	0x08
1	Channel number	0x01(CH1),0x02(CH2), 0x04(CH3),0x08(CH4), 0x10(CH5),0x20(CH6), 0x40(CH7),0x80(CH8)
2	Counter	0x00 ÷ 0xFF

Table 12. Channel Configuration frame format

On receipt of the *Channel Configuration* frame the PLC bridge sets the PLC modem with the new received transmission channel value and sends an acknowledgment message to the concentrator. Table 13 describe the acknowledgment frame format:

Byte	Description	Value
0	Identifier	0x09
1	Channel number	0x01(CH1), 0x02(CH2), 0x04(CH3), 0x08(CH4), 0x10(CH5), 0x20(CH6), 0x40(CH7), 0x80(CH8)
2	Counter	Counter received

Table 13. Channel Configuration ack frame format

The *Contactor Command* frame is sent from the concentrator to the PLC bridge to command the opening or closing of the contactor of the IPS for the connection or disconnection of the distributed generation/storage system from the utility network. The *Contactor Command* frame has the format in Table 14:

Byte	Description	Value
0	Identifier	0x00 (Closed Contactor) 0x80 (Open Contactor)
1	reserved	0x00
2	reserved	0x00

Table 14. Contactor Command frame format

On receipt of the *Contactor Command* frame, the PLC bridge, via a digital pin, signals the disconnection to the IPS, which commands the opening or closing of the contactor for disconnection or connection of the generation/ storage system to the distributor's electricity network.

The *Set Status* frame is sent from the concentrator to the PLC bridge to define the configuration of the inverter or IED that manages the distributed generation/ storage system. The format received is different depending on whether the configuration concerns the generation system (photovoltaic) or the storage system (batteries).

The *Set Status* frame for configuring the inverter/IED connected to a photovoltaic system contains one of the operating modes shown in 4.3.1 and the instantaneous power at which the system has to operate. The format is as follows:

Byte	Description	Value
byte 0	Inverter operational mode	0x41 (Standalone) 0x42 (GC_cos(φ) = 1) 0x43(GC_ Q = f(V)) 0x44 (PFC_cos(φ) = f(P))
byte 1	MSByte power	0x00 ÷ 0xFF
byte 2	MidSByte power	0x00 ÷ 0xFF
byte 3	LSByte power	0x00 ÷ 0xFF

Table 15. Set frame format for photovoltaic inverter/IED

For the storage system, on the other hand, the *Set Status* frame has the following format:

Byte	Description	Value
byte 0	Storage operational mode	0x51 (Store) 0x52 (Inject)
byte 1	MSByte power	0x00 ÷ 0xFF
byte 2	MidSByte power	0x00 ÷ 0xFF
byte 3	LSByte power	0x00 ÷ 0xFF

Table 16. Set frame format for storage system

The first byte of the frame defines the operation mode of the storage system among those described in 4.3.1 while the next three bytes define the instantaneous power value.

When a *Set Status* frame is received, the PLC bridge, after parsing the message, performs a wrapping operation in order to forward the configuration to the inverter/IED according to the ModBus/RTU protocol on standard

RS232. The implementation of communication via ModBus/RTU protocol is described in detail in the next paragraph.

The *Get Status* frame is sent from the concentrator to the PLC bridge when the operational status of the distributed generation and storage system is required. The Get Status frame has the following format:

Byte	Description	Value
byte 0	Identifier	0x20
byte 1	reserved	0x00
byte 2	reserved	0x00

Table 17. Get frame format

After receiving a *Get Status* the PLC Bridge requests the status of the plant by forwarding a message to the inverter/IED of the generation/storage system via ModBus/RTU protocol. The received information undergoes a wrapping operation before being transmitted to the concentrator. The response frame to a *Get Status* frame has the following format:

Byte	Description	Value
byte 0	frame header value	0x21
byte 1	photovoltaic data delimiter	0x01
byte 2	Inverter configuration	0x01 →standalone 0x02 →Gc_Cos(phi) 0x03 →Gc_Q 0x04 →PFC 0xFF →unknown
byte 3	MSB power	0x00 ÷ 0xFF
byte 4	MidSB power	0x00 ÷ 0xFF
byte 5	LSB power	0x00 ÷ 0xFF
byte 6	storage data delimiter	0x02
byte 7	soc (storage charge level)	0x00 ÷ 0x64 → 0% ÷ 100% 0xFF → unknown
byte 8	storage configuration	0x01 → storaging 0x02 → injection
byte 9	MSB storage-power	0x00 ÷ 0xFF
byte 10	MidSB storage-power	0x00 ÷ 0xFF
byte 11	LSB storage-power	0x00 ÷ 0xFF

Table 18. Get replay frame format

4.3.3.2.2 Modbus/RTU PLC Bridge frames

Communication between the PLC bridge and the inverter/IED of distributed generation systems is via a serial port (UART) using the RS232 standard and the ModBUS/RTU® communication protocol. The ModBUS/RTU® protocol provides 10 functions that write or read the status of a device on which it has been implemented. Each device status information is contained on two bytes.

In this specific case, only two functions of the ModBUS/RTU® protocol have been implemented on the PLC bridge for communication:

- *FUNCTION 16*: *Preset Multiple Registers*
- *FUNCTION 4: Read Input Register.*

The *FUNCTION 16: Preset Multiple Registers* allowing the value of a consecutive block of 16-bit registers to be set, is used by the PLC bridge when it is necessary to transfer an operating configuration to the inverter/IED of the generation/storage system. In particular, through *FUNCTION* 16, two separate Set commands have been implemented, one for generation and one for storage in accordance with the *Set Status* frames described in 4.3.3.2.1.

The *FUNCTION 16* for the configuration of the generation system has the format shown in Table 19, while for the configuration of the storage system it is shown in Table 20.

Byte Description	n. of byte
IED Address	1
ModBus function code	1
Start address	2
Registers number to be written	2
Register bytes number to be written	1
Inverter Configuration	2
InverterPower	4
CRC	2

Table 19. ModBus serial frame of FUNCTION 16 for the DGS configuration

Byte Description	n. of byte
IED Address	1
ModBus function code	1
Start address	2
Registers number to be written	2
Register bytes number to be written	1
Storage System Configuration	2
Storage System Power	4
CRC	2

Table 20. ModBus serial frame of FUNCTION 16 for the ESS configuration

The *FUNCTION 4: Read Input Register*, on the other hand, in accordance with the GET Status frame coming from the concentrator, allows to request all the information relating to the status of the generation/accumulation system contained in the 16-bit registers of the inverter/IED. The format of the serial frame for *FUNCTION 4* sent by the PLC bridge is as follows:

Byte Description	n. of byte
IED Address	1
ModBus function code	1
Start address	2
Registers number to be read	2
CRC	2

Table 21. ModBus serial frame of FUNCTION 4 for the information status register of GDS and ESS

On reception of a frame related to *FUNCTION 4*, the inverter/IED responds to the PLC bridge by sending a ModBUS/RTU® serial frame described in Table 22

Byte Description	n. of byte
IED Address	1
ModBus function code	1
Number of di transmitted bytes	1
Inverter Configuration	2
Inverter Power	4
Storage Charge Level	2
System Storage Configuration	2
System Storage Power	4
Photovoltaic Power Plate value	4
Storage Power Plate value	4
Storage Energy Plate value	4

Table 22. ModBus serial replay frame of FUNCTION 4 for the information status register of GDS and ESS

The plate values reported in the replay frame are used during the connection phase of the PLC bridge to the PRIME communication network.

4.3.4 PLC on MV Distribution Network

PLC was originally widely used in High Voltage transmission networks, primarily for protection and automation. It was also widely used in LV networks for AMR purposes in the recent decade. PLC technology, on the other hand, has yet to be utilised in MV distribution networks. As a result, many research on PLC signal propagation in MV cable or overhead networks, as well as power transformer behaviour at PLC frequency ranges [40,41,134,135], were conducted. In any case, one of the major challenges for PLC deployment in MV networks is the requirement for a large number of specialised PLC couplers to be deployed across the network. In fact, they must be installed in both primary and secondary substations, with the associated costs of equipment, MV cabinets, and other infrastructures, people for installation, and the additional indirect costs of service interruption. In order to address the aforementioned difficulties, [136] proposes a novel low-cost coupling approach. This technique employs the capacitive dividers already installed in MV switchboards for voltage detection as an MV PLC coupler [137]. As a result, no specific coupler installation or MV switchboard modification is required, resulting in a significant cost reduction for PLC deployment in MV networks. The proposed approach was evaluated in the frequency range of the CENELEC band [138,139] reserved in Europe for DSO signal broadcasts, as well as higher centre frequencies up to 200 kHz [21]. The solution demonstrated a flat frequency band of 15 kHz, allowing Frequency Shift Keying (FSK) and Phase Shift Keying (PSK) modulated signal transmission up to 28.8 kbit/s [129]. A deep insight on the specifics and the features of the prototype are present in [140].

A scheme of existing smart metering architecture is shown in Fig. 61. A smart meter provides information on energy transfers for each LV user or prosumer. An AMR concentrator collects and saves measured data from LV smart meters located downstream of the substation in each secondary substation.

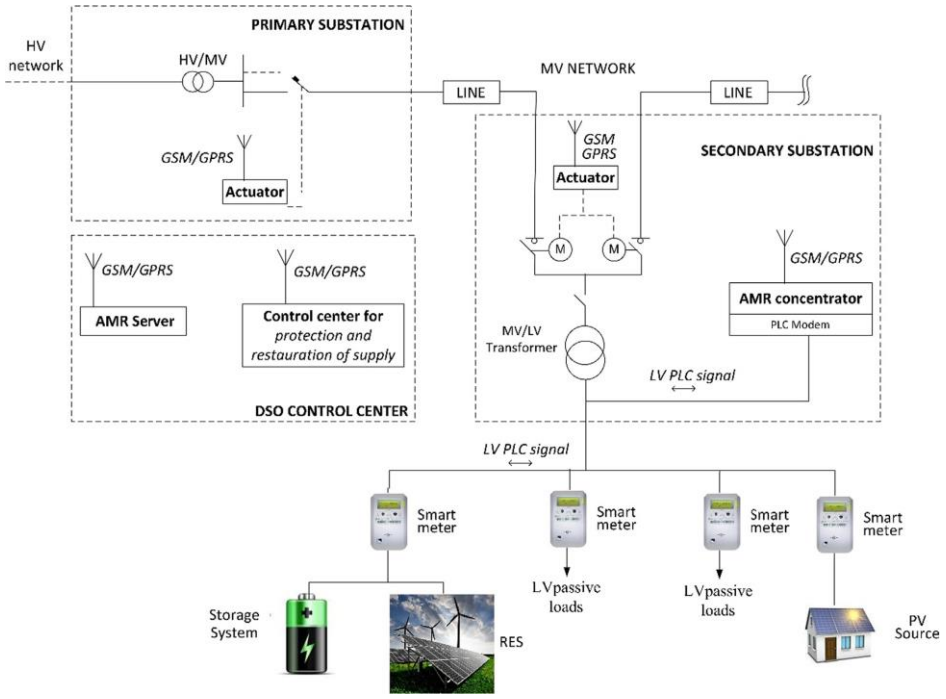

Fig. 61. Present smart metering architecture based on a wireless and LV PLC hybrid communication solution

The AMR server is deployed in the DSO control centre and queries the AMR concentrators on a regular basis (often once per day) to process and store the acquired data (mainly for billing purposes). Usually, the data link at the LV level between AMR concentrators and smart meters is established using power line communications (PLC), whereas AMR server and concentrators interact via a wireless modem (typically GPRS), which is widely available in urban situations. As a result, DSO manages its economic and infrastructure reliance on a wireless communication provider. Furthermore, such systems can be unreliable (especially in bad weather), and they can be vulnerable to cyber-attacks. To address the aforementioned issues, one feasible solution for AMR communication is the use of PLC at both the MV and LV levels. This solution, as said before, has several advantages: it has a low installation cost because power lines are already present; the PLC channel is completely under DSO control, which eliminates commercial and technical dependence on communication providers; and PLC is more secure from cyber-attacks because the communication system is not easily accessible to an intruder. Furthermore, PLC can be an appropriate solution for last-mile applications or contacting smart meters in remote urban or rural areas where other communication lines may be unavailable [36,41]. As previously stated, PLC is already employed at the LV level in distribution networks for AMR and has been recommended for DG applications. PLC use at the MV level, on the other hand, has been studied in recent years [34–39]. Some publications have confirmed that PLC signals traverse power transformers, even though attenuation is expected depending on the frequency and modulation technique used [43,135], particularly in the CENELEC band. Additional attenuations caused by line length and derivations can drop the signal amplitude below the noise level, limiting proper reception. Thus, commercial couplers are typically recommended in place of or in conjunction with PLC signal crossover approaches to boost signal strength in MV network points where larger attenuations are predicted. The usage of MV commercial couplers, on the

other hand, often requires substantial expenses for both equipment and installation, as well as service interruption. In this regard, the authors of [129,136,139] have patented a PLC coupling solution for MV networks based on the usage of capacitive dividers of voltage detecting systems (VDS), which are generally employed to expose the presence of mains voltage. The patented technology overcomes the restrictions of employing PLC at the MV level by requiring little equipment and installation while also minimising service interruptions. The innovative MV PLC coupler is a critical component of the approach provided in the preceding sections. To validate the practicality of the proposed smart metering architecture, an on-field experimental validation is carried out in the real case of Favignana Island's distribution network.

Fig. 62 depicts the proposed smart metering design. Each LV user or prosumer, like existing systems, has a smart meter. Secondary substations use LV AMR concentrators, however they are linked to MV PLC transceiver boxes (instead of wireless modems). To this aim, the innovative MV coupling solution, described in [21,140], is used to couple the PLC signal to the MV power network. A MV concentrator (MVC) is installed in the primary substation; it collects the measurement data of all the related secondary substations. These data can be used in computation algorithms typical of new smart city applications.

VDSs are used worldwide to expose the existence of mains voltage, assuring operator safety, according to IEC 61243-5 [137]. The VDS capacitive divider is made up of two capacitances that are connected between the MV bus-bars and the earth. The capacitance series' intermediate node is made available on a socket in the MV switchboard panel. When a mains voltage is applied to the capacitive divider terminals, the proportional voltage at the socket terminals is lowered. As a result, a voltage indicator, often a flashing light, can assist in quickly identifying the presence of mains voltage in the switchboard [137]. This connector is used by the new coupling system to inject and receive the PLC signal. A suitable electronic interface board is designed to allow the capacitive divider to function as a PLC coupler, with high impedance at low frequency (thus isolating the transceiver from mains voltage) and low impedance in the signal frequency region. The interface card's operation is based on establishing resonant behaviour with the VDS capacitances. Internal parameters, primarily variable inductances, are set to achieve this goal depending on observed VDS capacitances and desired operating frequency range [78]. The suggested interface card is less expensive than commercial MV couplers; additionally, it avoids MV switchboard upgrades, service interruption, and associated human expenditures (as the interface card can be safely connected to low voltage VDS socket).

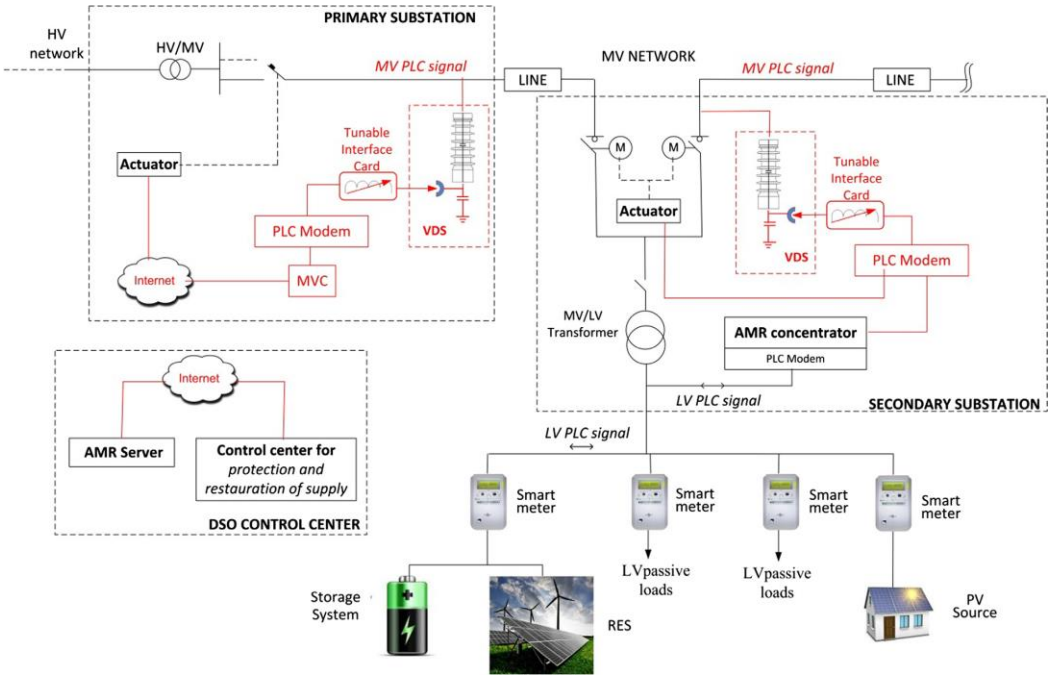

Fig. 62. Proposed smart metering architecture with low cost and easy to install PLC communication solutions both on LV and MV distribution networks

4.3.4.1 On-field experimental characterization of the MV PLC channel

An on-field experimental analysis of Favignana Island's MV and LV distribution networks was performed to validate the practicality of the MV PLC solution in a real-world scenario. In more detail, the Favignana electrical network is made up of three MV feeders that originate from a diesel power plant with a total capacity of 12 MW. The network is disconnected from the national power grid. In the three feeders that connect 40 MV/LV secondary substations, both MV cables and overhead lines are placed. The tests were performed on the MV feeder, which connects 29 secondary substations. The electrical loads are those found in tourist and residential areas. [141] reports rated statistics and some load measures for the considered network. Fig. 63 depicts a map of the MV and LV distribution network under test. In more detail, the experimental on-field site consists of two substations linked by a 1.1 km long MV line made up of unipolar cables of the RG7H1R type with a 50mm2 aluminium core cross-section and a copper shield (in Fig. 63, the MV line route is highlighted in red; the green route indicates the LV line, L1, used for the tests described in Section 4). The first test substation is called "*Gen. Di Vita*". It is in by-pass mode, with three MV switches connecting the MV bus-bars to the incoming line, outgoing line, and MV/LV power transformer (160 kVA) in that order. The second substation, known as "*4 Vanelle*", is a nodal substation with five MV switches for the incoming line, a 250 kVA MV/LV power transformer, and three outgoing MV lines that supply further secondary substations. In addition, three LV lines exit the MV/LV power transformer (one of those is the aforementioned L1, indicated with the green line in Fig. 63). To inject and receive the PLC signal, a

programmable PLC modem with the MV VDS PLC novel coupler was installed in both substations ("*Gen. Di Vita*" and "*4 Vanelle*").

Fig. 63. Portion of Favignana distribution network under test: the MV line connecting the two secondary substations "4 Vanelle" and "G. Di Vita" is highlighted in red; the LV line departing from substation "4 Vanelle" is in green.

A prototype box was built using a customizable PLC modem and a tuneable interface card (one for each substation, see Fig. 64). With no power interruption and no MV switchgear change, a customised connection was utilised to connect the tuneable interface card to the VDS socket at each end of the MV line [129]. To transmit nPSK modulated PLC signals, two ST7580 modems were employed. All on-field tests were carried out in the presence of alternating current (i.e. 20 kV, 50 Hz).

The MV PLC connection based on the new coupling solution was tested in three steps:

- firstly, the channel frequency response was used to tune interface card parameters, i.e. to obtain a resonant but enough flat frequency behaviour around the chosen centre frequency;
- secondly, the noise spectrum was measured at the interface card output, with the PLC modem switched off;
- thirdly, PLC transmission tests were carried out to verify the channel capacity in term of success rate at different modulation techniques.

The preceding steps enable accurate configuration of the interface card parameters, hence minimising the impact of stray parameters and noise on PLC signal transmission. In fact, the resonance condition between interface card and VDS equivalent capacitance is site specific, with both MV switchboard and stray

capacitances unknown. As a result, when installing an interface card in a new location, a tuning step is always required.

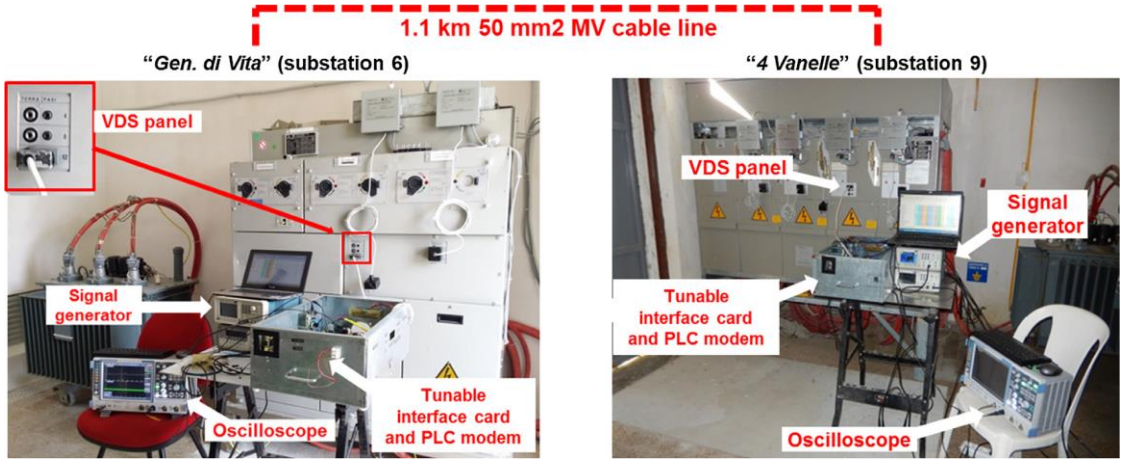

Fig. 64. Experimental set-up for the on-field tests of the MV PLC channel between "Gen di Vita" (6) and "4 Vanelle" (9) substations

On-site, the channel frequency response is acquired by sweeping a sinusoidal signal in the frequency range under study (50 kHz of SPAN around each chosen centre frequency) and analysing the FFT spectrum of the received signal. A digital oscilloscope was utilised to obtain measurements with high input impedance in the experiments given here, and the FFT spectrum of the received signal was analysed with a frequency resolution of 300 Hz. The frequency response test allows you to configure the interface card characteristics to have a suitable frequency band based on the modulation selected. In the case of nPSK modulation and a symbol rate of 9600 baud/s, a target 6 dB bandwidth of 15 kHz around the centre frequency is required. Because of the use of a VDS socket and the interface card's high impedance at power system frequencies, the on-field tuning operation can be performed in the presence of mains voltage, requiring no service interruptions during the interface card installation. .

In comparison with previous tests reported in [139], the on-field test campaign herein presented was aimed at demonstrating the effectiveness of the proposed solution in a wider frequency range, from 78 to 200 kHz. This frequency interval is considered for two reasons: transmission frequencies higher up to 200 kHz are allowed outside Europe (FCC band in United States, ARIB band in Japan, and so on); nPSK commercial PLC transceivers normally have a maximum frequency of 200 kHz.

Thanks to the interface card variable components, a resonant behaviour is obtained with a flat frequency response around each different centre frequency. Frequency response and noise evaluations reveal that increasing the frequency results in less noise and a bigger bandwidth, resulting in better transmission behaviour. This is also shown in the transmission testing. The collected findings validate the suggested NB-PLC coupling solution for various centre frequencies and modulation approaches. As a result, the suggested

approach can be utilised to efficiently transmit narrowband modulated signals over a wide frequency range, with a high success rate of up to 28.8 kbit/s.

4.3.5 Time dissemination System

A smart grid communication network's conceptual architecture can be separated into three layers:

- the home area network (HAN), which allows communication between end users' homes and the distribution network's (DN) service entry point;
- the field area network (FAN), which logically groups several HANs;
- the wide area network (WAN), which represents the electrical system's main communication network and allows communication between all FANs by merging and connecting local networks at regional or larger geographic levels.

Currently, there is no single solution that can meet the latency, bandwidth, and cost requirements of all of the multiple layers. As a result, smart grid communication networks are typically hybrid architectures made up of a variety of well-known communication media and protocols like Ethernet, PLC, long-term evolution (LTE), and others. The automation features of modern power grids necessitate the continuous monitoring of many electrical equipment parameters (e.g., voltage and current measurements, as well as operating conditions). In this case, the timestamping of all time-related information becomes critical [142]. Because the system is able to temporally correlate the phasors at distinct grid nodes [143,144], the measurement of PMUs [145] offers an accurate insight into the grid state at a certain time instant. On the existing hybrid communication infrastructure, modern FAN infrastructures use synchronisation algorithms that give accuracy on the order of hundreds of microseconds [32,146]. However, at this time, there isn't a synchronisation method that can be used as is at all levels—HAN, FAN, and WAN—at an economical cost. One of the most promising options is based on the communication channel broadcast of a reference signal (e.g., a chirp-based signal). "Frame synchronisation" has been achieved in the literature using a variety of strategies, the majority of which are based on specially crafted training sequences in the message header [147–150]. These techniques, on the other hand, necessitate a sophisticated optimization procedure that is difficult to scale to other network levels. A non-invasive and low-cost approach for the broadcast of time information across the MV grid is examined in [129]. The proposed approach takes advantage of the patented unique coupling technology for MV grid, which was described in previous studies in terms of bandwidth and attenuation [118,129]. The time information is encoded using the IRIG-B time code, which is commonly used by power substation measurement and control systems. On the power grid, chirp-based symbols are used to modulate the IRIG-B data. To avoid interference with PLC, the chirp-based symbols are sent via a dedicated band. In [151], the use of chirp-based time synchronisation on an MV power line was examined experimentally. The good results from past research activities are used to create a time dissemination system. A low-cost modulation and demodulation circuitry has been designed and validated using data obtained in laboratory.

4.3.5.1 Technologies Overview

Precision timing is essential for grid operation, monitoring, and protection in today's power systems. Data from geographically distant measuring equipment must be synced in a number of advanced applications, which necessitates the integration of common time information. Power system timing requirements have become increasingly rigorous in recent decades, depending on the applications examined [152]. Table 23 summarises the key grid applications that require time information and their associated accuracy requirements.

Application	Timing Requirements
Energy Billing	Measurements interval: Tens of minutes (15-30-60 mins)
SCADA Measurements	Reporting rate: few seconds (4÷6 secs)
Power quality measurements	Basic time interval: • 200ms (10/12 cycles for 50/60 Hz power systems); • 10sec (for power frequency measurements) Basic time-clock uncertainty (relative to UTC): • ±20/16.7ms (for 50/60 Hz power system)
Sequence of events / digital fault recording	Time resolution (relative to UTC): 50μs ÷ 1-2ms
Protective relays	Time resolution: 1ms (or better)
Synchrophasors/PMUs	Time resolution: 1μs (or better)

Table 23. Smart Grid Timing uses and Requirements

Synchronization constraints are frequently lax, especially at the distribution level. For power quality (PQ) measurements, the timeclock uncertainty is typically equivalent to one cycle time of the power supply. A global positioning system (GPS) receiver, network timing signals, or transmitted radio timing signals can all be used to achieve this synchronisation [98]. This allows the DSO to correlate events captured by numerous customers' PQ monitoring equipment. Time-synchronized data recorded by PQ monitors at the distribution level can be correlated with events recorded by fault recorders or protective relays at the transmission level if PQ disturbances at the distribution level trigger transmission-level events. SCADA measures have even tighter time constraints. Data sent to distribution grid operators (such as breaker status, transformer temperatures, voltage, current, and power measures) can be time-stamped, allowing the precise time of an incident to be determined. Scanning times for SCADA systems are typically a few seconds, and accuracy requirements are determined by the data to be registered. The majority of the above-mentioned timing requirements have been incorporated into national and international standards such as IEEE C37-118.1 [153] and IEC/IEEE 61850 [154]. Some criteria relating communication protocols timing requirements can also be found in this standard;

for example, synchronisation with an accuracy of 100µs divided by 1ms is required for substation local area network communication protocols (IEC 61850 GOOSE).

Several codes are defined in the IRIG standards [22] for transmitting time information over a serial connection. This type of coding is commonly used to disseminate the time data obtained by a GPS sensor. IRIG-B is the most often used code, but IRIG provides six distinct time codes (Table 24).

Code	Bit rate	Bit time	Bits per frame	Frame time	Frame rate
A	1000 Hz	1 ms	100	100 ms	10 Hz
B	100 Hz	10 ms	100	1000 ms	1 Hz
D	1/60 Hz	1 minute	60	1 hour	1/3600 Hz
E	10 Hz	100 ms	100	10 s	0.1 Hz
G	10 kHz	0.1 ms	100	10 ms	100 Hz
H	1 Hz	1 s	60	1 minute	1/60 Hz

Table 24. IRIG Timecode main characteristics

DC level shift (DCLS), pulse width coded without carrier, sine wave carrier (amplitude modulated) and Manchester modulation are all options in the IRIG standard for modulating serial time codes. Each of these modulations necessitates the definition of a position marker to identify the data field's position in the frame. The frame marker, also known as the sync marker, is used to indicate where the frame begins (SOF). The time code is divided into three fields in each version of the standard: binary-coded decimal time-of-year (BCD toy), binary-coded decimal year (BCD year), and straight binary seconds (SBS). The BCD toy field is used to code the month, day of the year, hour, minutes, seconds, and tenths of seconds, all of which are coded in BCD. The year is coded using the field BCD year (in BCD). Starting at 00:00 of the current day, the field SBS is used to code the second of the day. The field CF is defined by the standard. The values that should be assigned to such a field are determined by the user. For instance, such a field could be used to map the leap second data.

4.3.5.2 Proposed Architecture

In distribution systems, synchronisation structures are typically dependent on the usage of GPS signals in each secondary substation. GPS synchronisation, on the other hand, is vulnerable to cyberattacks and may have transient faults or unavailability due to poor sky accessibility [155–157]. Other methods should be used in place of (or in addition to) GPS systems to improve timing reliability and redundancy where synchronisation is required for power grid management. A synchronisation architecture based on telecommunication systems, such as those based on the use of precision time protocol (PTP) [157,158], or White Rabbit (WR) time protocol [159–161], is commonly advised in this circumstance. The fundamental disadvantage of such performing time synchronisation methods is that they want specialised communication infrastructure. The PTP protocol, for example, requires that the switches that make up the communication infrastructure be PTP compliant: even

one non-compliant switch can break the time distribution chain. As a result, when a new infrastructure may be built, such protocols are commonly employed. A new strategy is proposed in this work. It has the distinct advantage of being based on low-cost technology and requiring no specific communication infrastructure to be installed. Furthermore, the proposed solution can be utilised in conjunction with the above-mentioned ways to improve their reliability, or in place of them where time synchronisation difficulties are a low priority. In summary, the proposed technology attempts to disseminate a time synchronisation signal by linking it into the MV distribution network, avoiding any further installation expenditures. This signal travels along the MV segments, which are each a kilometer or fewer long. In greater detail, the architecture assumes that an MV network has at least one GPS device (or, more broadly, any other precise time source) that can deliver a synchronisation signal via a transceiver coupled to an MV coupler, as shown in Fig. 65.

The synchronisation signal flows over the MV network to additional secondary substations, which are also equipped with MV couplers and transceivers. Several transmission bands are available on the MV line, as shown in [151]. One of these frequency bands can be used to convey the timing signal, while the others can be utilised to transfer data using the PLC communication protocol (e.g., G3). As a result, the proposed time dissemination strategy has no impact on PLC communication channels. The reference time signal is then distributed to all of the substation's devices.

Inductive and capacitive signal couplers are the most common types of commercial signal couplers utilised in MV systems. Inductive couplers often have an opening magnetic core that offers galvanic isolation and enables for easy movement of the coupler itself around the power cable [162], without the need to turn off the power. Geometry and electric and magnetic features, such as air gap width, cable characteristic impedance, and core magnetic characteristics, all influence coupling efficacy [163,164]. In terms of the last part, it's worth noting that magnetic core behaviour is fundamentally nonlinear, and saturation can occur when power cable currents are high, causing signal distortions. Capacitive couplers, on the other hand, are directly linked to the power line; a suitable high impedance at mains frequency is accomplished by connecting an inductance and/or an isolation transformer in series with the MV capacitance [162]. In contrast to inductive devices, the installation of capacitive couplers necessitates a service interruption. All commercial solutions have drawbacks connected to their costs, which include not only the cost of the coupler but also the expenditures of equipment installation, switchboard reconfiguration, and service interruptions (if needed).

The innovative solution for PLC signal coupling in MV networks described in 4.3.4 allows exploiting some electrical elements normally present in MV switchboards. The proposed coupling solution is the base of the proposed solution for non-invasive time dissemination, because it guarantees to reach all secondary substation with reduced installation work, no service interruption or modification on the MV switchboards that are required, and very low cost, i.e., that of the electronic interface board. The solution which is described in next section has been developed in cooperation with University of Brescia and published in [165,166]

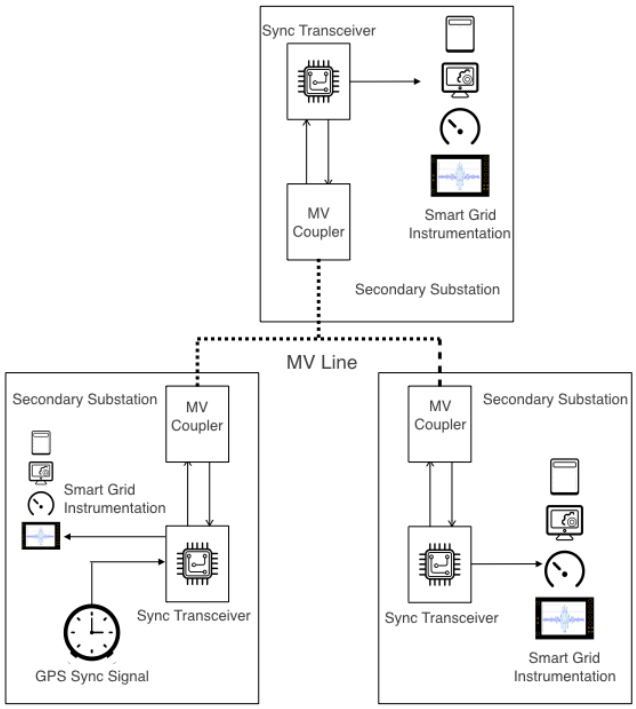

Fig. 65. Proposed synchronization system architecture on MV grid.

4.3.5.2.1 IRIG-B Time Code over MV Grid

IRIG-B is a standard frequently used in secondary substations to transmit time information via a serial communication channel, as described in 4.3.5.1. An IRIG-B interface is already built into a number of measurement and control devices. As a result, the IRIG-B time code has been proposed as a means of disseminating timing information across the MV power system. However, due to the unique characteristics of the transmission media, the modulation techniques established by the standard are not suited for transmission over the MV line. Chirp signals have good tolerance to channel noise when broadcast over an MV line, as proved experimentally in [151]. Thus, chirp signals can be utilised to modulate IRIG-B symbols on the MV line. IRIG-B needs the definition of two special markers: frame marker and position marker, as specified in the standard. The frame marker (also known as the sync marker in the rest of this thesis) is used to indicate the start of the IRIG-B frame. The position marker (also known as the position identifier, PI) is used to indicate the position of a data field in the IRIG-B frame (for example, second, minute, and hour). As a result, a modulation technique suited for transmitting the IRIGB frame necessitates the development of four symbols:

- two special symbols (sync and PI);
- two symbols expressing logic values ("0" and "1").

The duration of each symbol is 10 milliseconds, and the maximum number of bits per frame is 100, according to the IRIG-B standard. As a result, an IRIG-B frame lasts one second. An up-chirp (linear chirp from $f_0\ to\ f_1$) and down-chirp (linear chirp from $f_1\ to\ f_0$) to map the two separate logic values ("0" and "1") is one way to modulate digital information using a linear chirp signal delivered in the frequency band $[f_0 - f_1]$. IRIG-B, on

the other hand, requires two more symbols for sync and PI markers. To map up to four symbols, one feasible option is to combine up-chirp and down-chirp into a single sign. Each symbol has a duration of 10 milliseconds (as stated by the IRIG-B standard), while each chirp in a symbol has a duration of 5 milliseconds. Fig. 66 shows the chirp-based symbols used to map the IRIG-B marker and data.

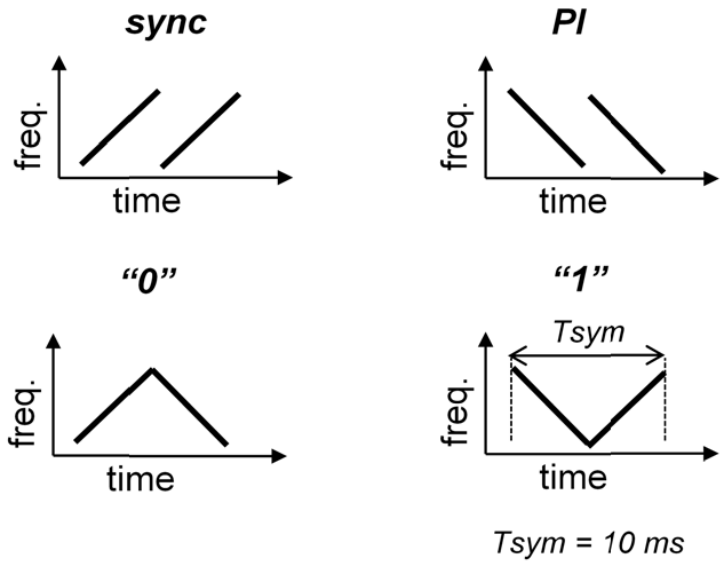

Fig. 66. Chirp-based symbols used to map IRIG-B marker and data value

Fig. 67 shows an example of an IRIG-B frame modulated with the suggested modulation strategy. In IRIG-B, the sync marker is used to start and end the frame. The start of sync symbol represents the SOF, which corresponds to the synchronisation event (i.e., the 1-pulse per second (1-PPS) signal generated by a GPS receiver, an atomic clock, or an IEEE 1588 Grand Master Clock). The PI marker divides the frame's data fields (for example, the seconds and minutes fields, as seen in Fig. 67). A BCD code is used to code each field of the IRIG-B frame.

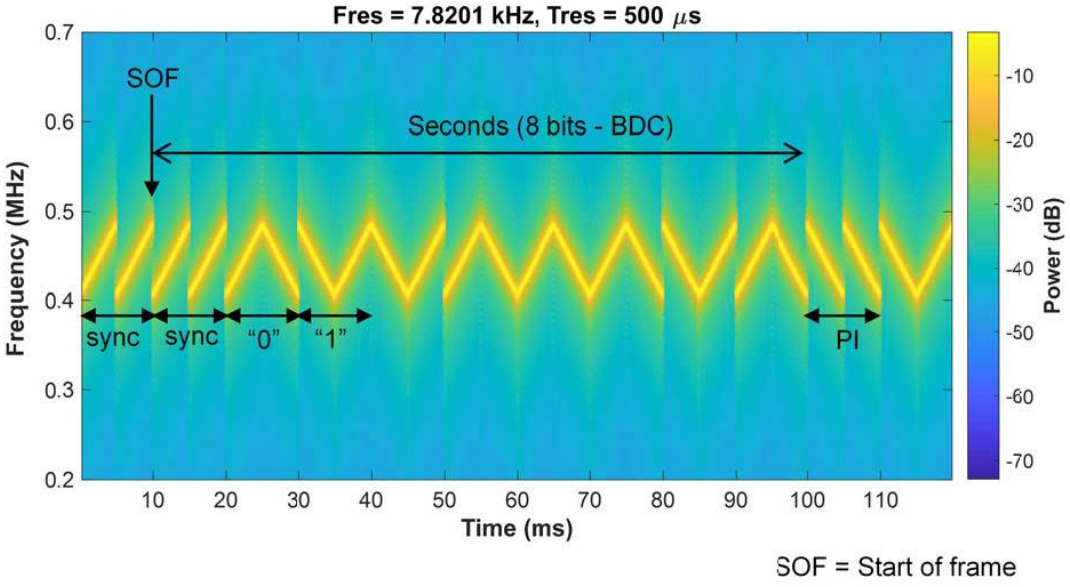

Fig. 67. Spectrogram of an IRIG-B frame modulated using the chirp-based modulation

4.3.5.2.2 Chirp-Based Modulation and Demodulation Circuitry

To keep the proposed approach's costs as low as possible, the Sync Transceiver's modulation and demodulation stages, which are used to transmit and recover the chirp-based symbol on the MV grid, should be as simple as possible. The block diagram of a modulation stage is shown in Fig. 68.

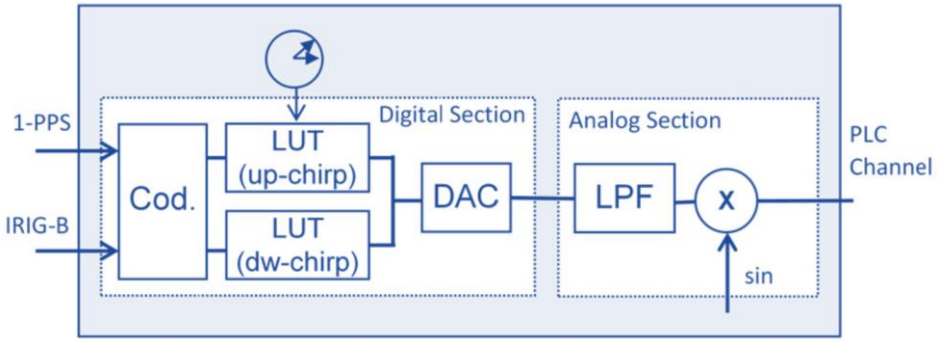

Fig. 68. Block diagram of the transmitted side modulation stage

The chirps are broadcast at a frequency of 405–485 kHz. Each chirp has an 80 kHz bandwidth. A suitable coding logic encodes the 1-PPS signal generated by a GPS receiver and the National Marine Electronics Association (NMEA) serial data (which provides the date and time) in a binary serial stream of data. The chirp-based symbols are then used to modulate each of these data according to the modulation strategy shown in Fig. 66. Look-up tables can be used to implement the up-chirp and down-chirp (LUTs). The up-chirp and down-chirp are created in the baseband (in the band 0–80 kHz) to save money on the digital-to-analogue converter (DAC). The external analogue front-end filters the signal created by the DAC (low-pass filter (LPF) with a frequency cut-off of 125 kHz) and uses an analogue multiplier to transform the generated chirp into the transmission band. The sinusoidal signal used to translate the chirp symbol has a frequency of 405 kHz. Because analogue transmissions have a maximum frequency of far below 1 MHz, the cost of the analogue front-end is still limited. The decoding of an IRIG-B frame is divided into two stages:

- The first step is to identify the SOF, which is used to identify the synchronisation event
- The second step is to decode the IRIG-B data sent in the frame.

The most difficult stage is identifying the SOF (indicated by the sync symbol), because the accuracy of time distribution is dependent on the accuracy of such an event's identification.

The demodulation circuitry, like the modulation stage, uses an analogue front-end to translate the incoming signal into baseband and reduce the sampling rate of the analogue-to-digital converter (ADC) block, as illustrated in Fig. 68. The analogue front-end requires a bandpass filter (BPF) tuned to the chirp band (405–485 kHz), an analogue multiplier that multiplies the filtered signal by a sinusoidal signal (at 405 kHz), and

finally an LPF (fc = 125 kHz). A 250-kSa/s ADC is used to acquire the filtered signal. To identify the SOF and decode the IRIG-B frame, the sampled data is digitally processed. A well-known method is to employ a marker to properly identify the time of arrival (ToA) of a frame delivered over a power grid. Markers with a high tolerance to noise, such as chirps or barker code, are utilised in PLC, as seen in [147–150]. Not just across wireless communication channels, but also over wired communication channels, the use of chirp signals for ToA detection appears to be particularly promising [167]. The usage of chirps in the suggested system is primarily for this purpose. With low processing power, the autocorrelation of the chirp—whose shape resembles a *sinc* function—may be easily calculated, and its peak can be used to determine chirp timing and so provide an accurate reception timestamp (see Fig. 69).

As shown in Fig. 70, the signal processed by the analogue front-end and sampled by an ADC is then cross-correlated with an ideal chirp. The maximum of the generated sinc-like function corresponds to the true chirp reception time. The receiver can then create the 1-PPS signal reference for external devices using this exact time reference. The estimated ToA estimation is given by

$$ToA_{est} = \underset{t\in\mathbb{R}}{\operatorname{argmax}}\{y(t)\}$$

in the ideal case of continuous time cross correlation of the chirp without prior sampling and quantization, where $y(t)$ is the result of the cross correlation between the ideal and real chirp signals. Only noise on the communication line limits the estimation's accuracy in this scenario.

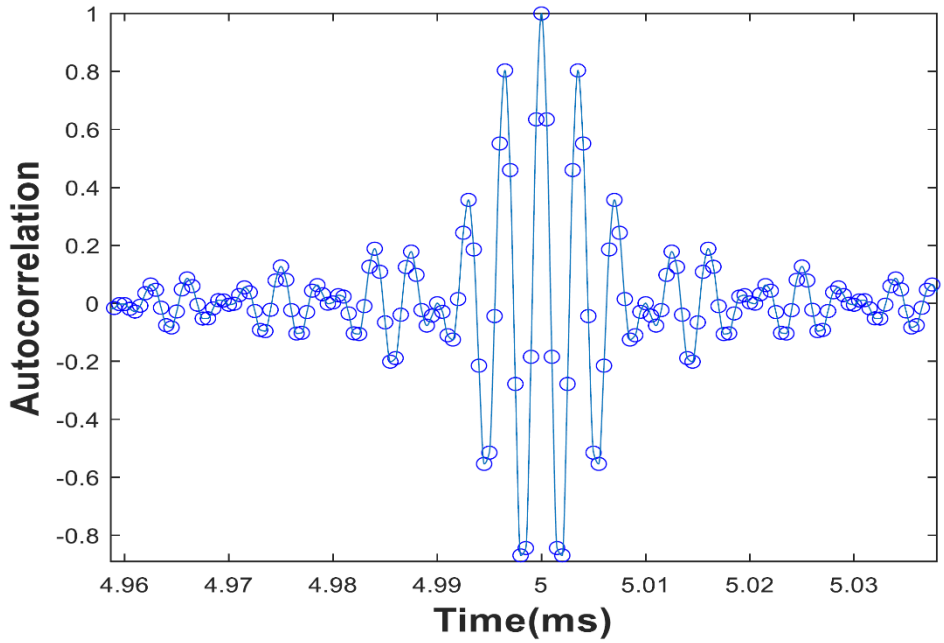

Fig. 69. Autocorrelation of a chirp. Solid line represent the autocorrelation while dots stands for its samples

The ADC sampling frequency, on the other hand, affects the temporal precision because analogue-to-digital conversion was chosen for its flexibility, convenience, and low cost. With respect to the input signal, the ADC sampling is asynchronous. Let $y[m]$ be the result of the discrete-time cross correlation between the reference chirp and the sampled input signal $s[m]$ ($s(t)$ sampled with sampling period T_s). The predicted ToA is then calculated using the formula

$$ToA_{est} = \underset{m\in\mathbb{Z}}{\operatorname{argmax}}\{y[m]\} * T_s = p * T_s$$

where $s[m] = s(m * T_s)$.

However, by interpolating the discrete values of the cross correlation, the peak's timestamping resolution can be improved. Because the correlation peak has a parabolic form around its maximum, a parabolic interpolator is a good fit. The estimated ToA is then:

$$ToA_{est} = \left(p + \frac{|y[p-1]| - |y[p+1]|}{2(|y[p-1]| - 2|y[p]| + |y[p+1]|)}\right) * T_s$$

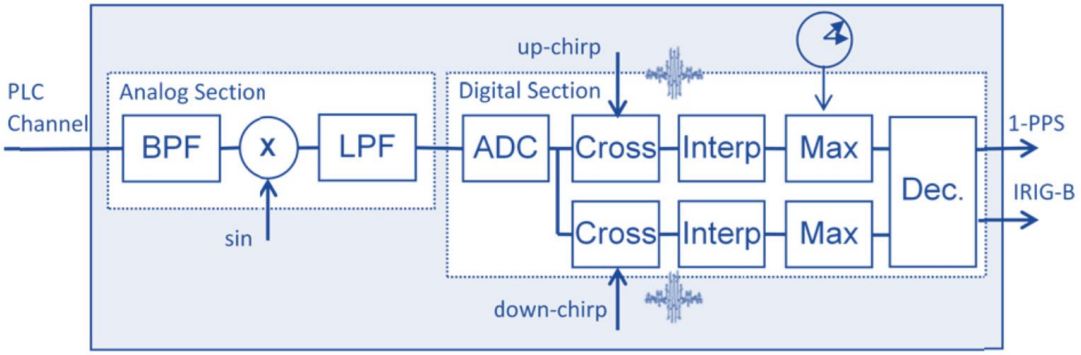

Fig. 70. Block diagram of the receiver side modulation stage

The approximation error can be relatively big when $y[p-1]$ and $y[p+1]$are far from the actual maximum, resulting in poor timestamping precision. A sample rate of 1 MSa/s is adequate to keep the parabolic interpolator's approximation errors below 5 ns. Low-cost ADCs, on the other hand, have a lower sample rate (typically 250 kSa/s). Given the requirement to deal with chirp signals in the baseband up to 80 kHz, a sampling frequency on the order of 250 kSa/s is employed in this particular case.

As a result, the suggested method is divided into two steps when applied to the signal of a 250 kSa/s ADC:

1. Stage 1: Post-processing algorithm for interpolating the signal from 250 kSa/s to 1 MSa/s after the matching filter. It's a shortened "sinc" reconstruction filter that looks at the 30 samples preceding and after the peak (for sake of computational efficiency).
2. Stage 2: Parabolic interpolator with three samples at the sinc peak.

4.3.5.3 Experimental Validation

Experiments were carried out in the absence of mains voltage on a laboratory test bench. Three MV power cables (single-pole, type RG7H1R, 50-mm2 aluminium core cross section, copper shield) were linked to capacitive dividers, similar to those often used in secondary substations MV switchboards, in the experimental setup (see Fig. 71 and Fig. 72). VDS panels (compatible with IEC 61243-5 MR type) were then connected to capacitive dividers [137]. An interface card was linked to each VDS socket terminal to broadcast and receive the signal. Variable inductors are embedded on the interface board and are used to match the equivalent capacity C_{eq}visible from socket terminals. These inductors are tuned to provide a resonant circuit in both transmission and reception, resulting in a low-impedance path to the ground. The resulting resonant circuit allows coupling the signal to the power line while avoiding short-circuiting the signal to ground in the transmitting region. An amplification stage and an impedance matching circuit are included on the interface card to boost the signal level. On the other hand, the signal is divided between the capacitive divider and the impedance between the VDS terminals and the earth at the receiving section. The resonant circuit reduces signal dispersion by increasing the resistance between the VDS terminals and the earth.

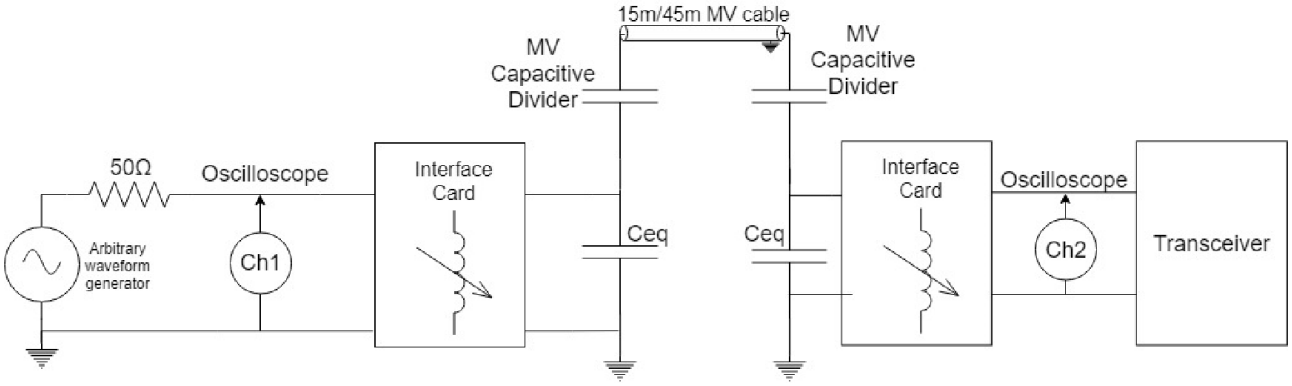

Fig. 71. Schematic of the experimental setup used for validating the tx of chirp on an MV line

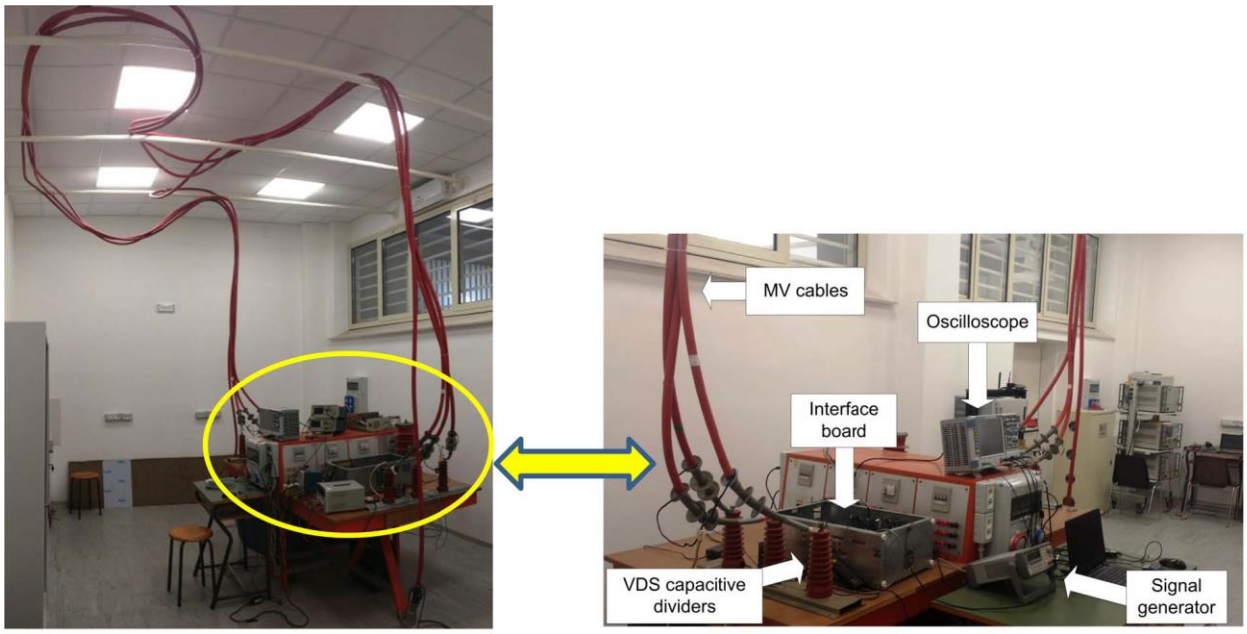

Fig. 72. Laboratory experimental setup

A passband active filter is included in the interface card to reduce noise and increase the signal–noise ratio (SNR). The frequency response of the inductors, filters, and impedance matching circuit is set to get a flat frequency response in the desired frequency range. The modem and interface card, as well as the system power supply, are housed in a metal box. An Agilent 33220A arbitrary waveform generator is utilised to create the chirp-based symbols used to map the IRIG-B frame for validation of the suggested technique. It's set up to create a generic waveform using sample data exported from MATLAB simulations. The final chirp symbol has a length of 10 ms and an amplitude of 1 Vpp. The rest of our analysis focuses on the transmission of sync symbols in particular, because the correctness of the external 1-PPS generation is solely dependent on the recognition of this symbol. A Rohde & Schwarz RTO 1044 digital oscilloscope was used to measure the transmitted and received signals, as well as the arbitrary waveform generator's trigger signal. The oscilloscope samples the power line with a sampling frequency of 100 Msamples/s. The samples are then numerically post-processed to approximate the analogue frontend and digital elaboration chain of the demodulation stage depicted in Fig. 69. The numerical elaboration depicted in Fig. 73 was used to replicate the analogue front-end.

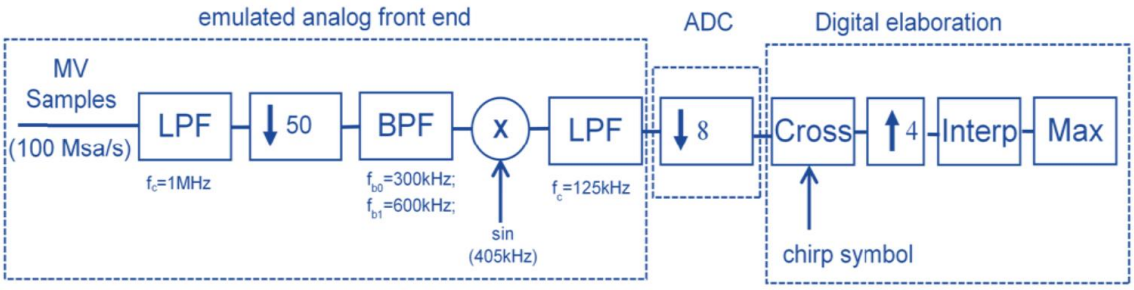

Fig. 73. Validation procedure based on digital elaboration

To limit the amount of samples to be processed by the subsequent phases, the captured signal is down-sampled offline by a factor of 50. The numerical data is then filtered using a digital finite impulse response (FIR) BPF adjusted to the chirp symbol's frequency spectrum. To translate the chirp in the baseband, these values are multiplied numerically with a sinusoidal signal. A digital FIR LPF filters the result of the multiplication, cutting off the spectral replicas. The ADC is then emulated with a sample rate of 250 kSa/s, equivalent to what is available in embedded systems, using a down-sampling stage. The down-sampled signal is then processed digitally, as detailed in 4.3.5.2.2. The tests were conducted with two different cable lengths (15 and 45 meters) with chirp symbols modulated in the frequency bands (405–485) kHz. Each test has been carried out 100 times.

4.3.5.3.1 Results

Chirp-based signals have already been shown to be successful in wireless communication channels for distributing time reference. However, the MV network (including the MV cable and coupling system) has unique characteristics that may impact chirp-based signal transmission. Previous research [151] has demonstrated that such a signal can be transmitted on the MV line in many frequency bands. To confirm the ability to modulate IRIG-B time coding with chirp-based signals, a special experimental analysis is necessary. The results of the characterisation performed on the experimental setup specified in above are here presented. Fig. 74 shows the spectrogram of a sync signal delivered over a 45-meter MV wire. The chirps signal that make up the sync symbol has a frequency range of [405–485] kHz. The sign has a duration of 10 milliseconds, as established by the IRIG-B protocol.

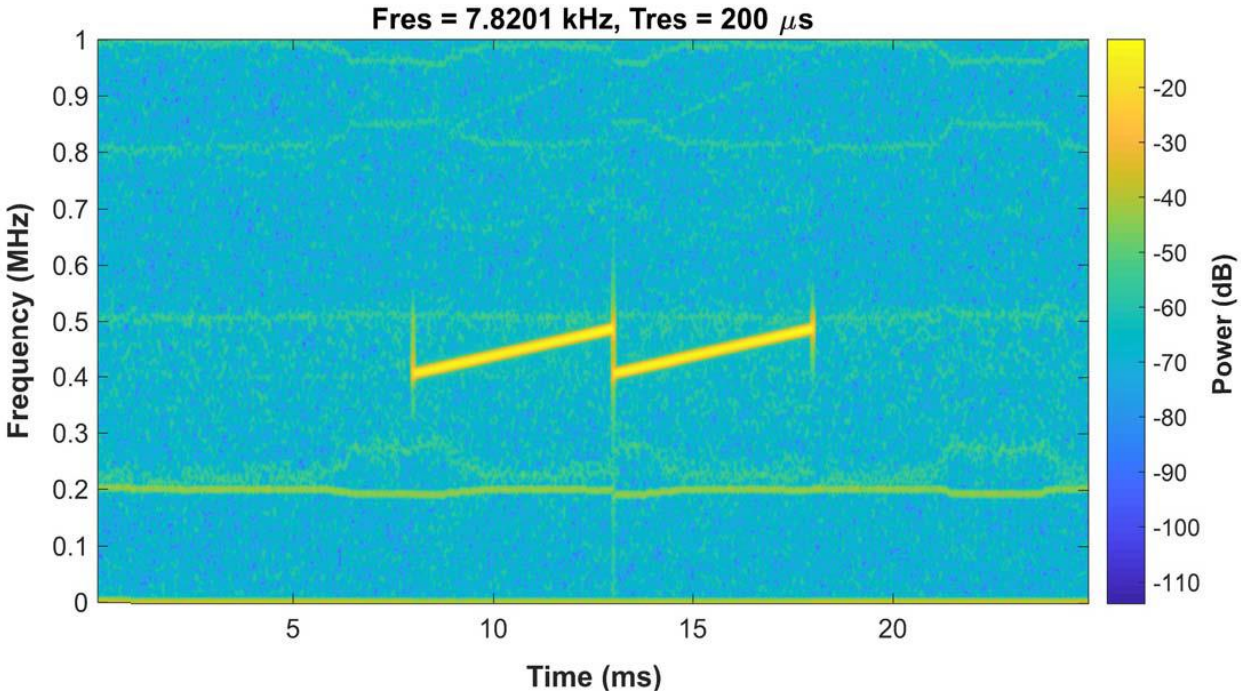

Fig. 74. Spectrogram of the sync symbol (symbol time = 10ms)

The sync symbol is used to identify the SOF and then to generate the reference 1-PPS, as mentioned in the preceding section. Because of the significance of such a symbol, the rest of the analysis concentrates on the MV grid's and coupling logic's impact on it. The characterisation was done using MV lines of various lengths while maintaining the same chirp bandwidth, i.e., 80 kHz, which is the maximum allowed by the MV coupling system. Using 15m and 45m cable lengths, Fig. 75 compares the sent and received chirp-based sync symbols (in the frequency spectrum [405–485] kHz). Each of the sync symbols was sampled at a rate of 2 MSa/s. Despite the short length of the MV line, the amplitude modulation effect on the received chirp is visible when comparing the subfigures (45 m in the longest case). This effect is mostly determined by the MV coupling system used.

The digital elaboration illustrated in Fig. 73 is used to process a sample of the data obtained from the experimental setup, as shown in Fig. 75. The spectrograms in Fig. 76 demonstrate the frequency content of the received sync symbol after the down sampling stage imitating the ADC. It should be observed that the elaboration steps depicted in Fig. 73 are capable of removing a significant portion of the frequency noises contained in the original signal depicted in Fig. 74. The quality of the received sync symbol is influenced in part by the length of the cables.

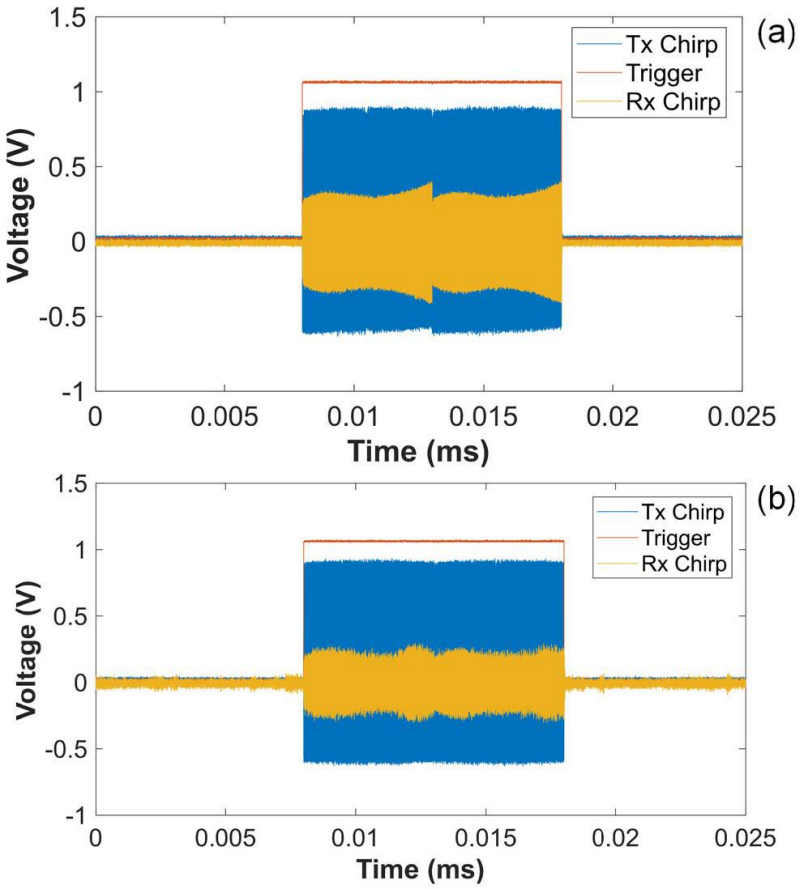

Fig. 75. Received chirp symbols vs trigger signal (orange line) and sent (blue line) (yellow line). 405–485 kHz is the frequency band. (a) 15 m and (b) 45 m cable length.

Following the characterisation of the sync symbol transmission on the MV line, the received sync symbol was post processed in the MATLAB environment to quantify the ToA identification accuracy. It's important to recall that the sync symbol's identification has a direct impact on the creation of the reference 1-PPS signal. To obtain the cross-correlation signal, the received sync symbol is cross-correlated with a locally synthetized symbol. After that, the cross-correlated signal is treated to improve ToA accuracy. As indicated in 4.3.5.2.2, the cross-correlation signal is interpolated. The midpoint of the sync symbol is represented by the maximum of the interpolated cross-correlation signal. On the transmission side, the time difference between the rising edge of the trigger signal (orange line in Fig. 75) utilised to generate the sync symbol and the peak of the cross-correlation signal has been used to estimate ToA accuracy. Table 25 summarises the findings of the characterisation done under various testing settings (each repeated 100 times). The cross-correlation function, whose peak corresponds to half of the chirp length, determines the mean value of this time interval. Such a value is constant and can be compensated under certain assumptions. Because the short length of the cables is taken into account throughout the test, the chirp propagation delay on the transmission line has only a little impact on the mean value. Under all of the parameters tested during the experimental characterisation, the ToA has a standard deviation of 0.5 seconds.

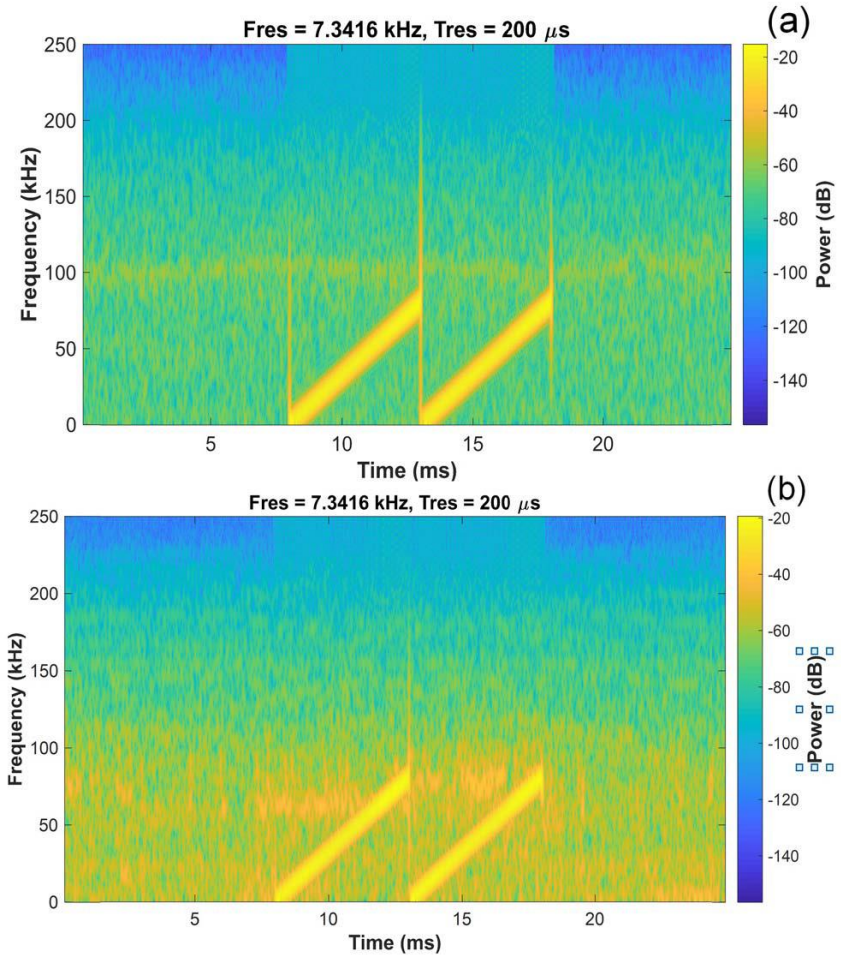

Fig. 76. Spectrogram of the received sync symbol after the digital elaboration (frequency resolution 7.3 kHz and time resolution 0.2 ms). Cable length: (a) 15 m and (b) 45 m.

The noise on the MV grid affects the jitter, which is defined as the highest fluctuation of the ToA during the experiment (100 samples). A longer MV line, as expected, has an impact on the accuracy of ToA estimation. With a 45-meter cable, the maximum jitter is 3.5 seconds. It should be emphasised that chirp-based symbol processing has been kept as basic as feasible in order to keep implementation costs low and to employ a low-cost platform.

Length	Time of Arrival		
	Mean()	Std.Dev ()	Jitter ()
15 m	3988	1.8	7
45 m	3990	1.9	7.5

Table 25. Statistical indices of the Evaluation of ToA under different cable lengths

5 CONCLUSIONS

The challenge of efficient integration of renewable energy sources at the MV and LV power grid levels has been addressed in this thesis. Indeed, the increased number of DGs and ESSs connected in various point-of-distribution networks, has resulted in their gradual metamorphosis into active networks with bidirectional energy flows. Thus, distribution networks should evolve into Smart Grids, with a greater number of monitoring, communication, and management systems to ensure many functionalities such as voltage and frequency regulation, anti-islanding protection, smart metering, power quality monitoring, system diagnostics, demand side management, and so on.

In this perspective, a novel architecture for MV and LV power grids and related advanced metering and ICT equipment have been proposed ,in order to enhance the penetration of renewable energy sources while also giving the DSO a proper control over them in order to make the system secure, stable, and reliable. The developed solutions allow to meet the requirements of the future power grid, thus,t enabling smart districts and smart cities paradigm implementation and exploitation. Actually, as shown in the previous chapters, the proposed architecture and related hardware and software solutions for metering and communication can allow contributing to the goals of:

- monitoring the network and remotely managing distributed energy sources. through innovative interface devices;
- improving the interaction between the interface devices and the main grid, thanks to new intelligent devices installed in secondary substations;
- enabling DSO with new features for power grid management, decision-making and forecasting, by means of the distributed measurement and communication infrastructure, equipped with new metering functionalities and the developed software tools.

This architecture includes a distributed measurement system for measuring active and reactive power at the secondary substation level. The collected data is transmitted to the DSO control centre via a proprietary wireless network, where it is processed by a load flow algorithm in the SCADA. As a result, the SCADA displays the actual flux on the MV network to the operator, signalling in real time if an inversion occurs in a branch. The informed operator can then act on the mapped controlled DER or ESS and modify the operating functionality to meet the DSO network stability criteria. To do this, the secondary substation, along with the PQAs, housing a special device known as a concentrator, which serves as a communication bridge between the DSO control centre and the remote devices deployed at the inverter level, according to the DSO. This is the DSO's HAP, and it's called PLC Remote Bridge. It connects with the inverter and the IPS to disconnect the user's production/storage facility as necessary. Both the concentrator and the PLC remote bridge use a ST microelectronic platform (EVALKIST8500-1 Evaluation Board) and communicate via the PLC link via the LV power wire. As a communication protocol, the PRIME 1.4 protocol was chosen. The concentrator software,

which serves as a communication bridge and network coordinator, was created on a Raspberry Pi 3 board by utilising a binary library for modem handling provided directly by ST Microelectronics. The proposed architecture has been implemented and tested both in the field and in the laboratory, with the results available in [95,116,125,126,152]. The PLC PRIME architecture was tested in the lab, and the findings are provided in [169]. The tests show that the design is suitable to be adopted by a distributor with a very low investment due to the use of the PLC and the reduced cost of the PQAs in comparison to other expensive equipment. Indeed, field testing were conducted on the Favignana and Ustica islands' MV and LV power grids. The findings demonstrated that the proposed design may be scaled up to a larger and more complex network.

Along with the proposed architecture some interesting topics are addressed in thesis. This topics embrace both the measurements and the PLC communication for smart grid evolution. The possibility to implement a power quality analyser on a low cost platform has been investigated. In detail the STCOMET (EVLKSTCOMET10-1) from ST microelectronics has been used. STCOMET is a smart meter board already used for energy billing and AMR purpose in various countries. The study on this board has been focus on implement the metrics of IEC-6100-4-30/4-7 for power quality and harmonics and inter-harmonics analysis. These metrics have been implemented in accordance with the standard, and an FFT-based algorithm has been built on the device, taking into account the platform's restricted resources. As a result of the platform's characteristics and constraints, an IEC-61000-4-3/4-7 Class S PQA has been implemented. Because the PQA has been implemented on a smart meter platform and placed at the user level, the DSO may take advantage of a highly distributed power quality measuring system and collect data for monitoring and quality of service analysis. It will be able to add more functionalities to the smart meter platform in the future to develop applications such as harmonic source localisation and so on. In order to do that a solid time dissemination system is needed. In section 4.3.5 a time dissemination over MV lines is proposed. It is based on the exploit of the PRIME protocol preamble where IRIG-B timecode is encoded in some chirp based symbols. The primary goal of the work on this topic is to investigate a low-cost system for disseminating time information via the distribution grid. The suggested modulation technique is both resilient to power line noise and simple to execute using low-cost electronic equipment. An experimental configuration for validating the possibility of transmitting IRIG-B time code over an MV line is provided in this thesis as well in [165]. Experiments on a genuine laboratory setting showed the validity of the suggested approach and show that the standard deviation of the sync symbol estimation is on the order of a few microseconds, even if the generated chirp has a limited frequency bandwidth (i.e., 80 kHz).

The Ph.D. research work has been carried out in cooperation with the Institute on Marine Engineering of the National Research Council (INM-CNR); collaborations have to be mentioned also with Industries, particularly STMicroelectronics, whose viewpoint has allowed to give an industrial interest to the research work.

The research work is already continuing after the Ph.D. experience, addressing some new developments concerning both measurement and communication features. To complete the time dissemination system

architecture, a gusset is ongoing; indeed, the devices clock sync over LV PLC is still in progress and need to be object of further insights. Moreover, future works includes the PQA implemented on the COMET platform upgrade to the Class A device and the full implementation and integration of the Hyperion software at the DSO control centre.

6 REFERENCES

[1] Senato 10a,13a,10a commisione CVA X Attività produttive. Atto del Governo 292 - Schema di decreto legislativo recante attuazione della direttiva (UE) 2018/2001 sulla promozione dell'energia da fonti rinnovabili. n.d.

[2] Croce V, Lazzaro M, Paternò G, Ziu D, Sanseverino ER, Monti A. Smart district energy optimization of flexible energy units for the integration of local energy storage. 2017 IEEE International Conference on Environment and Electrical Engineering and 2017 IEEE Industrial and Commercial Power Systems Europe (EEEIC / I CPS Europe), 2017, p. 1–6. https://doi.org/10.1109/EEEIC.2017.7977597.

[3] Chiarini R, Clerici P, Giuliani G, Gozo N, Massa G. Diffusione dei risultati e Network - Report RdS/PAR2018/039 2018.

[4] Kabalci E, Kabalci Y, editors. Smart Grids and Their Communication Systems. Singapore: Springer Singapore; 2019. https://doi.org/10.1007/978-981-13-1768-2.

[5] Jacobs M. 13 of the Largest Power Outages in History — and What They Tell Us About the 2003 Northeast Blackout. The Equation - Union of Concerned Scientist n.d. https://blog.ucsusa.org/mike-jacobs/2003-northeast-blackout-and-13-of-the-largest-power-outages-in-history-199/.

[6] Amin M, Schewe P. Preventing Blackouts in Scientific American. Scientific American 2007;296:60–7. https://doi.org/10.1038/scientificamerican0507-60.

[7] Amin M. Toward self-healing energy infrastructure systems. IEEE Computer Applications in Power 2001;14:20–8. https://doi.org/10.1109/67.893351.

[8] Massoud Amin S, Wollenberg BF. Toward a smart grid: power delivery for the 21st century. IEEE Power and Energy Magazine 2005;3:34–41. https://doi.org/10.1109/MPAE.2005.1507024.

[9] Khattak AR, Mahmud SA, Khan GM. The Power to Deliver: Trends in Smart Grid Solutions. IEEE Power and Energy Magazine 2012;10:56–64. https://doi.org/10.1109/MPE.2012.2196336.

[10] EPRI | SmartGrid Resource Center n.d. https://smartgrid.epri.com/.

[11] Smart Grids. NetlDoeGov n.d. http://www.netl.doe.gov/smartgrids.

[12] Momoh JA. Smart Grid: Fundamentals of Design and Analysis. John Wiley & Sons; 2012.

[13] Kroposki B, Johnson B, Zhang Y, Gevorgian V, Denholm P, Hodge B-M, et al. Achieving a 100% Renewable Grid: Operating Electric Power Systems with Extremely High Levels of Variable Renewable Energy. IEEE Power and Energy Magazine 2017;15:61–73. https://doi.org/10.1109/MPE.2016.2637122.

[14] Artale G, Caravello G, Cataliotti A, Cosentino V, Guaiana S, Di Cara D, et al. Implementation of a Management System for Prosumer Energy Storage Scheduling in Smart Grids. 20th IEEE Mediterranean Electrotechnical Conference, MELECON 2020 - Proceedings, 2020, p. 547–52. https://doi.org/10.1109/MELECON48756.2020.9140566.

[15] Shaukat N, Ali SM, Mehmood CA, Khan B, Jawad M, Farid U, et al. A survey on consumers empowerment, communication technologies, and renewable generation penetration within Smart Grid. Renewable and Sustainable Energy Reviews 2018;81:1453–75. https://doi.org/10.1016/j.rser.2017.05.208.

[16] Active demand side management for households in smart grids using optimization and artificial intelligence | Elsevier Enhanced Reader n.d. https://doi.org/10.1016/j.measurement.2017.10.010.

[17] Cataliotti A, Cosentino V, Crotti G, Delle Femine A, Di Cara D, Gallo D, et al. Compensation of nonlinearity of voltage and current instrument transformers.IEEE Trans. Instrum Meas 2019;68:1322–32.

[18] Rinaldi S. A Testing Framework for the Monitoring and Performance Analysis of Distributed Energy Systems. IEEE Trans Instrum Meas 2019;68:3831-3840,.

[19] Regola tecnica di riferimento per la connessione di utenti attivi e passivi alle reti BT delle imprese distributrici di energia elettrica" (Reference technical rules for the connection of active and passive users to the LV electrical Utilities 2016.

[20] Artale G. A Monitoring and Management System for Energy Storage Integration in Smart Grids. 2019 IEEE International Instrumentation and Measurement Technology Conference, Auckland, New Zealand: 2019, p. 803–8.

[21] Artale G, Cataliotti A, Cosentino V, Cara DD, Fiorelli R, Guaiana S, et al. A new PLC-based smart metering architecture for medium/low voltage grids: Feasibility and experimental characterization.

Measurement: Journal of the International Measurement Confederation 2018. https://doi.org/10.1016/j.measurement.2018.07.070.
[22] Morello R, Mukhopadhyay SC, Liu Z, Slomovitz D, Samantaray SR. Advances on Sensing Technologies for Smart Cities and Power Grids: A Review. IEEE Sensors Journal 2017;17:7596–610. https://doi.org/10.1109/JSEN.2017.2735539.
[23] Manditereza PT, Bansal R. Renewable distributed generation: The hidden challenges – A review from the protection perspective. Renewable and Sustainable Energy Reviews 2016;58:1457–65. https://doi.org/10.1016/j.rser.2015.12.276.
[24] Farhoodnea M, Mohamed A, Shareef H, Zayandehroodi H. Power Quality Impact of Renewable Energy based Generators and Electric Vehicles on Distribution Systems. Procedia Technology 2013;11:11–7. https://doi.org/10.1016/j.protcy.2013.12.156.
[25] Saxena N, Hussain I, Singh B, Vyas AL. Implementation of a Grid-Integrated PV-Battery System for Residential and Electrical Vehicle Applications. IEEE Trans Ind Electron 2018;65:6592–601. https://doi.org/10.1109/TIE.2017.2739712.
[26] Croce D, Giuliano F, Tinnirello I, Galatioto A, Bonomolo M, Beccali M, et al. Overgrid: A Fully Distributed Demand Response Architecture Based on Overlay Networks. IEEE Transactions on Automation Science and Engineering 2017;14:471–81. https://doi.org/10.1109/TASE.2016.2621890.
[27] Di Silvestre ML, Gallo P, Ippolito MG, Sanseverino ER, Zizzo G. A Technical Approach to the Energy Blockchain in Microgrids. IEEE Transactions on Industrial Informatics 2018;14:4792–803. https://doi.org/10.1109/TII.2018.2806357.
[28] Morello R, De Capua C, Fulco G, Mukhopadhyay SC. A Smart Power Meter to Monitor Energy Flow in Smart Grids: The Role of Advanced Sensing and IoT in the Electric Grid of the Future. IEEE Sensors J 2017;17:7828–37. https://doi.org/10.1109/JSEN.2017.2760014.
[29] Pasetti M, Rinaldi S, Manerba D. A Virtual Power Plant Architecture for the Demand-Side Management of Smart Prosumers. Applied Sciences 2018;8:432. https://doi.org/10.3390/app8030432.
[30] Kabalci E, Kabalci Y. A Measurement and Power Line Communication System Design for Renewable Smart Grids. Measurement Science Review 2013;13:248–52. https://doi.org/10.2478/msr-2013-0037.
[31] Cataliotti A, Cosentino V, Di Cara D, Russotto P, Telaretti E, Tine G. An Innovative Measurement Approach for Load Flow Analysis in MV Smart Grids. IEEE Trans Smart Grid 2016;7:889–96. https://doi.org/10.1109/TSG.2015.2430891.
[32] Rinaldi S, Della Giustina D, Ferrari P, Flammini A, Sisinni E. Time synchronization over heterogeneous network for smart grid application: Design and characterization of a real case. Ad Hoc Networks 2016;50:41–57. https://doi.org/10.1016/j.adhoc.2016.04.001.
[33] Sun Q, Li H, Ma Z, Wang C, Campillo J, Zhang Q, et al. A Comprehensive Review of Smart Energy Meters in Intelligent Energy Networks. IEEE Internet Things J 2016;3:464–79. https://doi.org/10.1109/JIOT.2015.2512325.
[34] Jamali S, Bahmanyar A, Bompard E. Fault location method for distribution networks using smart meters. Measurement 2017;102:150–7. https://doi.org/10.1016/j.measurement.2017.02.008.
[35] Artale G, Cataliotti A, Cosentino V, Di Cara D, Guaiana S, Nuccio S, et al. Smart interface devices for distributed generation in smart grids: The case of islanding. IEEE Sensors Journal 2017;17:7803–11. https://doi.org/10.1109/JSEN.2017.2726185.
[36] Kabalci Y. A survey on smart metering and smart grid communication. Renewable and Sustainable Energy Reviews 2016;57:302–18. https://doi.org/10.1016/j.rser.2015.12.114.
[37] Giustina DD, Rinaldi S. Hybrid Communication Network for the Smart Grid: Validation of a Field Test Experience. IEEE Transactions on Power Delivery 2015;30:2492–500. https://doi.org/10.1109/TPWRD.2015.2393836.
[38] Kiedrowski P. Toward More Efficient and More Secure Last Mile Smart Metering and Smart Lighting Communication Systems with the Use of PLC/RF Hybrid Technology. International Journal of Distributed Sensor Networks 2015;11:675926. https://doi.org/10.1155/2015/675926.
[39] Masood B, Baig S. Standardization and deployment scenario of next generation NB-PLC technologies. Renewable and Sustainable Energy Reviews 2016;65:1033–47. https://doi.org/10.1016/j.rser.2016.07.060.
[40] Cataliotti A, Cosentino V, Di Cara D, Guaiana S, Panzavecchia N, Tinè G. A New Solution for Low-Voltage Distributed Generation Interface Protection System. IEEE Transactions on Instrumentation and Measurement 2015;64:2086–95. https://doi.org/10.1109/TIM.2015.2421691.

[41] Papadopoulos TA, Kaloudas CG, Chrysochos AI, Papagiannis GK. Application of Narrowband Power-Line Communication in Medium-Voltage Smart Distribution Grids. IEEE Transactions on Power Delivery 2013;28:981–8. https://doi.org/10.1109/TPWRD.2012.2230344.
[42] Cataliotti A, Cosentino V, Di Cara D, Tinè G. Measurement Issues for the Characterization of Medium Voltage Grids Communications. IEEE Transactions on Instrumentation and Measurement 2013;62:2185–96. https://doi.org/10.1109/TIM.2013.2264861.
[43] Papadopoulos TA, Chrysochos AI, ElSamadouny A, Al-Dhahir N, Papagiannis GK. MIMO-OFDM narrowband-PLC in distribution systems: Impact of power transformers on achievable data rates. Electric Power Systems Research 2017;151:251–65. https://doi.org/10.1016/j.epsr.2017.05.039.
[44] Cataliotti A, Cosentino V, Di Cara D, Tinè G. Oil-filled MV/LV power-transformer behavior in narrow-band power-line communication systems. IEEE Transactions on Instrumentation and Measurement 2012;61:2642–52. https://doi.org/10.1109/TIM.2012.2209911.
[45] Huang Q, Jing S, Yi J, Zhen W. Innovative Testing and Measurement Solutions for Smart Grid: Huang/Innovative Testing and Measurement Solutions for Smart Grid. 2014. https://doi.org/10.1002/9781118889954.
[46] Ekanayake J, Liyanage K, Wu J, Yokoyama A, Jenkins N. Smart Grid: Technology and Applications. Chic Hester: John Wiley & Sons; 2012.
[47] Hirsch A, Parag Y, Guerrero JM. Microgrids: A review of technologies n.d.
[48] ș et al. YY. Enhancing smart grid with microgrids: Challenges and opportunities. Renewable Sustain Energy Rev 2017;72:205-214,.
[49] Marzal S. Current challenges and future trends in the field of communication architectures for microgrids. Renewable Sustain Energy Rev 2018;82:3610-3622,.
[50] Zia MF, Elbouchikhi E, Benbouzid M. Microgrids energy management systems: A critical review on methods, solutions, and prospects. Appl Energy 2018;222:1033-1055,.
[51] Han Y, Li H, Shen P, Coelho PEAA, Guerrero JM. Review of active and reactive power sharing strategies in hierarchical controlled microgrids. IEEE Trans Power Electron 2017;32:2427-2451,.
[52] Martirano L. Demand side management in microgrids for load control in nearly zero energy buildings. IEEE Trans Ind Appl 2017;53:1769-1779,.
[53] Tien DV, Gono R, Leonowicz Z. Reliability evaluation of the distribution systems using analytical technique. Proc. IEEE Int. Conf. Environ. Elect. Eng. IEEE Ind. Commercial Power Syst, Palermo, Italy: Europe; 2018, p. 1–5.
[54] Renjit AA, Mondal A, Illindala MS, Khalsa AS. Analytical methods for characterizing frequency dynamics in islanded microgrids with gensets and energy storage. IEEE Trans Ind Appl 2017;53:1815-1823,.
[55] Hayes BP, Gruber JK, Prodanovic M. A closed-loop state estimation tool for MV network monitoring and operation. IEEE Trans Smart Grid 2015;6:2116-2125,.
[56] Favuzza S. An analysis of the intertial response of small isolated power systems in presence of generation from renewable energy sources. Proc. IEEE 4th Int. Forum Res. Technol. Soc. Ind, 2018, p. 1–6.
[57] Kuang Y. A review of renewable energy utilization in islands. Renewable Sustain Energy Rev 2016;59:504-513,.
[58] Mendoza-Vizcaino J. Integral approach to energy planning and electric grid assessment in a renewable energy technology integration for a 50/50 target applied to a small island. ApplEnergy 2019;233:524-543,.
[59] Lu T, Wang Z, Ai Q, Lee W. Interactive model for energy management of clustered microgrids. IEEE Trans Ind Appl 2017;53:1739-1750,.
[60] Brenna M. Automatic distributed voltage control algorithm in smart grids applications. IEEE Trans Smart Grid 2013;4:877-885,.
[61] Brenna M, Foiadelli F, Longo M, Zaninelli D. Energy storage control for dispatching photovoltaic power. IEEE Trans Smart Grid 2018;9:2419-2428,.
[62] Andalib-Bin-Karim C, Liang X, Zhang H. Fuzzy-secondarycontroller- based virtual synchronous generator control scheme for interfacing inverters of renewable distributed generation in microgrids. IEEE Trans Ind Appl 2018;54:1047-1061,.
[63] García P, Arboleya P, Mohamed B, Vega AAC. Implementation of a hybrid distributed/centralized real-time monitoring system for a DC/AC microgrid with energy storage capabilities. IEEE Trans Ind Inform 2016;12:1900-1909,.
[64] Canova A, Giaccone L, Spertino F, Tartaglia M. Electrical impact of photovoltaic plant in distributed network. IEEE Trans Ind Appl 2009;45:341-347,.

[65] Hirsch A, Parag Y, Guerrero JM. Microgrids: A review of technologies, key drivers, and outstanding issues. Renewable Sustain Energy Rev 2018;90:402-411,.
[66] Abdi H, Beigvand SD, Scala ML. A review of optimal power flow studies applied to smart grids and microgrids. Renewable Sustain Energy Rev 2017;71:742-766,.
[67] Nguyen HK, Khodaei A, Han Z. Incentive mechanism design for integrated microgrids in peak ramp minimization problem. IEEE Trans Smart Grid 2018;9:5774-5785,.
[68] Liu J, Tang J, Ponci F, Monti A, Muscas C, Pegoraro PA. Tradeoffs in PMU deployment for state estimation in active distribution grids. IEEE Trans Smart Grid 2012;3:915-924,.
[69] Cataliotti A, Cosentino V, Cara DD, Tinè G. LV measurement device placement for load flow analysis in MV smart grids. IEEE Trans Instrum Meas 2016;65:999-1006,.
[70] Chen YC, Wang J, Domínguez-García AD, Sauer PW. Measurement-based estimation of the power flowJacobian matrix. IEEE Trans Smart Grid 2016;7:2507-2515,.
[71] Cataliotti A, Cosentino V, Di Cara D, Tinè G. LV Measurement device placement for load flow analysis in mv smart grids. IEEE Trans Instrum Meas 2016;65:999–1006.
[72] Scalable optimization methods for distribution networks with highPVintegration. IEEE Trans Smart Grid 2016;7:2061-2070,.
[73] Olivier F, Aristidou P, Ernst D, Cutsem T. Active management of low-voltage networks for mitigating overvoltages due to photovoltaic units. IEEE Trans Smart Grid 2016;7:926-936,.
[74] Stimoniaris D, Tsiamitros D, Dialynas E. Improved energy storage management and PV-active power control infrastructure and strategies for microgrids. IEEE Trans Power Syst 2016;31:813-820,.
[75] Sharma K, Saini LM. Power-line communications for smart grid: Progress, challenges, opportunities and status. Renewable SustainEnergy Rev 2017;67:704-751,.
[76] Salvadori F, Gehrke CS, Oliveira AC, Campos M, Sausen PS. Smart grid infrastructure using a hybrid network architecture. IEEE Trans Smart Grid 2013;4:1630-1639,.
[77] Rinaldi S, Bonafini F, Ferrari P, Flammini A, Sisinni E, Di Cara D, et al. Characterization of IP-Based Communication for Smart Grid Using Software-Defined Networking. IEEE Transactions on Instrumentation and Measurement 2018. https://doi.org/10.1109/TIM.2018.2831318.
[78] Artale G, Cataliotti A, Cosentino V, Di Cara D, Fiorelli R, Guaiana S, et al. A new low cost power line communication solution for smart grid monitoring and management. IEEE Instrumentation and Measurement Magazine 2018. https://doi.org/10.1109/MIM.2018.8327976.
[79] Morales-Velazquez L, Romero-Troncoso R de J, Herrera-Ruiz G, Morinigo-Sotelo D, Osornio-Rios RA. Smart sensor network for power quality monitoring in electrical installations. Measurement 2017;103:133–42. https://doi.org/10.1016/j.measurement.2017.02.032.
[80] Intelligent Electronic Device (IED) n.d. https://www.svri.nl/en/intelligent-electronic-device-ied/.
[81] Laaksonen H. IED Functionalities Fulfilling Future Smart Grid Requirements. International Journal of Distributed Energy Resources and Smart Grids 2013;9.
[82] Lu S, Repo DG, Della FA, Figuerola AL, Pikkarainen M. Real-time low voltage network monitoring-ICT architecture and field test experience. IEEE Trans Smart Grid 2015;6:2002–12.
[83] Pereira R, Figueiredo J, Melicio R, Mendes VMF, Martins J, Quadrado JC. Consumer energy management system with integration of smart meters. Energy Rep 2015;1:22–9.
[84] Artale G, Caravello G, Cataliotti A, Cosentino V, Cara DD, Guaiana S, et al. A virtual tool for load flow analysis in a micro-grid. Energies 2020;13. https://doi.org/10.3390/en13123173.
[85] Artale G, Caravello G, Cataliotti A, Cosentino V, Di Cara D, Dipaola N, et al. Pq and harmonic assessment issues on low-cost smart metering platforms: A case study. Sensors (Switzerland) 2020;20:1–27. https://doi.org/10.3390/s20216361.
[86] Castello P, Ferrari P, Flammini A, Muscas C, Pegoraro PA, Rinaldi S. A distributed pmu for electrical substations with wireless redundant process bus. IEEE Trans Instrum Meas 2015;64:1149–57.
[87] Delle Femine A, Gallo D, Landi C, Luiso M. The design of a low cost phasor measurement unit. Energies 2019;12:2648.
[88] Tosato P, Macii D, Luiso M, Davide B, Daniele G, Carmine L. A tuned lightweight estimation algorithm for low-cost phasor measurement units. IEEE Trans Instrum Meas 2018;67:1047–57.
[89] Castello P, Ferrero R, Pegoraro PA, Toscani S. E ect of unbalance on positive-sequence synchrophasor, frequency, and rocof estimations. IEEE Trans Instrum Meas 2018;67:1036–46.
[90] Pegoraro PA, Meloni A, Atzori L, Castello P, Sulis S. PMU-Based distribution system state estimation with adaptive accuracy exploiting local decision metrics and iot paradigm. IEEE Trans Instrum Meas 2017;66:704–14.

[91] Cataliotti A, Cervellera C, Cosentino V, Di Cara D, Gaggero M, Maccio D, et al. An improved load flow method for MV networks based on LV load measurements and estimations. IEEE Trans Instrum Meas 2018;68:430–8.
[92] Artale G, Cataliotti A, Cosentino V, Di Cara D, Guaiana S, Telaretti E, et al. Incremental heuristic approach for meter placement in radial distribution systems. Energies 2019;12:3917.
[93] Rinaldi S, Della Giustina D, Ferrari P, Flammini A. Distributed monitoring system for voltage dip classification over distribution grid. Sustain Energy Grids Netw 2016;6:70–80.
[94] Bucci G, Ciancetta F, D'Innocenzo F, Fiorucci E, Ometto A. Development of a low cost power meter based on a digital signal controller. Int J Emerg Electr Power Syst 2018:19.
[95] De Souza WA, Marafao FP, Liberado EV, Diniz IS, Serni PJA. Power quality, smart meters and additional information from di erent power terms. IEEE Latin America Trans 2015;13:158–65.
[96] Caramia P, Carpinelli G, Verde P. Power Quality Indices in Liberalized Markets. Chichester, UK: John Wiley & Sons, Ltd; 2009.
[97] Artale G, Cataliotti A, Cosentino V, Guaiana S, Di Cara D, Panzavecchia N, et al. PQ Metrics Implementation on Low Cost Smart Metering Platforms. A Case Study Analysis. 2018 IEEE 9th International Workshop on Applied Measurements for Power Systems (AMPS), Bologna: IEEE; 2018, p. 1–6. https://doi.org/10.1109/AMPS.2018.8494866.
[98] I.E.C. Electromagnetic Compatibility (EMC)—Part 4-30: Testing and Measurement Techniques—Power Quality Measurement Methods. Geneva, Switzerland: IEC; 2015.
[99] I.E.C. Electromagnetic Compatibility (EMC)—Part 4-7: Testing and Measurement Techniques—General Guide on Harmonics and Interharmonics Measurements and Instrumentation, for Power Supply Systems and Equipment Connected Thereto. Geneva, Switzerland: IEC; 2002.
[100] I.E.C./T.R. Instrument Transformers—The Use of Instrument Transformers for Power Quality Measurements. Geneva, Switzerland: IEC; 2012.
[101] EN ES. Voltage Characteristics of Electricity Supplied by Public Electricity Networks. Brussels, Belgium: CENELEC; 2015.
[102] AN4732 A. STCOMET Smart Meter and Power Line Communication System-on-Chip Development Kit. Geneva, Switzerland: STMIcroelectronics; 2017.
[103] Cataliotti A. An improved load flow method for MV networks based on LV load measurements and estimations. IEEE Trans Instrum Meas 2019;68:430-438,.
[104] Kersting WH. Distribution System Modeling and Analysis. 3rd ed. Las Cruces, NM, USA: CRC Press; 2012.
[105] IEEE Standard Communication Delivery Time Performance Requirements for Electric Power Substation Automation, IEEE Standard 1646-2004 2005.
[106] Artale G, Cataliotti A, Cosentino V, Di Cara D, Guaiana S, Panzavecchia N, et al. Real-Time Power Flow Monitoring and Control System for Microgrids Integration in Islanded Scenarios. IEEE Trans on Ind Applicat 2019;55:7186–97. https://doi.org/10.1109/TIA.2019.2932967.
[107] JRC Photovoltaic Geographical Information System (PVGIS) - European Commission n.d. https://re.jrc.ec.europa.eu/pvg_tools/en/#PVP.
[108] Riva Sanseverino E, Buono L, Di Silvestre ML, Zizzo G, Ippolito MG, Favuzza S, et al. A distributed minimum losses optimal power flow for islanded microgrids. Electric Power Systems Research 2017;152:271–83. https://doi.org/10.1016/j.epsr.2017.07.014.
[109] Jadhav AM, Patne NR, Guerrero JM. A Novel Approach to Neighborhood Fair Energy Trading in a Distribution Network of Multiple Microgrid Clusters. IEEE Transactions on Industrial Electronics 2019;66:1520–31. https://doi.org/10.1109/TIE.2018.2815945.
[110] Lu X. Implementing PRIME for Robust and Reliable Power Line Communication (PLC) 2013.
[111] Dostert K. Powerline communications. Upper Saddle River, NJ: Prentice Hall; 2001.
[112] Held G. Understanding Broadband over Power Line. CRC Press; 2016.
[113] Iniewski K, editor. Broadband over Power Line Communications: Home Networking, Broadband Access, and Smart Power Grids. Internet Networks, CRC Press; 2010.
[114] Pighi R, Raheli R. On multicarrier signal transmission for high-voltage power lines. International Symposium on Power Line Communications and Its Applications, 2005., 2005, p. 32–6. https://doi.org/10.1109/ISPLC.2005.1430460.
[115] Hyun D, Lee Y. A Study on the Compound Communication Network over the High Voltage Power Line for Distribution Automation System. 2008 International Conference on Information Security and Assurance (isa 2008), 2008, p. 410–4. https://doi.org/10.1109/ISA.2008.28.

[116] Aquilue R, Gutierrez I, Pijoan JL, Sanchez G. High-Voltage Multicarrier Spread-Spectrum System Field Test. IEEE Transactions on Power Delivery 2009;24:1112–21. https://doi.org/10.1109/TPWRD.2008.2002847.
[117] Cataliotti A, Daidone A, Tinè G. Power line communication in medium voltage systems: characterization of MV cables. IEEE Transactions on Power Delivery 2008;23:1896–902. https://doi.org/10.1109/TPWRD.2008.919048.
[118] Artale G, Cataliotti A, Cosentino V, Di Cara D, Fiorelli R, Guaiana S, et al. A new coupling solution for G3-PLC employment in MV smart grids. Energies 2019;12. https://doi.org/10.3390/en12132474.
[119] P.Meier MB, HWidmer, Rubinstein A, Rachidi F, Rubinstein M. Pathloss as a function of frequency, distance and network topology for various LV and MV European powerline networks,"The OPERA Consortium, Project Deliverable. EC/IST FP6 Project 2005.
[120] Cataliotti A, Cosentino V, Guaiana S, Di Cara D, Panzavecchia N, Tinè G. Experimental investigation on PLC signal crossing of power transformers. Conference Record - IEEE Instrumentation and Measurement Technology Conference, 2014. https://doi.org/10.1109/I2MTC.2014.6860941.
[121] Nordell DE. Communication systems for distribution automation. Proceedings of the IEEE Transmission and Distribution Conference and Exposition, Bogota, Colombia: 2008.
[122] Mak S, Moore T. TWACS, a new viable twoway automatic communication system for distribution networks. Part II: inbound communication. IEEE Transactions on Power Apparatus and Systems 1984;103:2141-2147,.
[123] Mak S, Reed D. TWACS, a new viable twoway automatic communication system for distribution networks. Part I: outbound communication. IEEE Transactions on Power Apparatus and Systems 1982;101:2941-2949,.
[124] Ankou A, Arribas M, Arzuaga A, Arzuaga T, Berganza I, Bertoni G, et al. Specification for PoweRline Intelligent Metering Evolution n.d.
[125] Razazian K, Umari M, Kamalizad A, Loginov V, Navid M. G3-PLC specification for powerline communication: Overview, system simulation and field trial results. Proceedings of the 14th Annual International Symposium on Power Line Communications and its Applications (ISPLC '10, Brazil: Rio de Janeiro; 2010, p. 313-318,.
[126] Sendin A, Kim IH, Bois S, Munoz A, Llano A. PRIME v1.4 evolution: A future proof of reality beyond metering. 2014 IEEE International Conference on Smart Grid Communications (SmartGridComm), 2014, p. 332–7. https://doi.org/10.1109/SmartGridComm.2014.7007668.
[127] Corchado JA, Manero E, Cortés JA, Sanz A, Díez-del-Río L. Application-layer Performance Analysis of PRIME in Smart Metering Networks 2016.
[128] Alliance PRIME. Powerline related intelligent metering evolution (PRIME n.d.
[129] Artale G, Cataliotti A, Cosentino V, Di Cara D, Fiorelli R, Guaiana S, et al. A new low cost coupling system for power line communication on medium voltage smart grids. IEEE Trans Smart Grid 2018;9:3321–9.
[130] Cataliotti A, Cipriani G, Cosentino V, Di Cara D, Di Dio V, Guaiana S, et al. A prototypal architecture of a IEEE 21451 network for smart grid applications based on power line communications. IEEE Sensors Journal 2015. https://doi.org/10.1109/JSEN.2014.2336377.
[131] Artale G, Caravello G, Cataliotti A, Cosentino V, Di Cara D, Fiorelli R, et al. Implementation of a PLC Field Analyzer on a G3 Modem Platform. Conference Record - IEEE Instrumentation and Measurement Technology Conference, vol. 2021- May, 2021. https://doi.org/10.1109/I2MTC50364.2021.9459937.
[132] ctypes — A foreign function library for Python — Python 3.10.0 documentation n.d. https://docs.python.org/3/library/ctypes.html.
[133] rfc4122 n.d. https://datatracker.ietf.org/doc/html/rfc4122.html.
[134] Bali MC, Rebai C. Improved maximum likelihood S-FSK receiver for PLC modem in AMR. J ElectrComput Eng 2012:452402.
[135] Cataliotti A, Di Cara D, Tinè G. Model of line to shield power line communication system on a medium voltage network. Proc. IEEE I2MTC, Austin, TX: 2010, p. 1459–62.
[136] Fiorelli R, Cataliotti A, Di Cara D, Tinè G. Coupling circuit for power line communications 2014.
[137] Live working – Voltage detectors – Part 1: capacitive type to be used for voltages exceeding 1 kV a.c 2009.

[138] Electrotechnical Standardization EC. Signalling on low-voltage electrical installations in the frequency range 3 kHz to 148,5 kHz - Part 1: General requirements, frequency bands and electromagnetic disturbances 2010.
[139] Artale G, Cataliotti A, Cosentino V, Di Cara D, Tinè G. Development of a coupling system for medium voltage power line communication in the CENELEC a frequency band. Proc. IEEE AMPS 2016, Aachen, Germany, Sept: 2016, p. 103–7.
[140] Artale G, Cataliotti A, Cosentino V, Guaiana S, Di Cara D, Panzavecchia N, et al. An Innovative Coupling Solution for Power Line Communication in MV Electrical Networks. Proceedings - 2019 IEEE 1st Global Power, Energy and Communication Conference, GPECOM 2019, 2019. https://doi.org/10.1109/GPECOM.2019.8778524.
[141] Cataliotti A, Cosentino V, Nuccio S, Di Cara D, Panzavecchia N, Tinè G. A simplified approach for load flow analysis in MV smart grids based on LV power measurements. I2MTC 2017 - 2017 IEEE International Instrumentation and Measurement Technology Conference, Proceedings, 2017. https://doi.org/10.1109/I2MTC.2017.7969686.
[142] Novosel D, Madani V, Bhargava B, Vu K, Cole J. Dawn of the grid synchronization. IEEE Power Energy Mag 2008;6:49-60,.
[143] Pegoraro PA, Brady K, Castello P, Muscas C, Meier A. Line impedance estimation based on synchrophasor measurements for power distribution systems. IEEE Trans Instrum Meas 2019;68:1002-1013,.
[144] Blair SM, Syed MH, Roscoe AJ, Burt GM, Braun J-P. Measurement and analysis of PMU reporting latency for smart grid protection and control applications. IEEE Access 2019;7:48689-48698,.
[145] Tosato P, Macii D, Fontanelli D, Brunelli D, Laverty D. A software-based low-jitter servo clock for inexpensive phasor measurement units. Proc. IEEE Int. Symp. Precis. Clock Synchronization Meas., Control, Commun. (ISPCS, 2018, p. 1–6.
[146] Rinaldi S, Ferrari P, Flammini A, Sisinni E, Vezzoli A. Uncertainty analysis in time distribution mechanisms for OMS smart meters: The last-mile time synchronization issue. IEEE Trans Instrum Meas 2019;68:693-703,.
[147] Bello LL, Raucea A, Patti G, Mirabella O. L-PTP: A novel clock synchronization protocol for powerline networks. Proc. IEEE 17th Int. Conf. Emerg. Technol. Factory Automat. (ETFA, Krakow, Poland: 2012, p. 1–4.
[148] Gaderer G, Loschmidt P, Treytl A, Kerö N. Internal and external clock synchronization in a power line network. Proc. PTTI Syst. Appl. Meeting, 2006, p. 213–22.
[149] Bumiller G, Lampe L. Fast burst synchronization for PLC systems. Proc. IEEE Int. Symp. Power Line Commun. Appl, 2007, p. 26–8.
[150] Liang D, Niu D, Zhang BH, Fu K, Bo ZQ. A design and implementation of timing synchronization algorithm for OFDMbased powerline communication. Proc. IEEE Int. Symp. Power Line Commun, Appl: 2012, p. 27–30.
[151] Rinaldi S. An experimental characterization of time of arrival accuracy for time synchronization of medium voltage smart grid solutions. Proc. IEEE 10th Int. Workshop Appl. Meas. Power Syst. (AMPS, 2019, p. 1–6.
[152] Time Synchronization in the Electric Power System, NASPI Time Synchronization Task Force 2017.
[153] IEEE Standard for Synchrophasor Measurements for Power Systems. IEEE Standard C371181-2011 (Revision of IEEE Std C37118-2005 2011:1–61.
[154] Communication Networks and Systems for Power Utility Automation 2019.
[155] Jiang X, Zhang J, Harding BJ, Makela JJ, Dominguez-Garcia AD. Spoofing GPS receiver clock offset of phasor measurement units. IEEE Trans Power Syst 2013;28:3253-3262,.
[156] Shereen E, Delcourt M, Barreto S, Dan G, Boudec J-YL, Paolone M. Feasibility of time synchronization attacks against PMUbased state-estimation. IEEE Trans Instrum Meas n.d. https://doi.org/10.1109/TIM.2019.2939942.
[157] IEEE Standard for a Precision Clock Synchronization Protocol for Networked Measurement and Control Systems 2008:1–300.
[158] Lixia M, Benigni A, Flammini A, Muscas C, Ponci F, Monti A. A software-only PTP synchronization for power system state estimation with PMUs. IEEE Trans Instrum Meas 2012;61:1476-1485,.
[159] Serrano J. The white rabbit project. Proc. ICALEPCS TUC, Kobe, Japan: 2009, p. 93–5.
[160] Lipinski M. White rabbit applications and enhancements. Proc. IEEE Int. Symp. Precis. Clock Synchronization Meas., Control, Commun. (ISPCS, 2018, p. 1–4.

[161] Ramos F, Gutierrez-Rivas JL, Lopez-Jimenez J, Caracuel B, Diaz J. Accurate timing networks for dependable smart grid applications. IEEE Trans Ind Informat 2018;14:2076-2084,.
[162] Lampe LA, Tonello M, Swart TG. Power Line Communications: Principles, Standards and Applications From Multimedia to Smart Grid. 2nd ed. Hoboken, NJ, USA: Wiley; 2016.
[163] Yu Q, Holmes TW, Naishadham K. RF equivalent circuit modeling of ferrite-core inductors and characterization of core materials. IEEE Trans Electromagn Compat 2002;44:258-262,.
[164] Wang X-Y, Gao X. The typical designs of PLC network in MV distribution network. Proc. IEEE Int. Symp. Power Line Commun, Appl: 2012, p. 19–23.
[165] Rinaldi S, Pasetti M, Bonafini F, Ferrari P, Flammini A, Sisinni E, et al. Design of a Time Dissemination System Using Chirp Modulation for Medium Voltage Smart Grid Applications. IEEE Transactions on Instrumentation and Measurement 2020;69:6686–95. https://doi.org/10.1109/TIM.2020.2975372.
[166] Rinaldi S, Di Cara D, Panzavecchia N, Tine G, Bonafini F, Ferrari P, et al. An experimental characterization of time of arrival accuracy for time synchronization of medium voltage smart grid solutions. AMPS 2019 - 2019 10th IEEE International Workshop on Applied Measurements for Power Systems, Proceedings, 2019. https://doi.org/10.1109/AMPS.2019.8897769.
[167] Boumard S, Mammela A. Synchronization using chirp training sequences in multipath channels. Proc. IEEE Global Telecommun. Conf, Washington, DC, USA: GLOBECOM; 2007, p. 4030–4.
[168] Artale G, Brandauer C, Caravello G, Cataliotti A, Cosentino V, Di Cara D, et al. A resilient distributed measurement system for smart grid application. vol. 1284 CCIS. 2020. https://doi.org/10.1007/978-3-030-59000-0_11.
[169] Artale G, Caravello G, Cataliotti A, Cosentino V, Di Cara D, Ditta V, et al. A PLC based monitoring and remote control architecture for Distributed Generation and Storage systems in LV smart grids. 2021 IEEE 6th International Forum on Research and Technology for Society and Industry (RTSI), Naples, Italy: IEEE; 2021, p. 255–60. https://doi.org/10.1109/RTSI50628.2021.9597316.